

GEOLOGY FOR SOCIETY

SINCE 1858



**GEOLOGICAL
SURVEY OF
NORWAY**

· NGU ·

NGU REPORT
2021.023

Landscape changes and bedrock
reconstruction in Gjerdrum area.
Methodological approach and
main results



REPORT

Report no.: 2021.023		ISSN: 0800-3416 (print) ISSN: 2387-3515 (online)		Grading: Open	
Title: Landscape changes and bedrock reconstruction in Gjerdrum area. Methodological approach and main results					
Authors: Ivanna Penna and Inger-Lise Solberg			Client:		
County: Viken			Commune: Gjerdrum		
Map-sheet name (M=1:250.000)			Map-sheet no. and -name (M=1:50.000)		
Deposit name and grid-reference:			Number of pages: 82		Price (NOK):
			Map enclosures:		
Fieldwork carried out:		Date of report: 29.09.2021		Project no.: 394800	Person responsible: 
Summary: <p>On 30 December 2020 a quick-clay landslide occurred in Gjerdrum, Norway. Because of the severe consequences, the Norwegian government appointed an external expert committee to investigate the landslide. In order to investigate the changes in the landscape that could have contributed to the destabilisation of the slopes, a wide approach was necessary. For this, the Geological Survey of Norway (NGU) has contributed with several GIS analyses and 3D modelling.</p> <p>This report is a documentation of the methods utilised during the work done by NGU. The data quality of the input data for the analyses and modelling are also presented. The main results of the work are shown, but not discussed with regard to the underlying causes and/or triggers of the landslide. Most of the results are used and discussed in the report of the Gjerdrum committee.</p>					
Keywords:		Landslide		Gjerdrum	
Terrain modelling		LiDAR		Orthophoto	
Landscape changes		3D model		Erosion	

Preface

On 30 December 2020, a quick-clay landslide occurred in Ask, the municipality centre in Gjerdrum (Viken county, Norway). Ten people lost their lives in the landslide, and more than 1600 people were evacuated. The landslide occurred during the night.

The Norwegian government appointed on 5 February 2021 an external expert committee to investigate the causes of the Gjerdrum landslide and assess measures to strengthen the prevention of quick-clay landslides throughout the country (Regjeringen 2021).

In order to investigate the changes in the landscape that could have contributed to the destabilisation of the slopes, a wide approach was necessary. For this, the Geological Survey of Norway (NGU) has contributed with several GIS analyses and 3D modelling.

This report is a documentation of the methods, parameters of the work done by NGU. The data quality of the input data for the analyses and modelling is also presented. The results of the work are shown, but not discussed with regard to the underlying causes and/or triggering of the landslide. Most of the results are used and discussed in the report of the Gjerdrum committee, published 29 September 2021.

Table of contents

1.	Introduction.....	6
2.	General methodology	7
3.	Geological context.....	8
4.	Brief geomorphological description of the landslide.....	9
5.	Landslide: Volume calculations	10
5.1	Methodology	11
5.2	Results.....	11
6.	Land use changes: Overview of infill and urbanisation	13
6.1	Methodology	14
6.2	Results.....	14
7.	Spatial and temporal distribution of landscape changes.....	18
7.1	Methodology	18
7.2	Results.....	20
8.	Land infill in Nystulia: terrain changes	22
8.1	Methodology	22
8.2	Results.....	23
9.	Changes in forest cover	24
9.1	Methodology	24
9.2	Results.....	24
10.	Land infill in Holmen: Volume calculation	26
10.1	Methodology	26
10.2	Results.....	26
11.	Watershed extension in time	27
11.1	Methodology	28
11.2	Results.....	28
12.	Changes in the stream path of Brådalsbekken-Tistilbekken.....	33
12.1	Methodology	33
12.2	Results.....	35
13.	Changes in the long profile of the Brådalsbekken and Tistilbekken.....	39
13.1	Methodology	39
13.2	Results.....	39
14.	Changes observed in cross sections of the streams	42
14.1	Methodology	42
14.2	Results.....	42

15.	Streambed changes in the lower section of Tistilbekken	45
15.1	Methodology	45
15.2	Results.....	47
16.	Slope changes at the bottom of Tistilbekken creek.....	49
16.1	Methodology	49
16.2	Results.....	50
17.	Stream Power Index	53
17.1	Methodology	53
17.2	Results.....	53
18.	Bedrock topography and sediment thicknesses	55
18.1	Methodology	56
18.2	Results.....	58
19.	Closing remarks	61
20.	References.....	62
21.	Acknowledgement	63

1. Introduction

On 30 December 2020 a quick-clay landslide occurred in Ask, the municipality centre in Gjerdrum (Viken county, Norway) (Figure 1). The purpose of the present study is to investigate changes in the landscape that could have contributed to the destabilisation of the slopes in Ask. For this, a broad approach is necessary.

Landscape changes result from the interaction of natural and human-driven processes. Remote sensing data and GIS analyses can be used to determine the spatial and temporal distribution of those changes, as well as their magnitude. This report explores the changes by carrying out several analyses on historical aerial photos and airborne LiDAR datasets. Furthermore, we reconstruct the bedrock topography below the marine sediments in the area using subsurface data.

After a general overview of the main methods used in the report, a short overview of the geological setting is given. This is followed by two chapters dealing with the geomorphology and volumes of the quick-clay landslide on 30 December 2020. The main parts of the report show the results from analyses of landscape changes the years before the landslide event. Finally, the results of the modelling of bedrock topography are presented.

Important localities are (Figure 1):

Tistilbekken: This stream runs from Ask centre down to the landslide area west of Holmen. Here it becomes a pond, and after this the stream is partly piped before it flows into Tangeelva.

Brådalsbekken: This short stream is located west of Tistilbekken. Downstream the confluence the stream is called Tistilbekken.

The culvert: A ca. 44 m long pipe/culvert for Tistilbekken is just downstream the confluence with Brådalsbekken. A fairway of the golf course is located over the culvert.

The pond: This is a small pool in Tistilbekken southwest of Holmen.

The golf course: This is the Gjerdrum Golfklubb area and mainly located west of Brådalsbekken-Tistilbekken.

Holmen: Byvegen 1-5 is located in the south-eastern part of the detachment area of the 30 December landslide.

Nystulia: This is a developed area located in the northern part of the detachment area of the 30 December landslide.

Brådalsfjellet: This developed area is located about 1 km west of Ask centre.

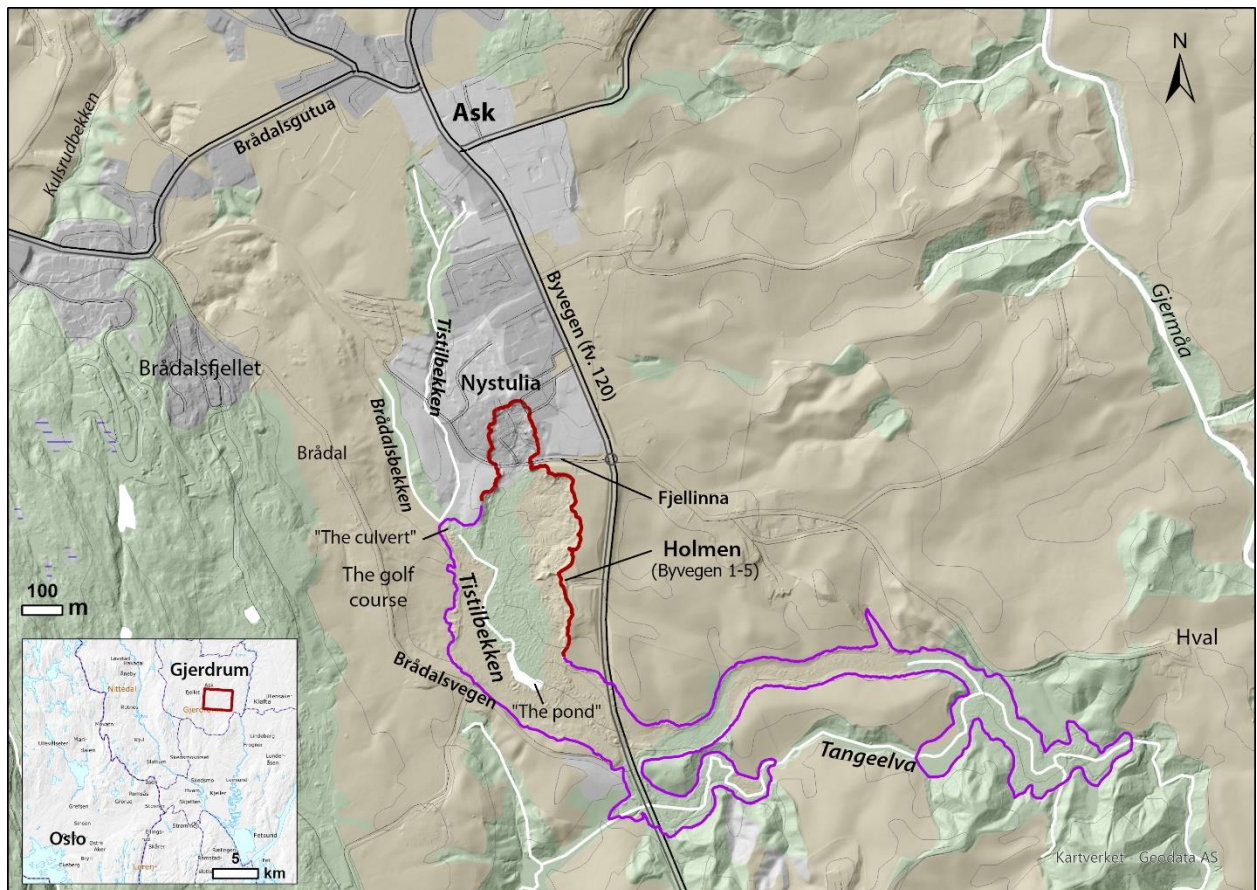


Figure 1. Location of the study area, extension of the 2020 landslide event and main localities mentioned in the text. The red line represents the headscarp of the landslide and the purple line corresponds to the outlet area.

2. General methodology

For the mapping, computations, and analyses in this study, the following software programmes were used:

- ArcGIS® software version 10.8.1. by ESRI
- Cloud Compare software version 2.11.1
- GRASS GIS software
- Grapher™ (Golden Software, LLC)

LiDAR (Light Detection and Ranging) data from different years were used for most of the analyses. See Appendix 1 for a short description of the LiDAR method. In addition, vertical aerial photos/orthophotos were used. LiDAR-data/DTMs and vertical aerial photos are from Kartverket (2021a, b). Photogrammetric models were provided by the Norwegian Water Resources and Energy Directorate (NVE) and produced by COWI (see Appendix 2).

For the Ask area, LiDAR datasets from 2007, 2013, 2015, 2020 and 2021 are available and were used in the analyses. In addition, there are vertical aerial photos captured over many years in Ask; the oldest is from 1946. The datasets (year, resolution etc.) are presented in each chapter, depending on which data were used for the different analyses.

For the bedrock modelling, different datasets are used: geotechnical borehole data, groundwater wells, geophysical data and field observation points.

3. Geological context

The Gjerdrum area was below sea level during the deglaciation of the last ice age (Østmo & Olsen 1978). The marine limit in the area is about 205 m a.s.l., and the “Romeriksfjorden” was filled with marine sediments (Figure 2). In the Ask area, marine clay was deposited locally with thin layers of silt or fine-grained sand. During the Holocene, the area was isostatically lifted, and gradually rivers and streams started to erode the deposits. As the marine clay was leached by groundwater, quick clay developed in layers and pockets. When the streams eroded the sediments, the slopes became unstable, leading to landslide activity. There are several traces of ravines and landslides in Gjerdrum (Figure 3).

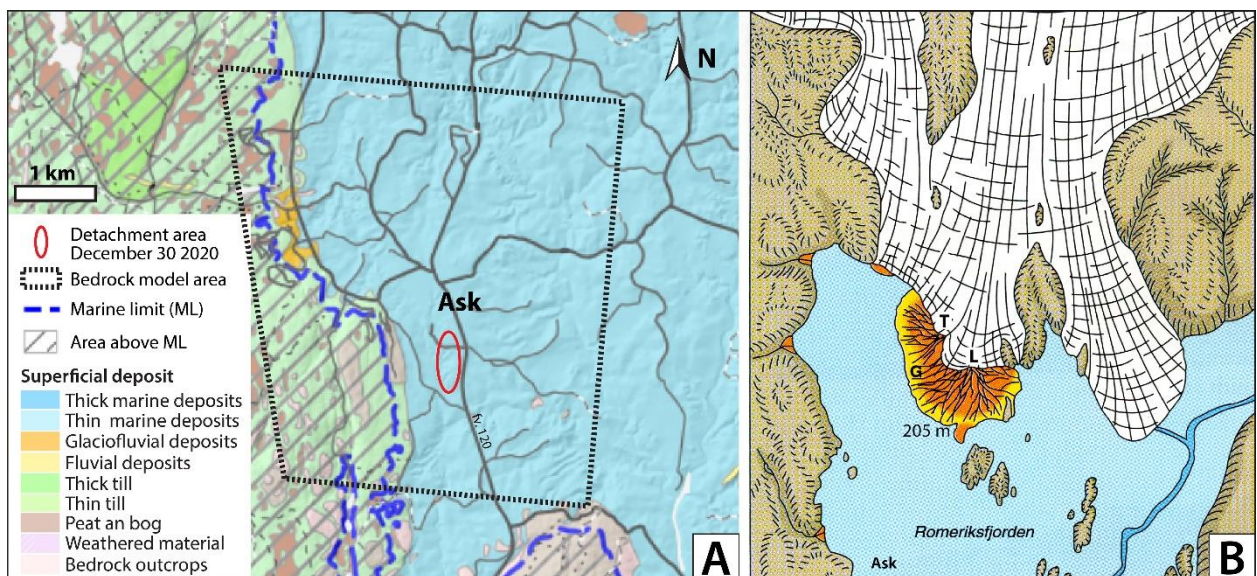


Figure 2. (A) Quaternary geological map with marine limit for parts of Gjerdrum municipality. The area is mapped by Østmo & Olsen (1978); see NGU (2021a) for more mapped details. (B) Romerike about 9 500 ¹⁴C years BP. The large ice-marginal delta (orange) was built up to and above the former sea level. The figure is modified from Barger (2005).

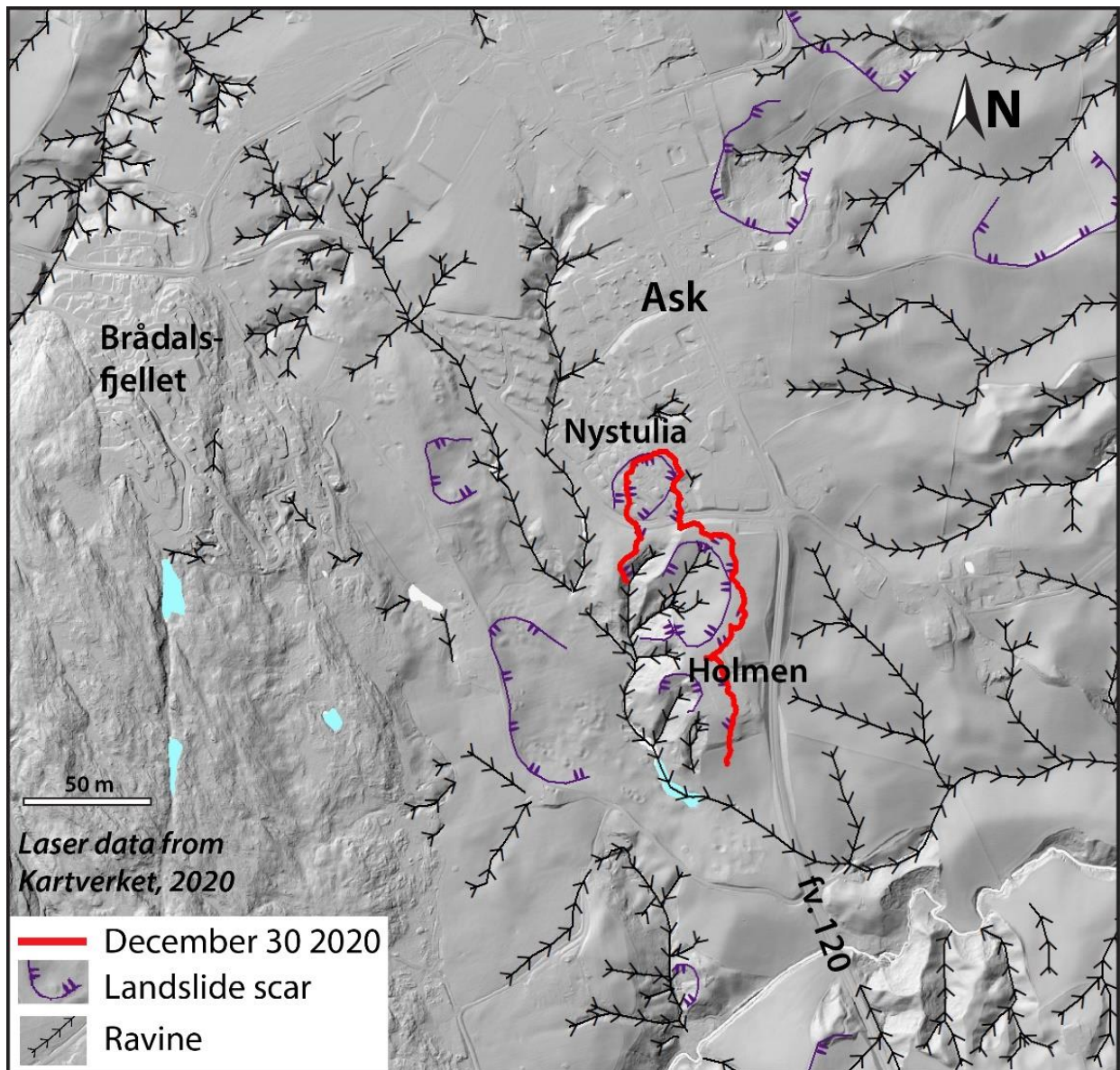


Figure 3. There are a lot of traces of ravines and landslides in Gjerdrum. The mapping of these landforms is based on terrain models and orthophotos from Kartverket (2021a).

4. Brief geomorphological description of the landslide

On 30 December 2020, a quick-clay landslide took place southwest of Ask centre in Gjerdrum. The detachment area was about 0.12 km², and the outlet area was about 0.26 km². The deposits had a maximum runout length of about 2 km. The landslide deposits split into two branches, one along the Tistilbekken ravine (the stream was partly in pipes here), and a shorter one along the Tangeelva (Figure 1 and Figure 4). The landslide deposits blocked ravines, forming several dams. The largest dam covered 0.03 km² and extended 1 km in Tangeelva upstream the road fv. 120.

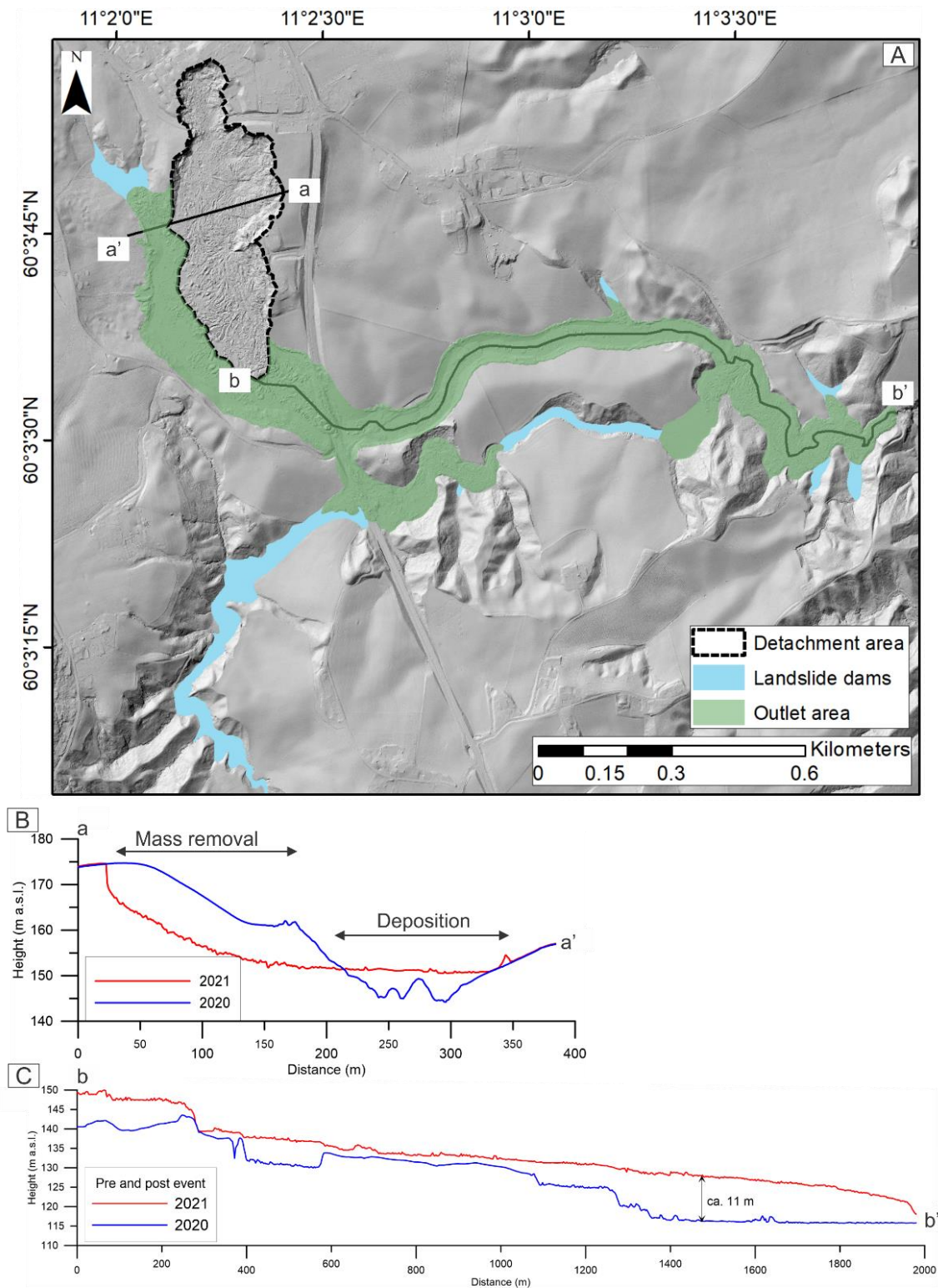


Figure 4. (A) Hillshade map and main landforms related to the quick-clay landslide on 30 December 2020 in Gjerdrum. (B) Cross section with pre and post event topographies at the detachment area. (C) Cross section with pre and post event topographies along the outlet area.

5. Landslide: Volume calculations

The volume of a landslide is a key parameter controlling its propagation distance and, therefore, its damage capacity. A major problem with estimating the volume of a landslide is the determination of the shape of its sliding surface, which is frequently buried with parts of

the detached material. In addition, the determination of the depth of the sliding surface is often based on sparse data (Jaboyedoff et al. 2020). A way to overcome this issue is to use high-resolution elevation models and, as much as possible, subsurface information. In this chapter, we present the results of the computation of the 2020 landslide and the input data used for its calculation.

5.1 Methodology

The general approach to compute the detached and deposited volumes was the subtraction of digital terrain models (DTMs), such as the reconstructed sliding surface and the 2020 and 2021 topography (Table 1).

The sliding surface was reconstructed and delivered by Multiconsult as part of their further development of a Leapfrog 3D model for the landslide area (Multiconsult 2021). The density of points in the sliding surface area was 0.15 points/m², and with this data, a raster of 1 m resolution was built with the Inverse Distance Weighted (*IDW*) tool from ArcMap. This tool interpolates a raster surface from points using an inverse distance weighted technique.

Table 1. Airborne LiDAR DTMs used for volume computations

Name and Year	Resolution (m)	Date of acquisition
Gjerdrum 5pkt 2021	0.25	08.01.2021
Gjerdrum Ullensaker Nannestad 5 pkt 2020	0.25	19.04.2020

The detached volume resulted from the computation of the height differences between the 2020 topography and the reconstructed sliding surface. We carried out the computation of the volume of the deposited material in two steps: 1) height difference between the 2021 topography and the sliding surface. This provided the volume of mobilised material resting over the sliding surface in the detachment area and 2) height differences between the 2021 and the 2020 topographies. These computations provided the volume of the material deposited in the outlet area. In all cases, the height differences were determined using the *Raster Calculator* tool from ArcMap, and the volumes resulted from the multiplication of the sum of height differences in the output raster of the *Raster Calculator* by the area of a single pixel.

5.2 Results

The area of detachment is elongated, with its longest axis oriented N-S. The maximum height difference between the 2020 topography and the sliding surface is observed in the vicinity of Holmen. The volume of mobilised material was determined in 1.35 million m³, and the sediments slid along a spoon-like surface, with the toe located at the height of Tistilbekken creek in 2020 (ca. 140-144 m a.s.l.). Parts of the displaced material remained over the sliding surface, which constitutes a total volume of 0.470 million m³ (Figure 5).

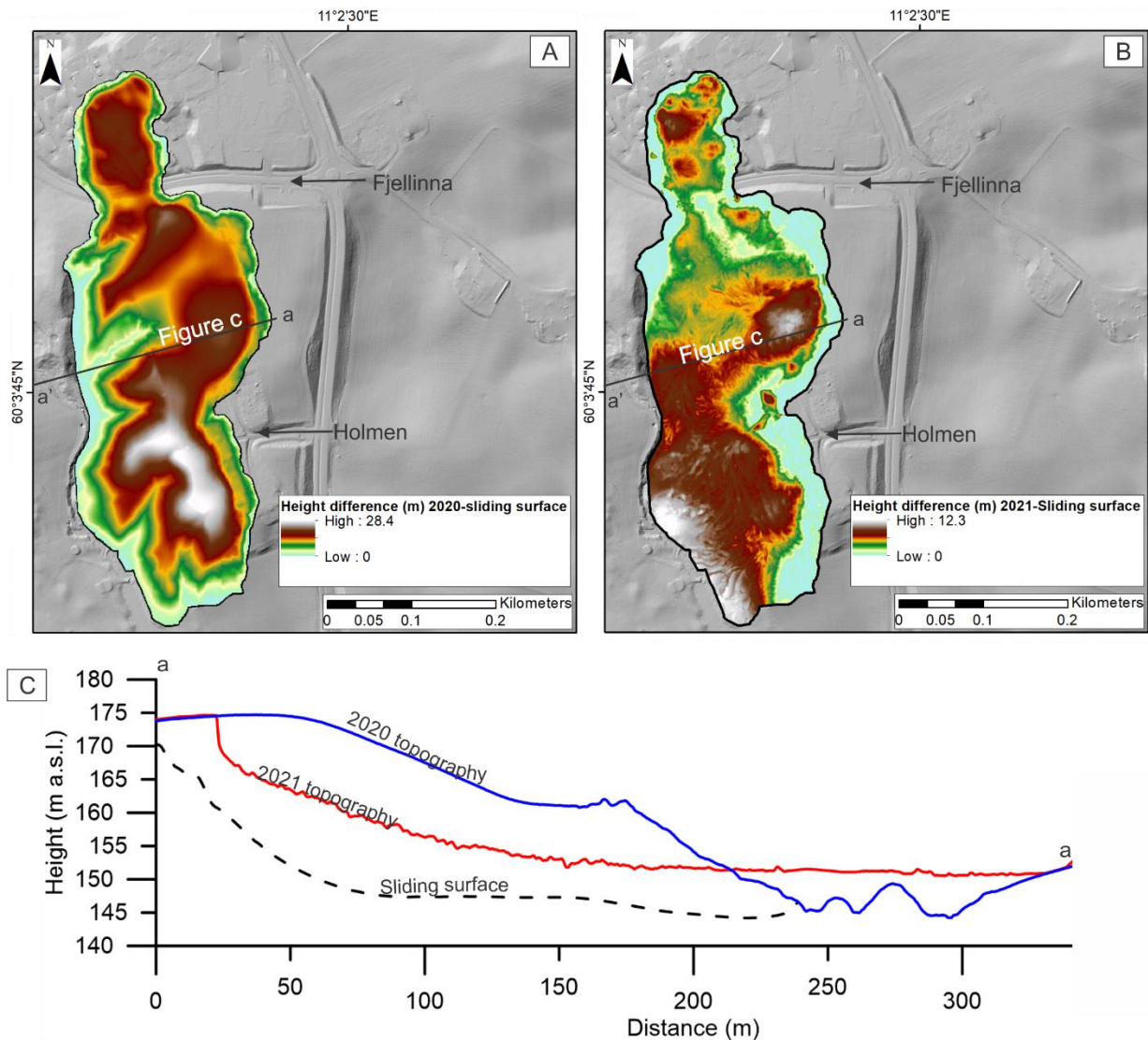


Figure 5. (A) Map of height differences between the sliding surface and the 2020 topography in the detachment zone, with 2020 hillshade as base map. (B) Map of height differences between the 2021 topography and the sliding surface in the detachment zone, with 2020 hillshade as base map. (C) Cross-section showing the three surfaces involved in the volume computation.

The backscarp of the landslide was up to 175-178 m a.s.l. and the distal part of the deposits lies at around 115 m a.s.l. The deposits in the outlet area present a variable thickness from the detachment zone to the distal part. The sectors with higher thickness correspond to places where topographical constraints have controlled the deposition and behaviour of the flow. Upstream the fv. 120, the higher thickness relates to the height of the road which by constituting an obstacle, dammed the flow. 140 m east of the fv. 120, a part of Tistilbekken that was not piped, was filled. Immediately south of this sector, a narrow section in the Tangeelva could have created a bottle-neck effect, reducing the velocity of the flow and leading to the deposition of material. In the distal part of the deposit, a wide section in the valley close to the confluence between Tistilbekken and Tangeelva, plus a narrow section in the distal area of the deposit, could have contributed to reducing the velocity of the flow. In the outlet area, the deposit has a volume of 0.926 million m³.

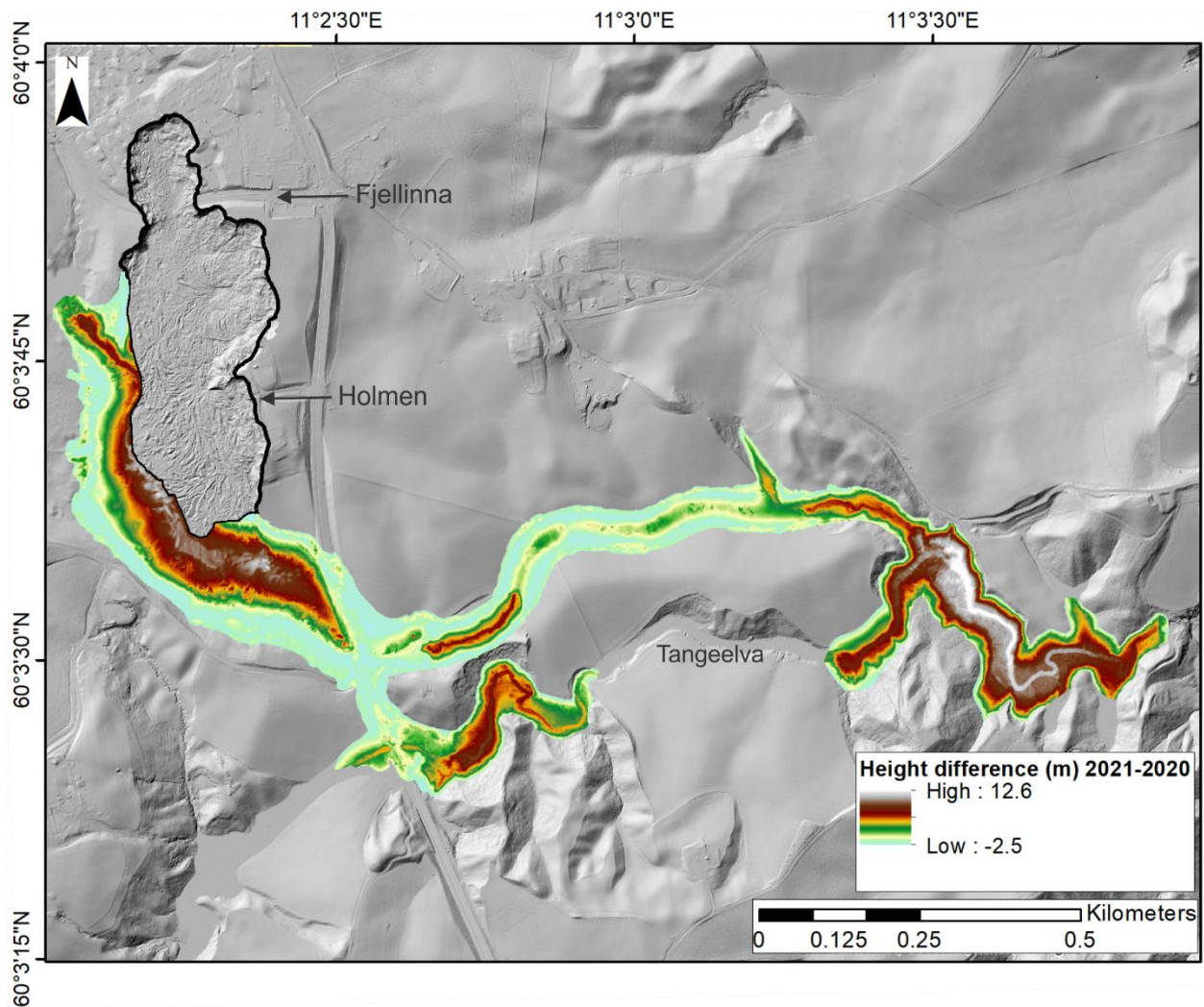


Figure 6. Map of height differences between the 2021 and 2020 topography for the outlet area.

The difference between the volume of the mobilised material and the deposited volume can be explained by the entrainment of trees in the detachment area and along the path of the landslide. All the trees in the detachment area and along the path of the landslide were removed. A minor proportion of the difference could owe to potential air pockets in the deposits due to trees and other obstacles, and to the different resolutions of the 2020 and 2021 topography.

6. Land use changes: Overview of infill and urbanisation

Ask and its adjacent areas have experienced land-use changes: e.g. urban development has increased and agricultural lands have decreased. Furthermore, as urbanisation increased, surface changes occurred (infill and removal of soil) (see an example in chapter 8), and the forest cover was reduced (chapter 9). In this chapter, we present an overview of the main changes observed concerning infill and urbanisation.

6.1 Methodology

Areas with land infill: Areas undergoing land infill were determined based on the interpretation of aerial pictures from 1969 to 2007, photogrammetric reconstructions based on aerial pictures, and airborne LiDAR datasets from 2007 to 2020.

Rooftop mapping: The area covered by rooftops was determined by interpretation and mapping of aerial photos from the projects listed below and available at “Norge i bilder” (Kartverket 2021b), and the FKB-Bygning from Geonorge.no.

- Øvre Romerike 2020
- Fet Gjerdrum 2007
- Gjerdrum 2004
- Ask 17 mai 1991
- Ask juni 1974
- Ask juli 1969

Road network mapping: The road network has been mapped along time using the aerial photos of the projects listed above.

6.2 Results

Between 1974 and 2020 agricultural ground levelling, and filling and removal of sediments due to construction activities, were carried out in several parts of the area (Figure 7). The upper and lower sections of Brådalsbekken show land infill between 1974-1984. Infill in the upper part of Tistilbekken continued between 2007-2013.

Land infill is often carried out to increase the extension of agricultural lands or for the development of new urban areas. Land infilling is conducted for both these reasons in Ask. An increase in urban areas has been observed since 1969. The area southwest of Ask centre was developed in several stages, mainly around 1993 and from 2004. Nystulia is the area that experienced most of the growth, and houses there were built from around 2007.

The surfaces covered by rooftops in 2020 is five times greater than in 1969; see Table 2 and Figure 8. The exponential growth of the surface covered by rooftops is due to the urbanisation of the area.

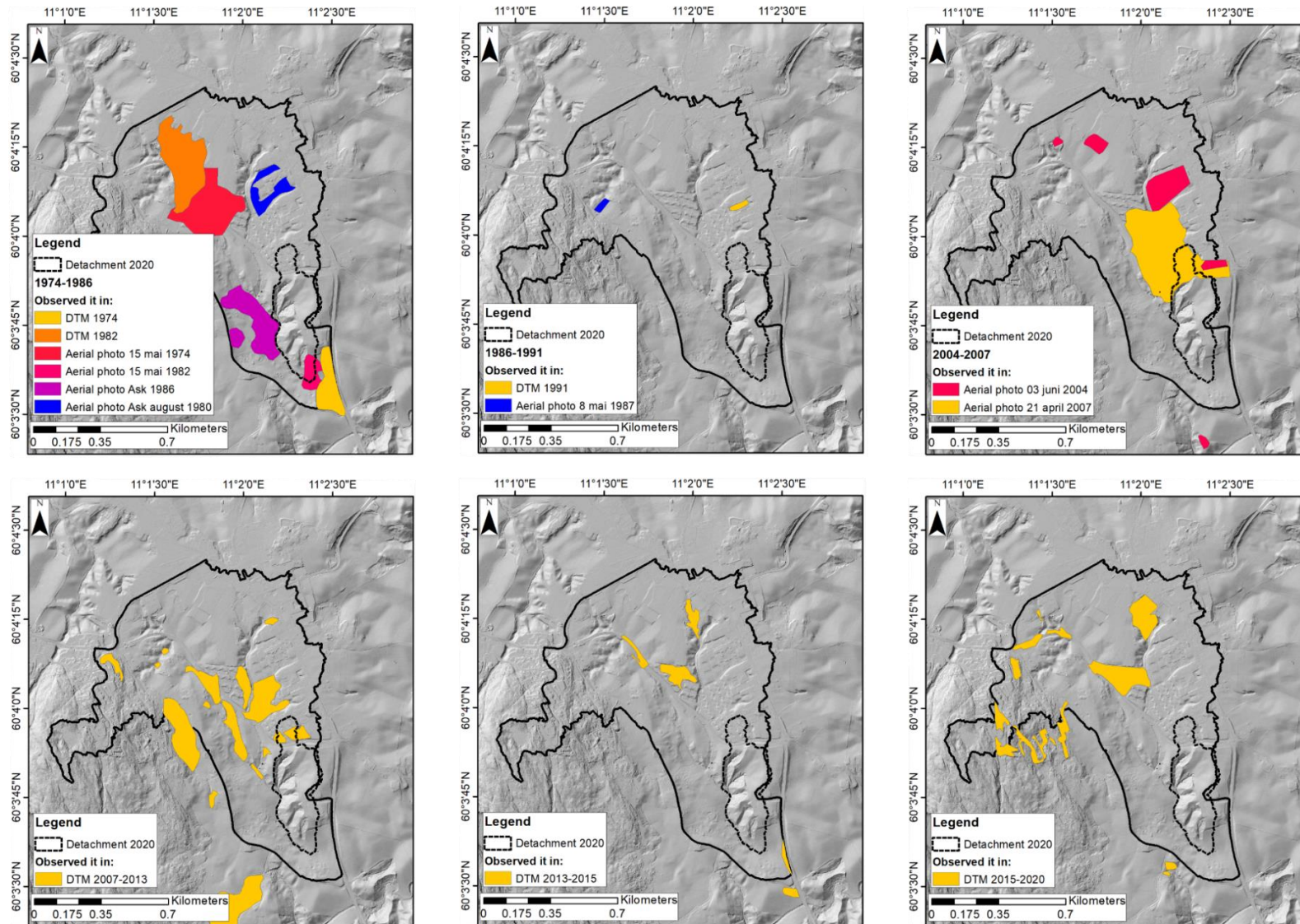


Figure 7. Areas with infill from 1974 to 2020. The background hillshade shows the 2020 topography. The black line corresponds to the limits of the 2020 watershed, the black dashed line corresponds to the detachment area of the 2020 landslide event.

Table 2. Evolution of surfaces covered by rooftops since 1969.

Year	Area covered by rooftops (m ²)
1969	18 715
1974	21 611
1991	30 876
2004	52 348
2007	58 877
2020	94 344

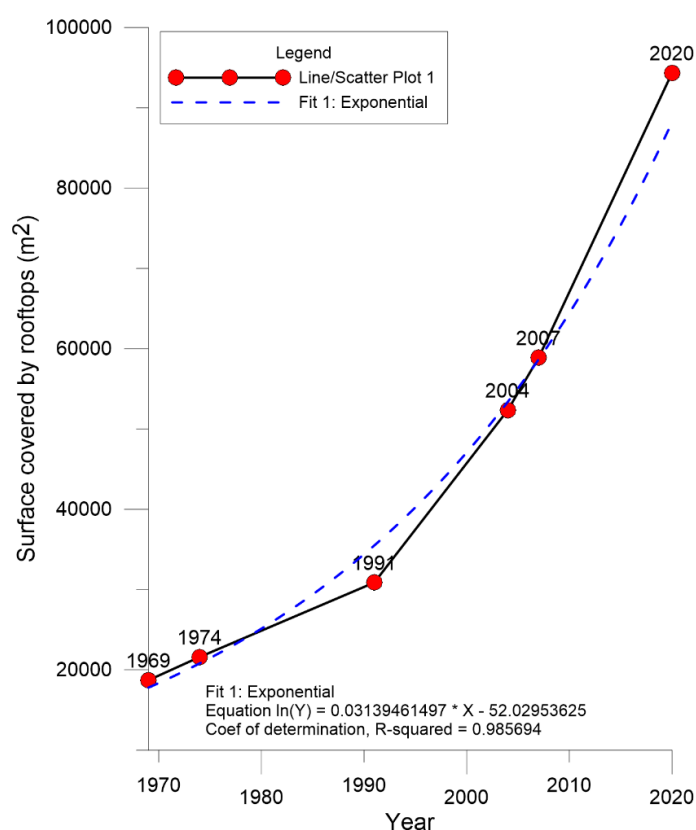


Figure 8. Surfaces covered by rooftops in time, for the area covered by the 2020 watershed.

As with the urbanisation through more buildings, we also see an expansion of the road network since the end of the 1960's. In 1969, the main existing roads were Byvegen (fv. 120), Brådalsvegen and Brådalsgutua (Figure 1). Between 1970 and 1974, parts of the path of Byvegen, close to its intersection with Brådalsvegen, were changed. Figure 9 shows that there were no significant changes between 1974 and 1991. However, after 2007 there was an increase in the development of the road network and the construction of houses. The main areas that were developed were Nystulia and Brådalsfjellet.

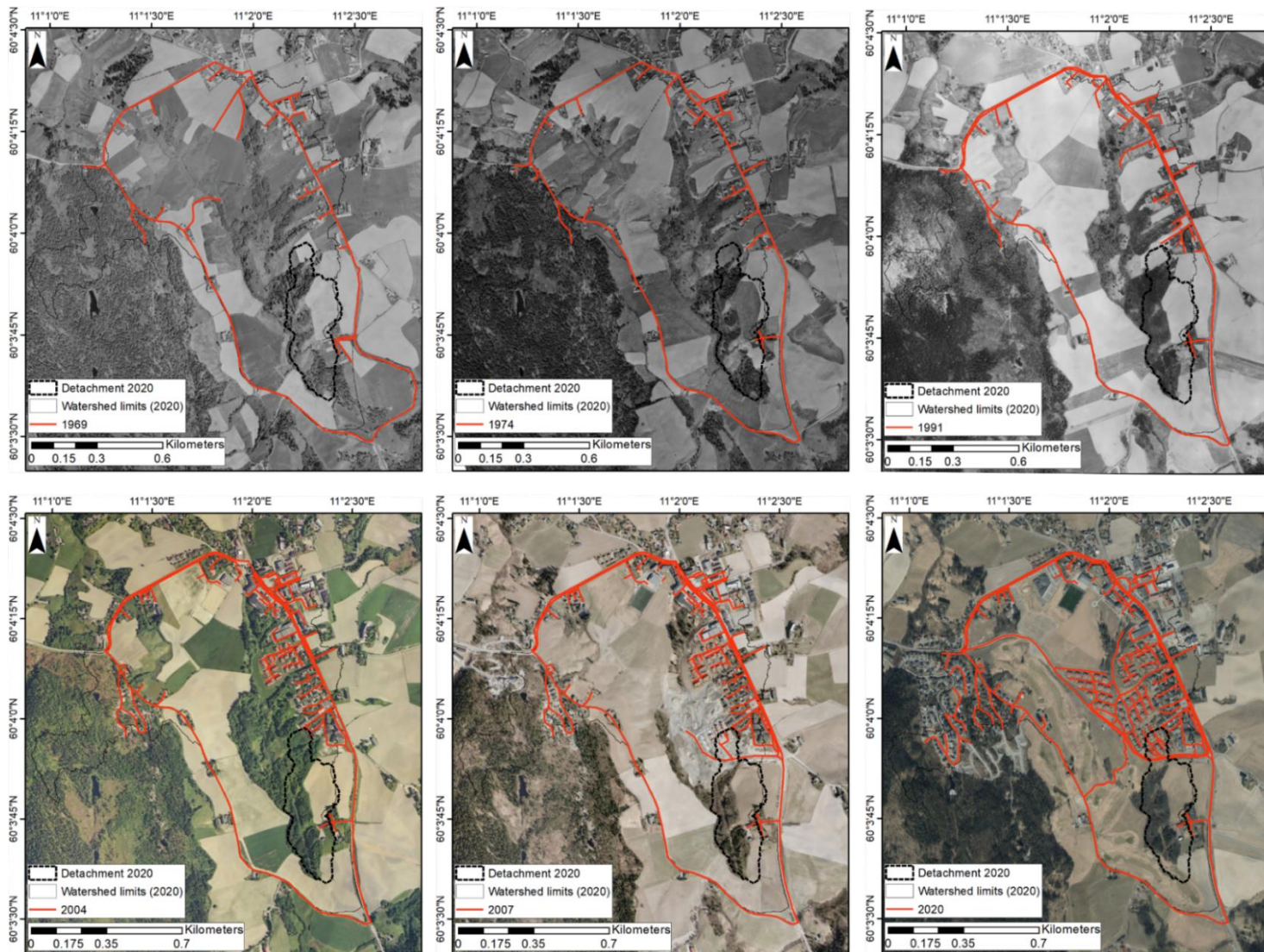


Figure 9. Development of roads between 1969 and 2020 for the area within the 2020 watershed.

7. Spatial and temporal distribution of landscape changes

Natural and anthropogenic-driven landscape changes can be accurately detected using repeated high-resolution DTMs. Comparing DTMs acquired at different times allows us to attain the DEMs of differences (DoD), representing those changes. In this chapter, we explore the landscape changes for the period 2007-2020 that were detected using airborne LiDAR DTMs (Kartverket 2021a). We present the location and magnitude (height difference) of those changes.

7.1 Methodology

We compared the DTM of 2013 to 2007, 2015 to 2013, and 2020 to 2015 (Table 3). The differences in DTMs heights were computed by subtracting rasters (new minus old) with the *Raster Calculator* tool from ArcMap. This tool computed the vertical differences of the overlapping rasters on a cell-by-cell basis.

Table 3. Airborne LiDAR DTMs used to determine surface changes in time.

Name and Year	Resolution (m)	Date of acquisition
Gjerdrum Ullensaker Nannestad 5 pkt 2020	0.25	19.04.2020
NDH Askerhus 2 pkt 2015	0.5	03.12.2015
Romeriksåsene 07 pkt 2013	1	06.07.2013
Romerike 07 pkt 2007	1	01.01.2007

To discriminate changes due to real surface changes from uncertainties associated with the elevation values of the DTMs, we analysed their accuracy and calculated the thresholds of detection. To determine the accuracy of the datasets, we used ground control points (GCP) provided by NVE. The points were measured with GPS Leica GS16 in April 2021. We calculated the height difference between each GCP and each LiDAR dataset, computed the mean MAE (mean average error) and the RMSE (root mean square error) for each dataset and the thresholds of detection for the periods 2007-2013, 2013-2015, and 2015-2020 (Table 4, Table 5 and Table 6).

Table 4. Measured differences in height between GCP and LiDAR datasets for seven different points in the Ask area.

ID	1	2	3	4	5	6	7
x	613213.3	613276.7	613416.7	613420.1	613448.4	613252.39	613213.81
y	6660052	6660203	6660528	6660531	6660450	6660512.08	6660464.93
GPS 2021	153.636	155.505	179.101	179.26	179.143	163.525	159.211
DTM 2020	153.5767	155.4721	179.1022	179.2705	179.0388	163.532791	159.248489
DTM 2015	153.4032	155.3108	178.9262	179.0574	178.8934	163.353561	159.121445

ID	1	2	3	4	5	6	7
DTM 2013	153.5592	155.5374	179.0769	179.2331	179.033	163.5614	159.2231
DTM 2007	153.6212	158.5188	179.1994	179.3417	177.1171	161.605392	158.262039
Dz2020 (m)	0.059317	0.032924	-0.0012	-0.01052	0.104243	-0.007791	-0.037489
Dz2015 (m)	0.232756	0.194209	0.174837	0.202642	0.249567	0.171439	0.089555
Dz2013 (m)	0.0768	-0.0324	0.0241	0.0269	0.11	-0.0364	-0.0121
Dz2007 (m)	0.014754	-3.01375	-0.09842	-0.08172	2.025874	1.919608	0.948961

Note: Dz-year: Difference in height between GCP and LiDAR. In red are we highlight the outliers.

Table 5. MAE and RMSE for the LiDAR datasets.

2007		2013		2015		2020	
Dz Min (m)	-0.098417	Min	-0.0364	Min	0.089555	Min	-0.037489
Dz Max (m)	0.948961	Max	0.11	Max	0.249567	Max	0.104243
MAE = δz	0.28596325	MAE	0.045529	MAE = δz	0.187857857	MAE = δz	0.036212886
RMSE	1.594136	RMSE	0.055836	RMSE	0.193914	RMSE	0.049349

Errors on DTMs can be propagated into DoD as (Brasington et al. 2003; Wheaton et al. 2010):

$$\delta(z) = \text{SQRT}((\delta z \text{ new dem}^2) + (\delta z \text{ old dem}^2))$$

Then, for this work the threshold of detection obtained from error propagation is the following (Table 6):

Table 6. Threshold of detection for the periods considered.

Period	Threshold (m)
2007-2013	0.29
2013-2015	0.19
2015-2020	0.19

Finally, we have done a conservative analysis and applied a 50 cm confidence threshold.

Slight differences observed between 2007-2013 and 2013-2015 correspond to densely vegetated areas. These differences can relate to height errors caused by the difficulty of the LiDAR pulse to penetrate vegetation and get the ground echo.

7.2 Results

The topography in Ask and adjacent areas has undergone several changes between 2007 and 2020. Most of them occurred between 2007 and 2013. Below we summarise the location of the main changes by period analysed:

- **2007-2013** (Figure 10A): The changes primarily extend from the upper-central part of Brådalsbekken down to the pond in the lower part of Tistilbekken. Soil removal occurred upstream from the confluence of Brådalsbekken and Tistilbekken, in the local drainage divide area (A.2). In addition, a depression located in Brådal, west of Brådalsvegen, was filled (A.1).
- **2013-2015** (Figure 10B): Some changes are observed in the upper and central part of Brådalsbekken (B.1) and south of Ask centre, where a ravine was filled.
- **2015-2020** (Figure 10C): Some changes are observed in the upper and central part of Brådalsbekken (C.1), in parts of Ask centre and in Brådalsfjellet.

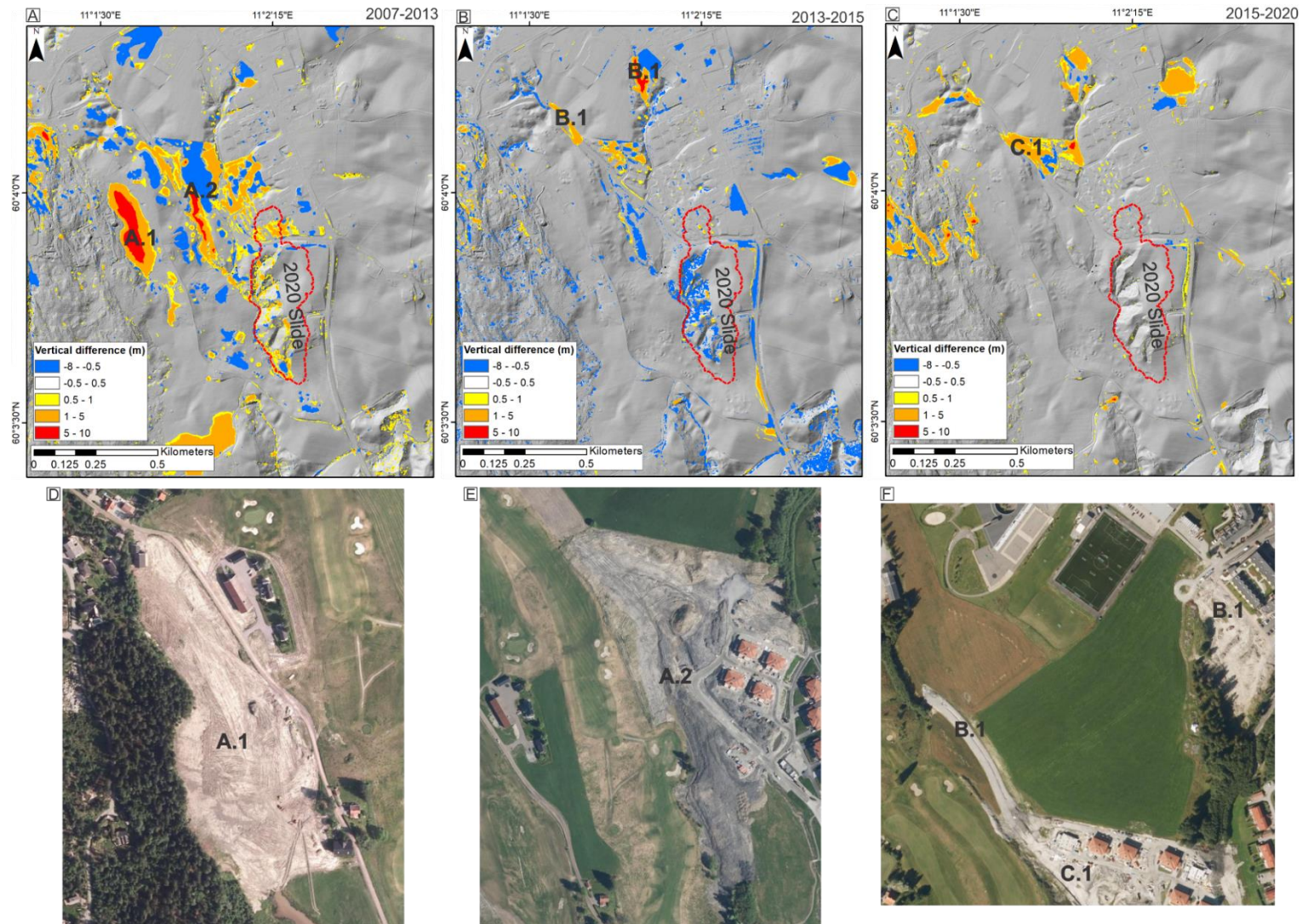


Figure 10. Spatial and temporal distribution of landscape changes in Ask and adjacent areas. For (A)-(C) the 2020 hillshade is used as background. (D) and (E): Orthophoto showing the changes in A.1 and A.2 (projects: D - Oslo 2011 and E - Romeriksåsene 2013). (F): Orthophoto showing the changes in B.1 and B.2 and point C.1 (project Oslo-Østlandet 2016). Note: Positive values correspond to infill and negative values to mass removal.

8. Land infill in Nystulia: terrain changes

In Nystulia, an old landslide scar and two ravines were filled after 2006 to develop a new urban area. Around 2007, houses were built in Nystulia and along nearby Fjellinna road. In this chapter, we present the terrain changes in the area of Nystulia and Fjellinna.

8.1 Methodology

To establish the magnitude of changes of the terrain in Nystulia, we compared a DTM produced from a photogrammetric model of 1991 made by COWI (see methodology in Appendix 2) with the DTM of 2020 derived from airborne LiDAR data (Kartverket 2021a). But before the comparison, we determined the accuracy of the 1991 DTM by using the location of ground control points (GCP; Figure 11). The GPs were dug in test pits by the Norwegian Geotechnical Institute (NGI) (Gregersen & Moholdt 2006). Then, we calculated the height difference between each GCP and the 1991 and the 2020 DTM. After that, the mean absolute error (MAE) and the root mean square error (RMSE) for each dataset was computed (Table 7).

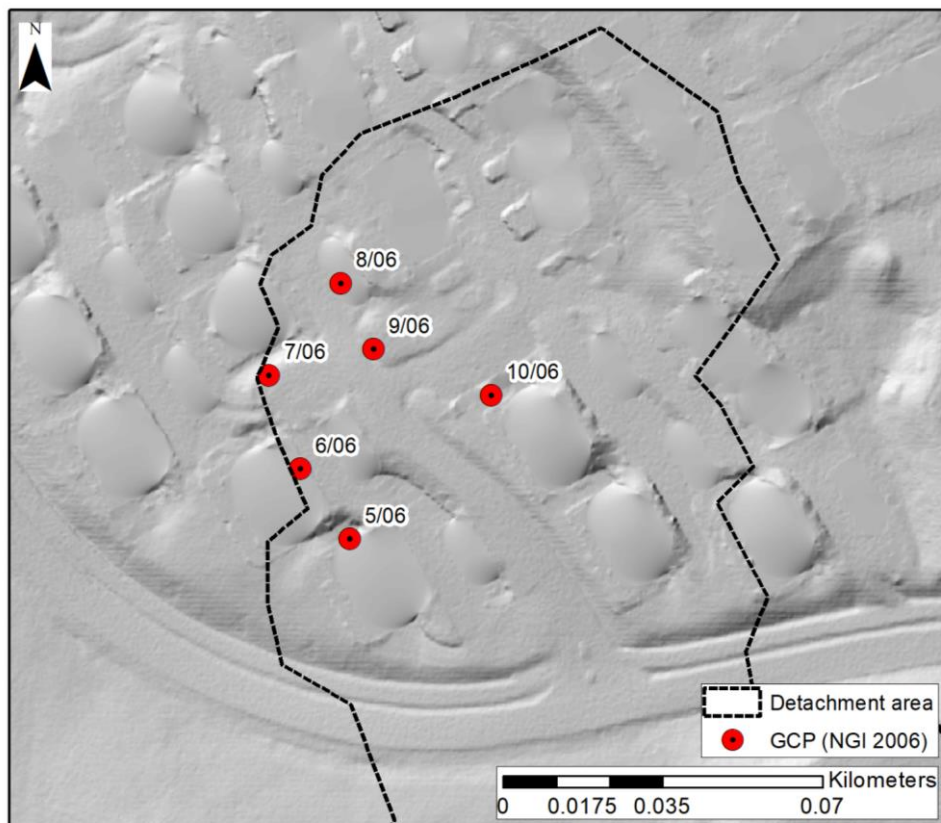


Figure 11. Location of GCP used for the analysis of the accuracy of the 1991 photogrammetric model in Nystulia area. Note: the labels of GCP points are the same as in the NGI report (Gregersen & Moholdt 2006).

Table 7. Control of accuracy for the 1991 photogrammetric model in Nystulia area.

ID	x	y	z (2006)	z (1991)	z (2020)	Dz (m) (1991-2006)	Dz (m) (1991-2020)	Dz (m) (2020-2006)
6/06	613319.5	6660404	163.137	163.02	166.6	0.117	3.58	3.463
5/06	613330.4	6660389	162.879	163.099	165.337	-0.22	2.238	2.458
7/06	613312.7	6660425	164.757	164.847	166.834	-0.09	1.987	2.077
8/06	613328.4	6660445	167.913	168.143	168.842	-0.23	0.699	0.929
9/06	613335.5	6660430	166.042	166.404	168.813	-0.362	2.409	2.771
10/06	613361.4	6660420	165.69	166.33	169.917	-0.64	3.587	4.227

Accuracy 1991	
Min Dz (m)	-0.64
Max Dz (m)	0.117
MAE	0.2765
RMSE	0.332599

8.2 Results

Figure 12 shows that in parts of the Nystulia area some mounds were lowered (sediments removal), and the ravines and the scar of a small landslide were filled.

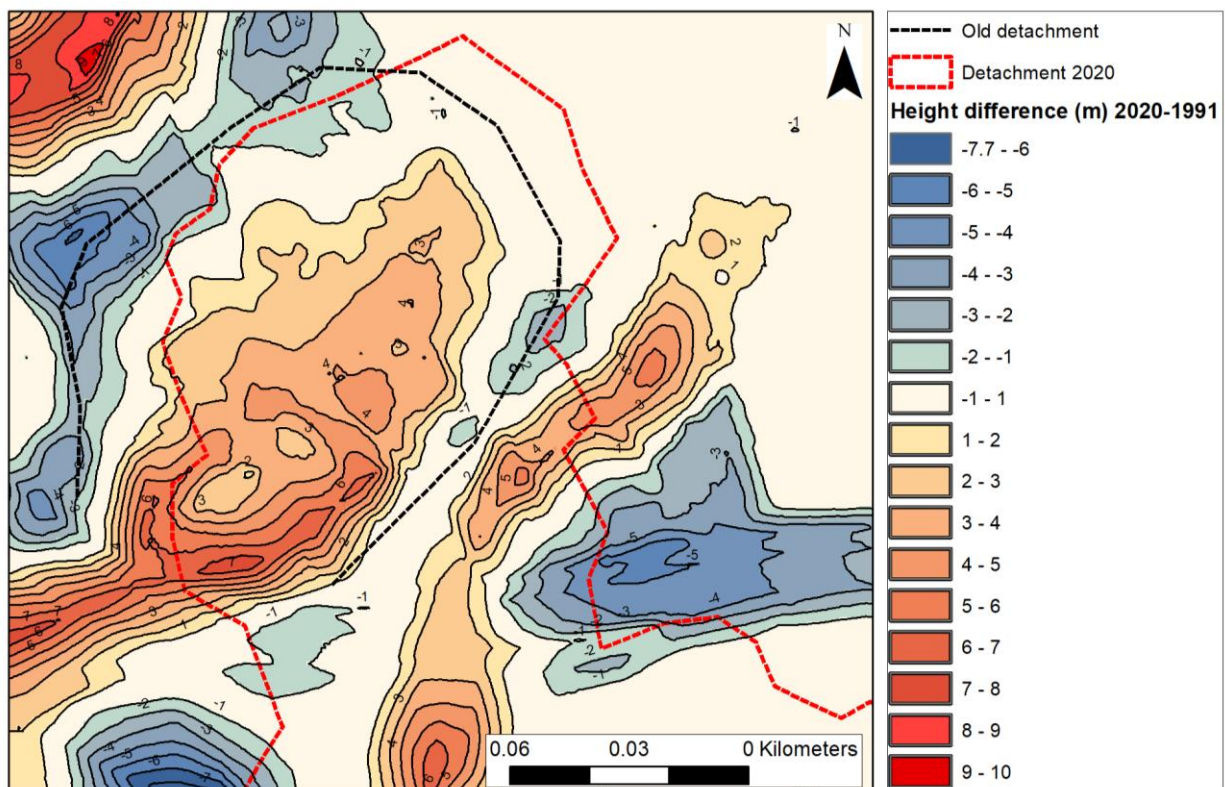


Figure 12. Land infill and removal in Nystulia area. Terrain models from 1991 and 2020 are compared.

9. Changes in forest cover

The loss of forested surfaces impacts watershed dynamics. It can increase surface runoff and stream discharges, which in turn can impact erosion rates. In this chapter, we study the changes in the forested surface in the watershed of Ask.

9.1 Methodology

The mapping of the forested areas was achieved using orthophotos from 1969 to 2020 (Table 8). The mapped areas correspond to sectors of the watershed with a high density of trees, excluding small patches of trees around houses or lines of trees along roads. The proportion of the area covered by forest is computed for the size of the watershed at the time of the datasets used (Table 8).

Table 8. List of datasets used for mapping the forest cover in time. The periods with a higher deforestation rate are highlighted (orange).

Project used for mapping	Forest coverage (km ²)	Watershed size (km ²)	Proportion of the watershed with forest cover
Ask Juli 1969	0.254	1.062	24 %
Ask 15 May 1974	0.242	1.062	23 %
Ask 29 May 1991	0.239	1.062	22 %
Gjerdrum 2004	0.214	1.062	20 %
Fet Gjerdrum 2007	0.134	1.062	13 %
Oslo 2011	0.132	1.062	12 %
Romeriksåsene 2013	0.12	1.062	11 %
Oslo-Øslandet 2016	0.13	1.126	12 %
Øvre Romerike 2020	0.115	1.126	10 %

9.2 Results

The forest cover decreased after 1969 by ca. 45 %. Most of its reduction occurred in the central part of the Brådalsbekken and Tistilbekken, and in Brådalsfjellet area (Figure 1 and Figure 13). The highest deforestation rate corresponds to the period 2004-2007 (Figure 14; Table 8). Between 1969-2004 (35 years) ca. 0.04 km² of forest were lost. In contrast, 0.08 km² were lost between 2004 and 2007, which means deforestation was 20 times faster than in 1969-2004. The apparent increase in the proportion of the watershed (catchment area) with forest cover between 2013 and 2016 owes to the increase in the size of the watershed in the Brådalsfjellet area (see chapter 11).

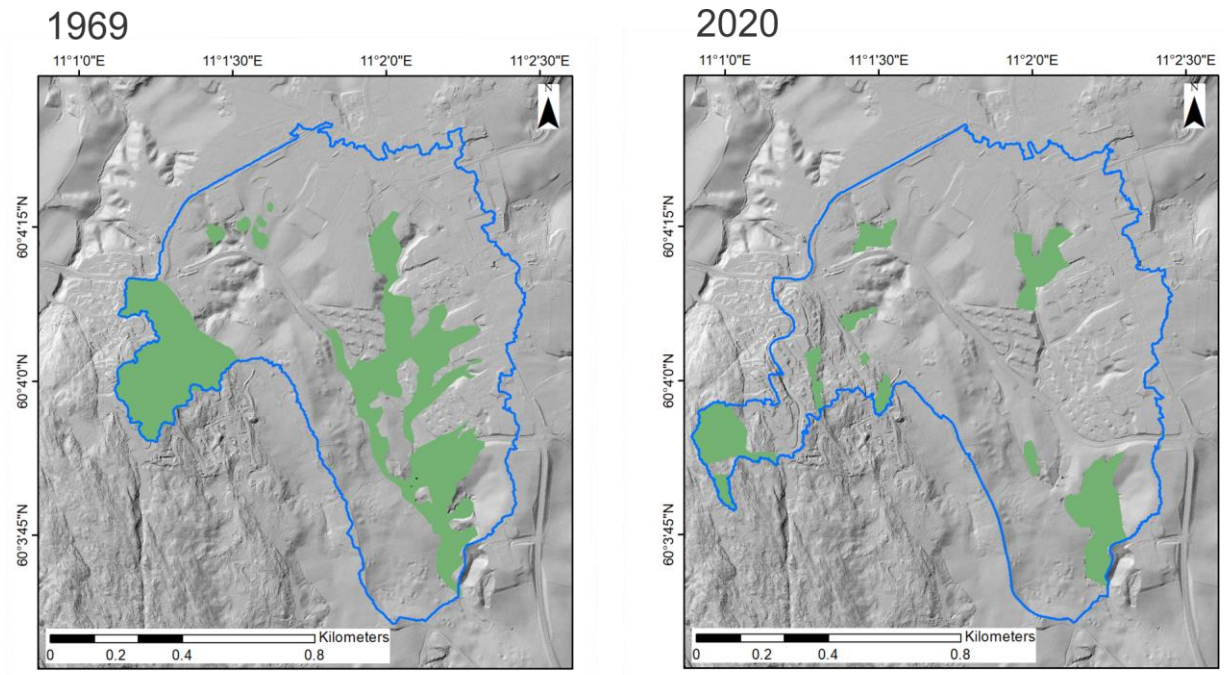


Figure 13. Forest coverage for 1969 and 2020. The blue lines correspond to the area draining upstream from the pond, mapped using the 2007 and 2020 DTMs. Appendix 3 contains the maps for the periods not included in this figure.

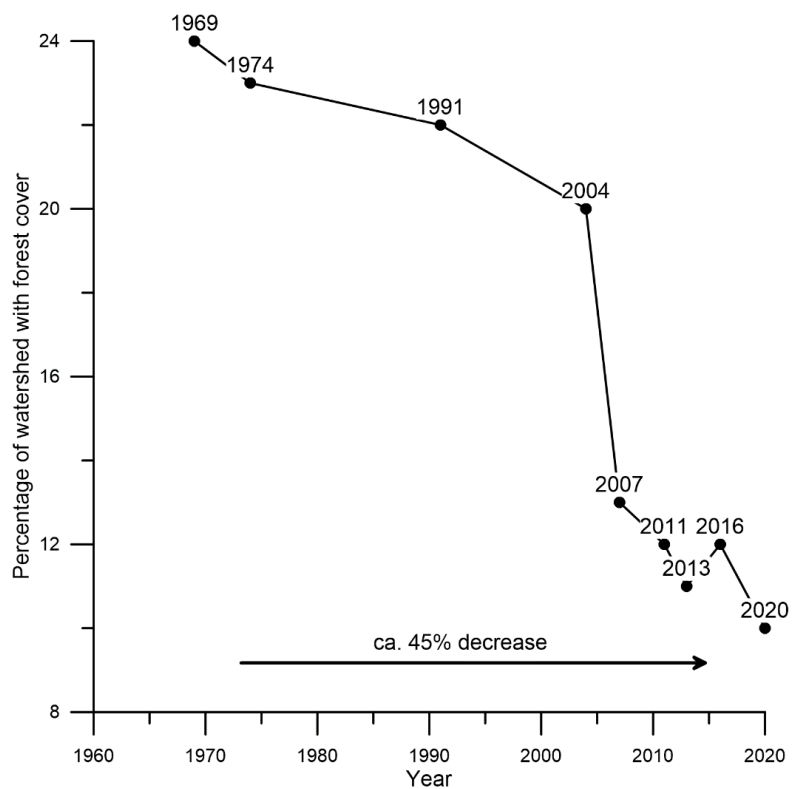


Figure 14. Evolution of the forest cover in time-based on mapping of orthophotos.

10. Land infill in Holmen: Volume calculation

In the western part of Holmen, land infilling increased stepwise since the 1970's, as shown on aerial photos from the area (Kartverket 2021b). Infilling has also taken place after 2007, and LiDAR data is therefore used to calculate the volume of the infill after this year.

10.1 Methodology

A cloud-to-mesh (C2M) analysis was done using the Cloud Compare software to determine the volume of the land infill in the Holmen area between 2007 and 2020, following the procedure represented in chapter 15 (Figure 31A). We used as input data the 2007 and 2020 LiDAR point clouds.

The C2M comparison was carried out using the 2020-point cloud as reference (mesh), and the 2007 as compared point cloud. From the comparison we obtained a point cloud with height differences (Figure 15). Then, we used the *IDW* interpolation tool from ArcMap to produce a 50 cm resolution raster of height differences. With this raster, the infill volume for the period 2007-2020 was computed as the sum of the height differences, multiplied by the area of a single pixel.

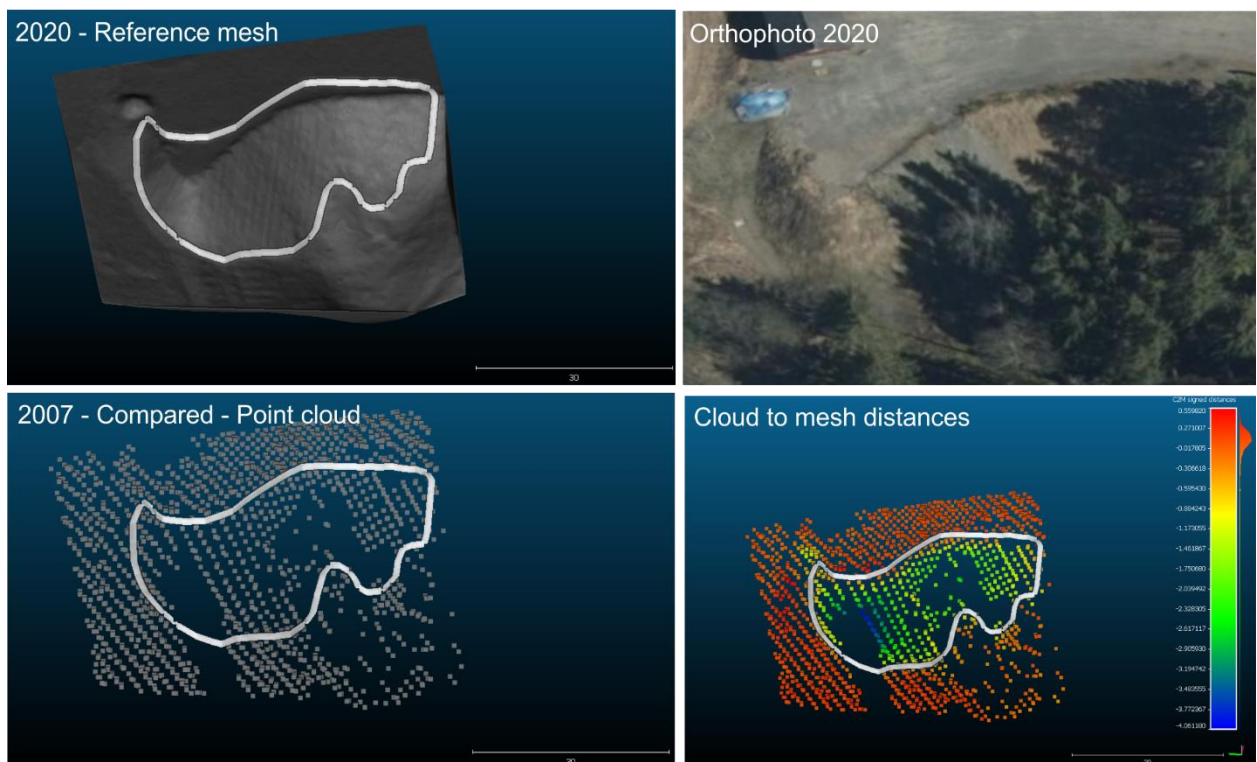


Figure 15. Computation of cloud-to-mesh distances for Holmen area.

10.2 Results

Holmen is located in the lower section of Tistilbekken, in the catchment area of a small tributary (Figure 1). The comparison of LiDAR datasets allowed us to detect a volumetric

change of ca. 1200 m³ (Figure 16A). The volumetric increase occurred mainly between 2007 and 2015 (Figure 16B).

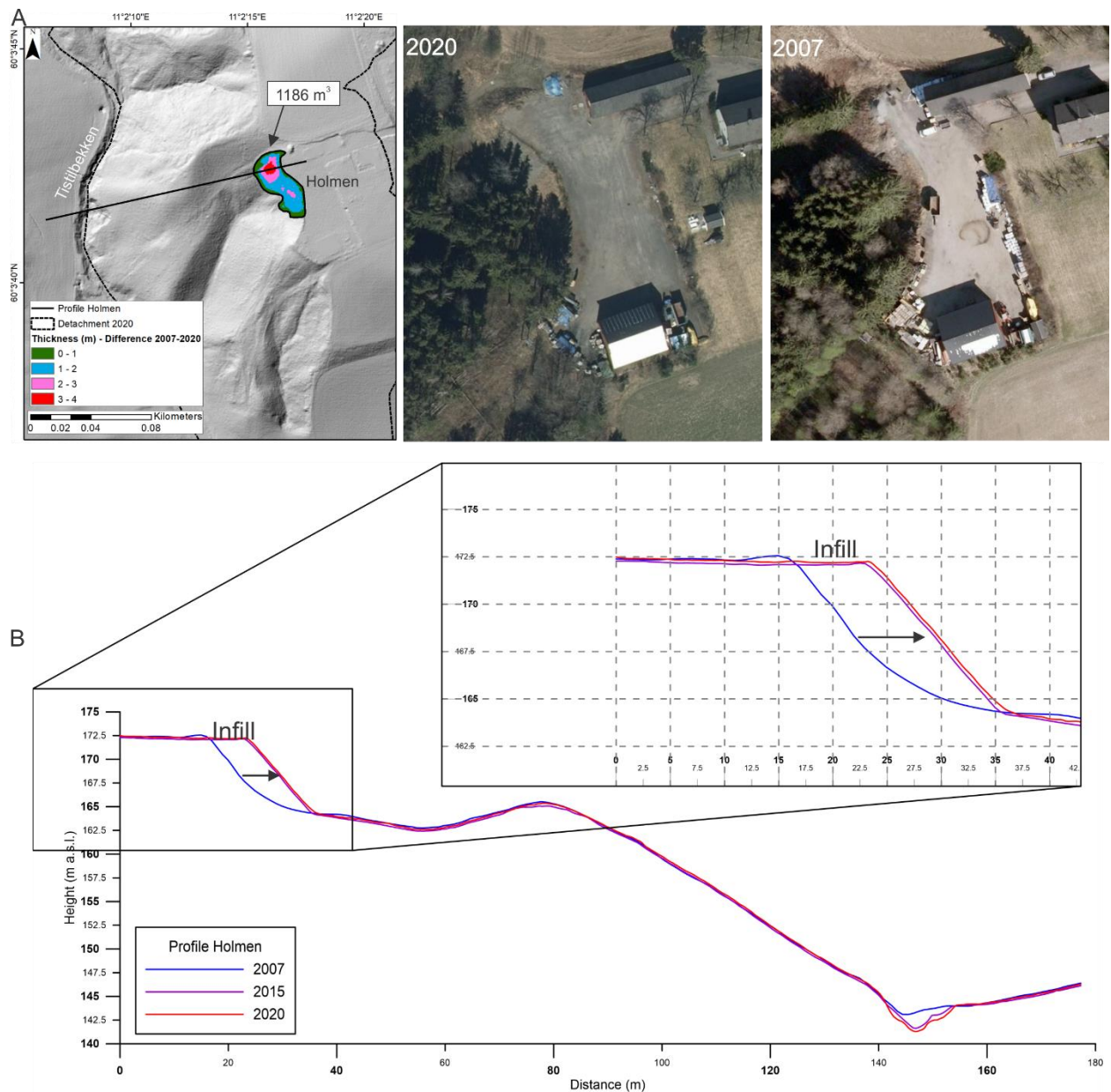


Figure 16. (A) Hillshade with thickness map of the land infill and aerial photos of the area from 2007 and 2020. (B) Profile showing the differences between the 2007 and the 2020 topography.

11. Watershed extension in time

The size changes of a watershed (catchment area) over time may be caused by natural or anthropogenic processes. Urbanisation is a major driver of change, by re-shaping surfaces and creating impervious surfaces by constructing roads, rooftops, parking areas, etc. (O'Driscoll et al. 2010).

High-resolution digital elevation models are key inputs for the automatic detection of a watershed's limits and the determination of changes. The automatically detected limits are dependent on the resolution of the DTMs. If a temporal analysis is done and changes in watershed extent are observed, it is essential to determine the magnitude of changes driven by real surface changes from those owing to different resolution of DTMs used for the watershed delimitation. In this chapter, we establish the extent of the Ask watershed in 2007 and 2020 and analyse the controlling factors of the observed differences. It must be pointed out that our analysis does not include the sewage systems but only topographic conditions.

11.1 Methodology

The watersheds (catchment areas) for 2007 and 2020 were automatically detected using the *Watershed* tool of ArcMap. This tool uses as input data: 1) Flow direction (the direction of flow out of each cell composing a DTM), 2) Flow accumulation (accumulated flow to each cell of a raster), and 3) An outlet (or pour point) corresponds to the lowest point of a watershed to be delineated. The watershed is determined as the upslope area contributing to flow to a defined outlet or pour point. In this study, the pour point was placed close to the interception between Byvegen and Brådalsvegen. The limits of the watershed were calculated using the *D8 method*, which models the flow direction from each cell to its steepest downslope neighbour.

Once the watershed areas had been determined, we investigated the origin of the detected differences. For this, we did three different computations: 1) differences in watershed extent for 2020 and 2007 at 1 m, 50 cm and 25 cm resolution; 2) differences in watershed extent between 2007 and 2020 at 1m, 50 cm, and 25 cm resolution each, and 3) differences in watershed extent using 1 m resolution for 2007 and 25 cm resolution for 2020.

The comparison of the areas was made using the *Symmetrical Difference* tool in ArcMap, a tool that can compute the geometric intersection of two polygons, identifying the areas that do not overlap. The output of the *Symmetrical Difference* is a multipart feature which was then separated into a singlepart feature with the *Multi to Singlepart* tool.

11.2 Results

The watershed for 2007 and 2020 measure ca. 1 171 000 m² and ca. 1 234 000 m², respectively.

When comparing the watershed extent for the same year but at different resolutions, the biggest polygon representing a difference measures ca. 4300 m² (Figure 17). For 2007, the sum of all the polygons representing differences in watershed extent between 1 m and 50 cm resolution is ca. 8500 m², and between 50 cm and 25 cm resolution, the sum is ca. 380 m². For 2020, the sum of differences in watershed extent between 1 m and 50 cm resolution is ca. 14 400 m² and between 50 cm and 25 cm it is ca. 4760 m².

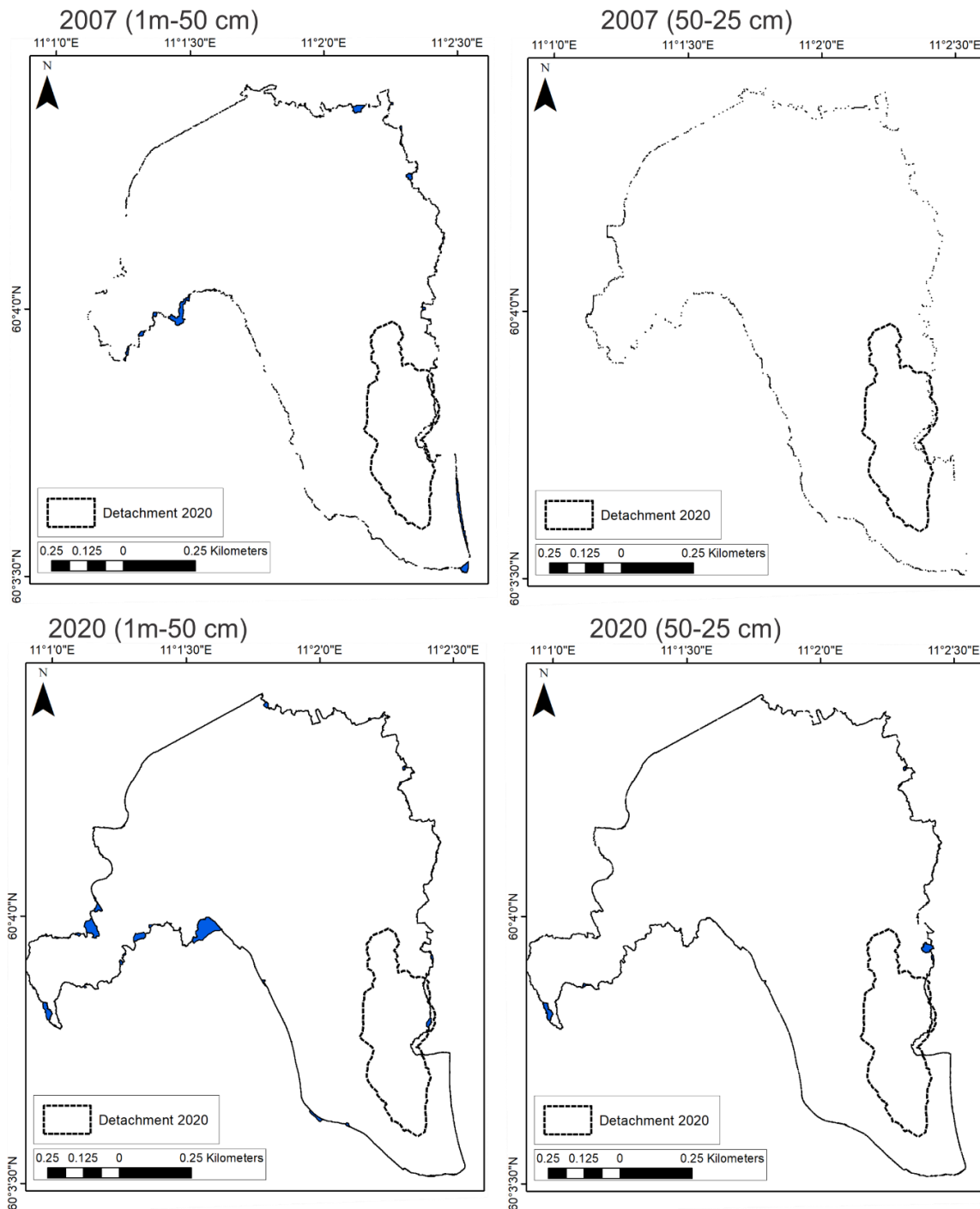


Figure 17. Differences in watershed extension computed for 2007 and 2020 at different resolution each. The blue polygons correspond to significant differences in the limits of the watershed. The apparent line delimiting the watershed is composed of several small polygons representing differences in the limits of the watershed.

When comparing the datasets of 2020 and 2007 the observed differences are up to ca. 53 000 m² (Figure 18). And the sum of differences is ca. 10 times higher than for same years at different resolutions. With both datasets at 1 m resolution the difference in watershed extent is 127 833 m², at 50 cm is 130 456 m², at 25 cm is 130 315 m² and using the original resolution of the dataset the difference is 125 162 m².

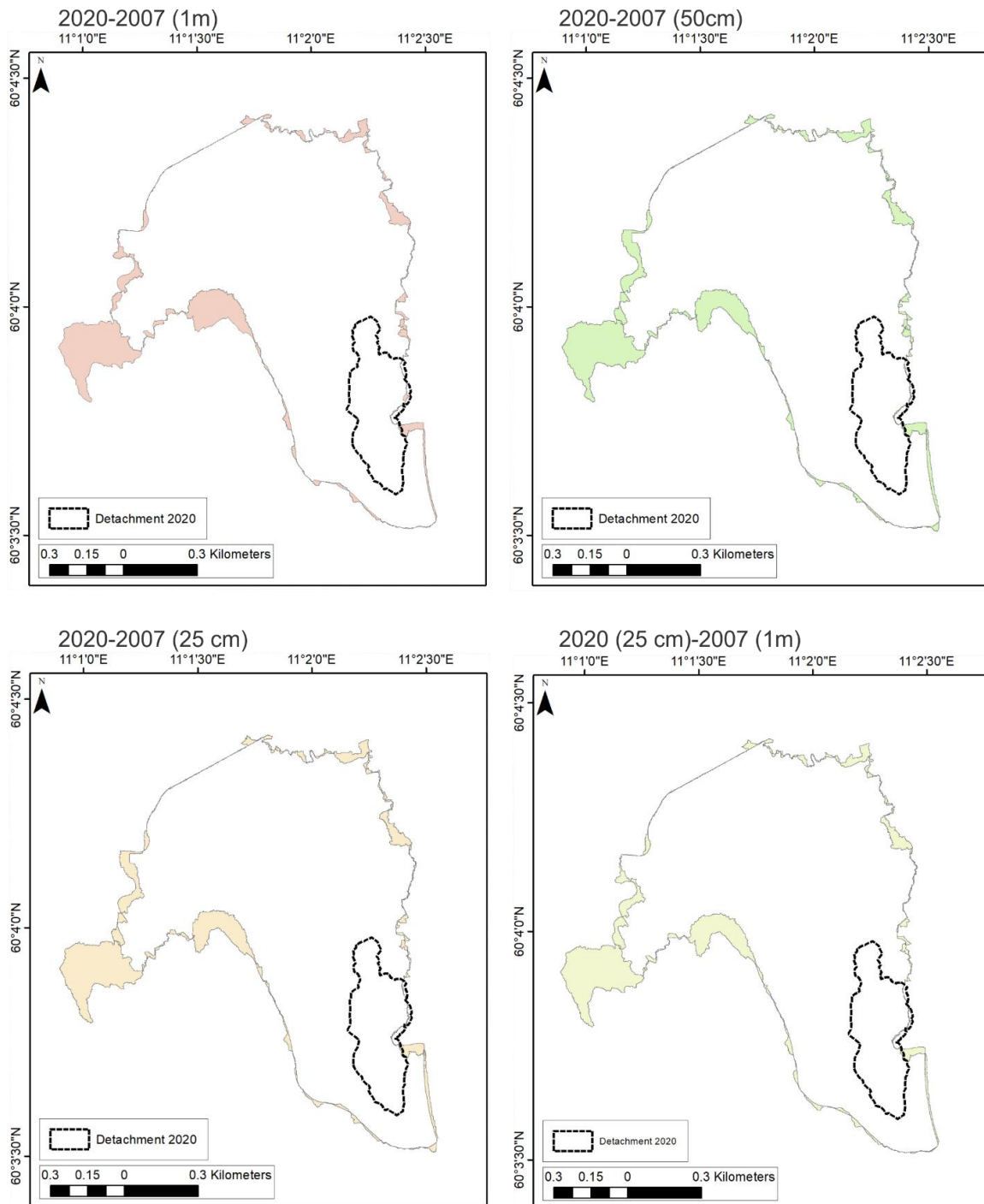


Figure 18. Differences in watershed extension computed across years.

Our results show that changes caused by DTM resolution are minor, and that major changes in Ask watershed relate to landscape changes (Figure 19).

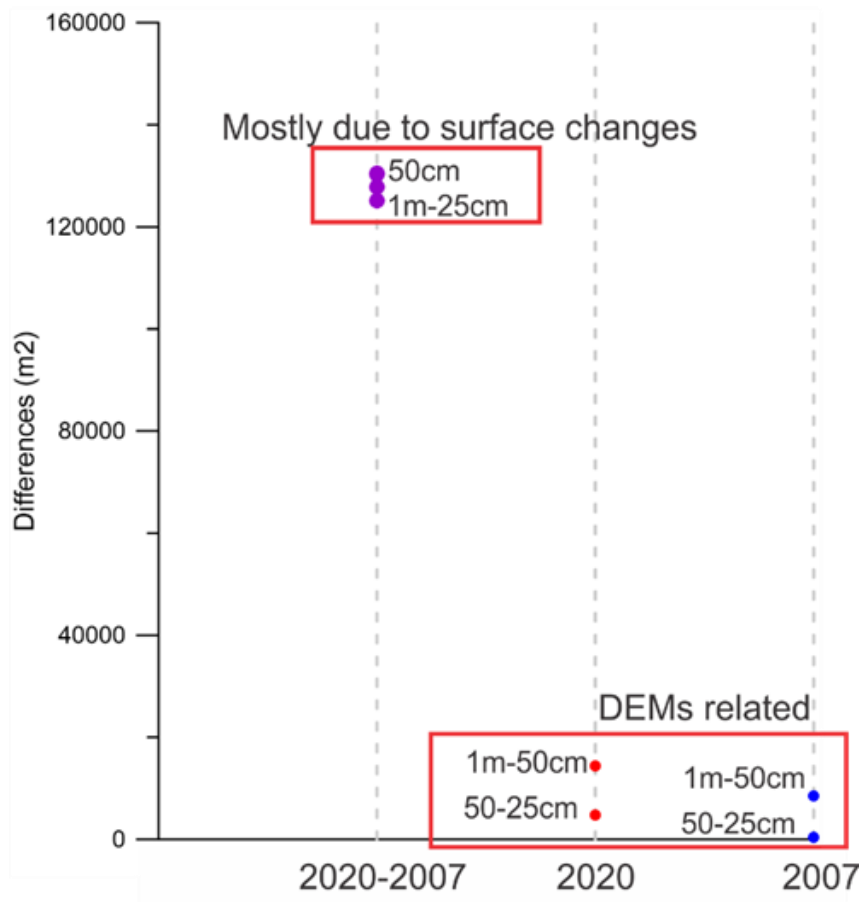


Figure 19. Magnitude of differences depending on the controlling factor.

When we used the area of 2007 as reference, we could identify which sectors increased the extent of the watershed between 2007 and 2020, and which sectors decreased it (Figure 20A). With a 29 210 m² decrease and a 92 860 m² increase, the net increase is 63 650 m². Two main areas changed: one is on the western side of Brådalsvegen where a depression (old ravine) was filled in 2011 (Figure 20B and Figure 10A). The other is in Brådalsfjellet where urbanisation took place and the construction of a road in 2015/2016 seems to have changed the location of the drainage divide (Figure 20C).

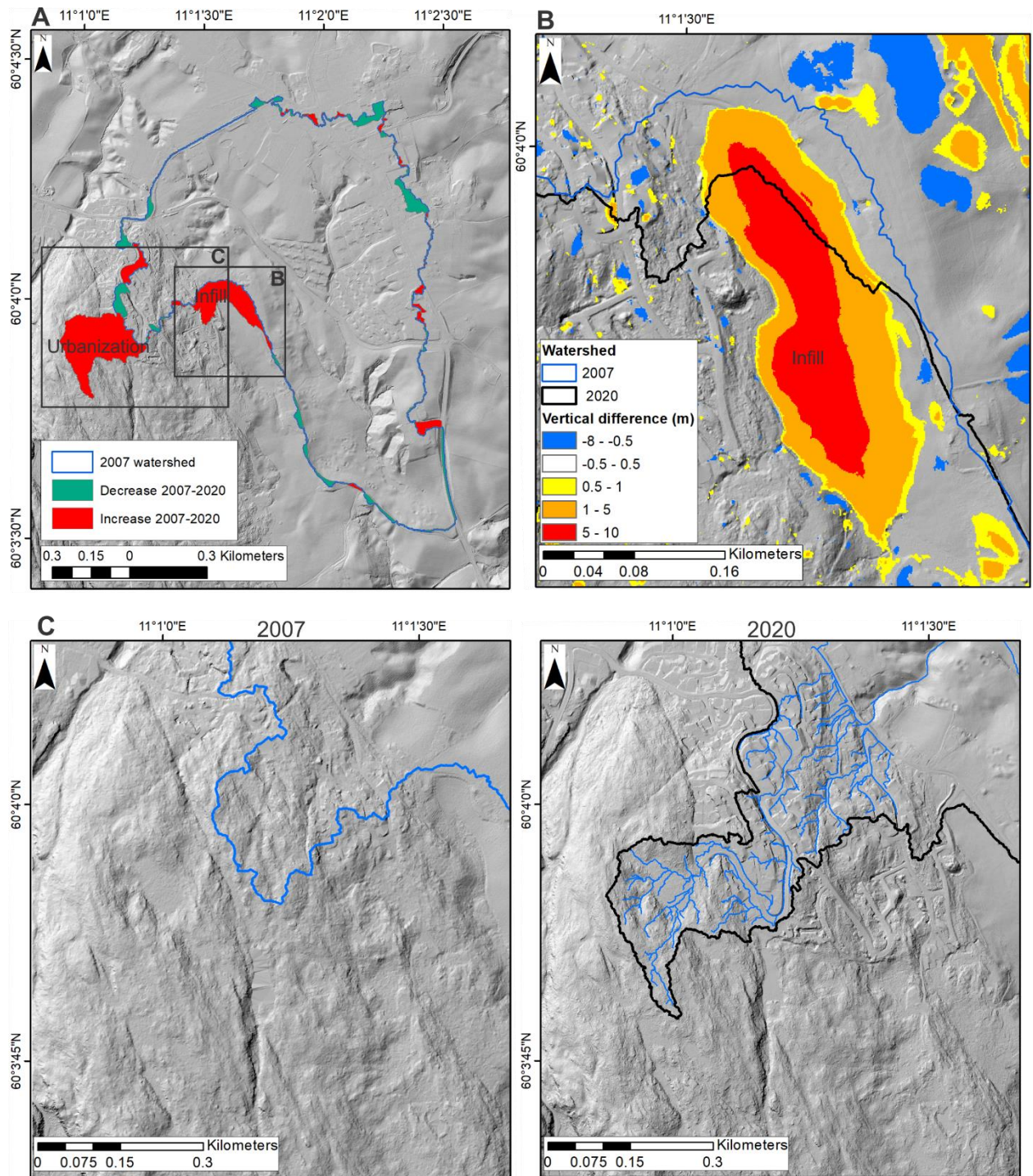


Figure 20. A) Zones showing increase and decrease in watershed extent considering the limits of the 2007 watershed as a reference. B) Map showing the thickness of land infill west of Brådalsvegen and the 2007 and 2020 watershed limits. C) 2007 and 2020 hillshade maps showing the limits of the watershed for those years. The 2020 map shows the drainage network developed on the urbanised area.

12. Changes in the stream path of Brådalsbekken-Tistilbekken

Fluvial courses can change their path naturally or induced by human activities. In this chapter, we explore the timing and the potential drivers of changes of Brådalsbekken-Tistilbekken.

12.1 Methodology

The path of Brådalsbekken-Tistilbekken (Figure 1) has been mapped using historical aerial photos and LiDAR DTMs (Table 9).

Table 9. List of datasets used for mapping the path of Brådalsbekken-Tistilbekken

Project	Type of data
Ask 1953	Orthophoto
Ask 1955	Orthophoto
Ask 1960	Orthophoto
Ask Juli 1969	Orthophoto
Ask 16 mai 1974	Orthophoto
Ask 1976	Orthophoto
Ask 15 mai 1982	Orthophoto
Ask 1986	Orthophoto
Nittedal - Skedsmo - Fet - Sørumsund 1986	Orthophoto
Ask 17 mai 1986	Orthophoto
Ask 1993	Orthophoto
Romerike 07 pkt 2007	Airborne LIDAR
Øvre Romerike 2012	Orthophoto
NDH Askerhus 2 pkt 2015	Airborne LIDAR
Gjerdrum Ullensaker Nannestad 5 pkt 2020	Airborne LIDAR

The 2020 path was used as a reference to determine whether the creek has migrated in time. The *Euclidean Distance* tool from ArcMap allowed us to produce, on a buffer of 20 m, a raster with distance from the 2020 creek path. In the Euclidean distance raster, positive values were assigned on the west side of the creek, and negative values on the east side (Figure 21).

Each mapped line representing the creek at a particular time was converted into points with 0.2 m as a fixed interval with the *Generate Points along Lines* tool from ArcMap. The points were then interpolated with the Euclidean distance raster (*Extract value to points* tool from ArcMap) to get the points' distance to the 2020 river.

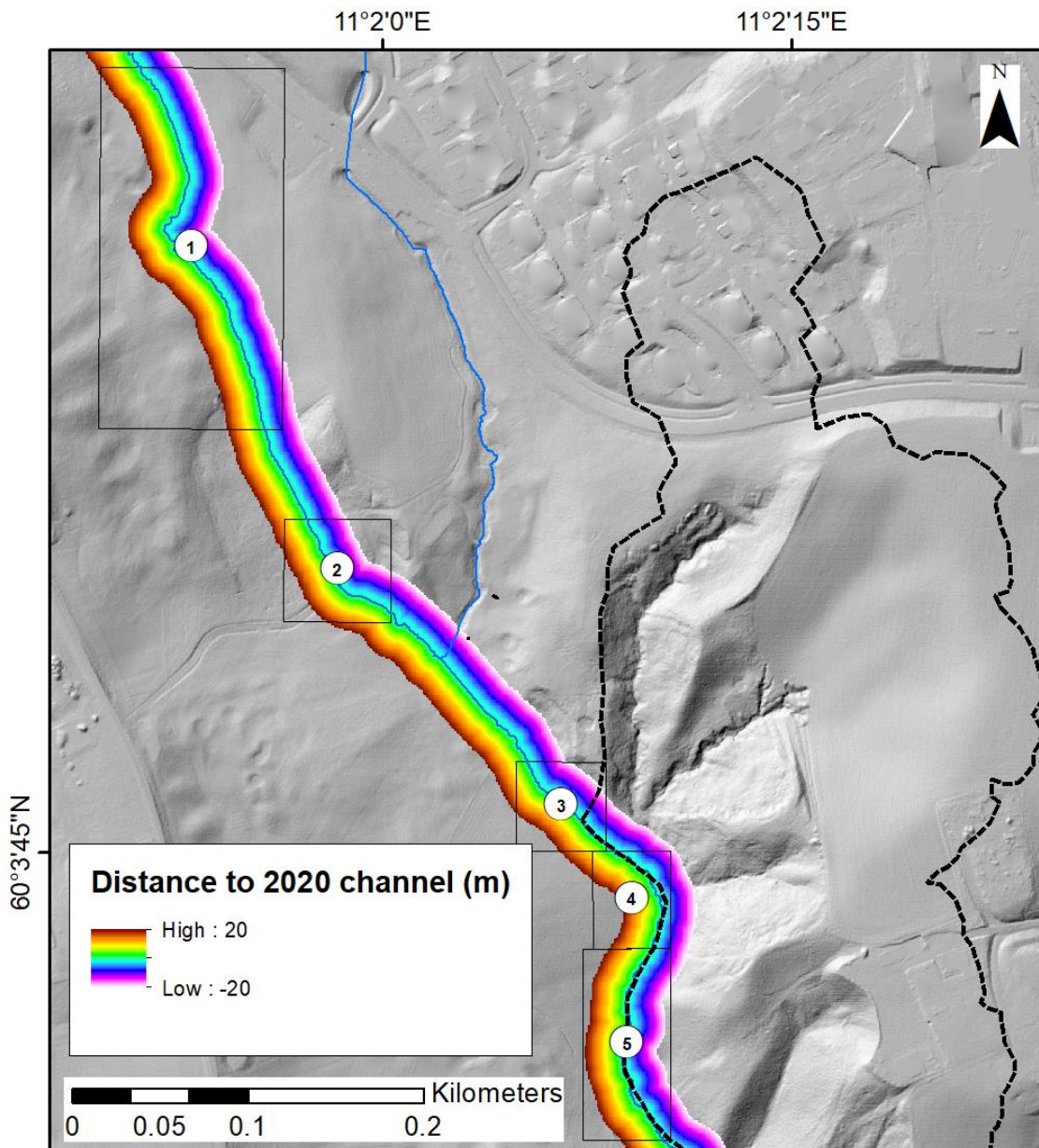


Figure 21. Euclidean distance along the path of the main creek.

Figure 22 summarises the methodology used to establish distance to the 2020 path.

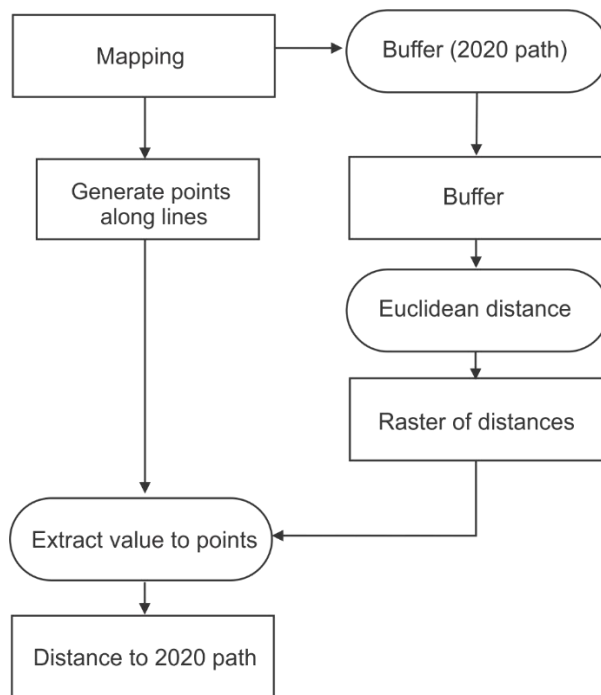


Figure 22. Scheme showing the methodology used to determine the distance between past creek path and the 2020 path.

Detailed analyses have been done in 5 Areas of Interest (AOI). The histograms showing the distribution of distances at each area can be seen in Appendix 4.

12.2 Results

Our analysis show sections both with significant and without changes. Some of the significant changes coincide with places where human activities e.g. land infill have altered the path.

We summarise the main changes in the Areas of Interest (AOI) 1-5 in Figure 23:

- AOI_1: No significant changes are observed for the period 1974-2007. The main change here occurred between 2007 and 2015, when construction activities induced the change, displacing the creek towards the west.
- AOI_2: No significant changes are observed between 1969 and 2020.
- AOI_3: The path in 1974 locates east of the 2020 path.
- AOI_4: The path of 1986 locates west of the 2020 path. This means the path became closer to the slope where the landslide occurred (migration to the east).
- AOI_5: Since 1969, the distance of the creek and the 2020 path gets shorter. This means the path is reaching closer to the slope where the landslide occurred (migration to the east).

See Figure 24 and Figure 25 for details about the areas 1-5.

The highest displacement for areas 4 and 5 seems to have occurred between May 1986 and 1993. Aerial photos show a land infill made in this section of Tistilbekken between May and November 1986. This area, and area 1, are those showing the most significant changes in the path of the creek.

Errors in the orthorectification can produce differences between the real and the mapped creek path at a certain time. However, errors in orthorectification cannot explain several meters of displacement for projects that have passed the quality test as those used in this work. In AOI 5, the horizontal distance between the May 1986 and the 2020 path is above 6 m. COWI (2018) estimated an error on X of 0.14 m and Y of 0.18 m for the orthophoto Nittedal-Skedsmo-Fet-Sørsum in May 1986.

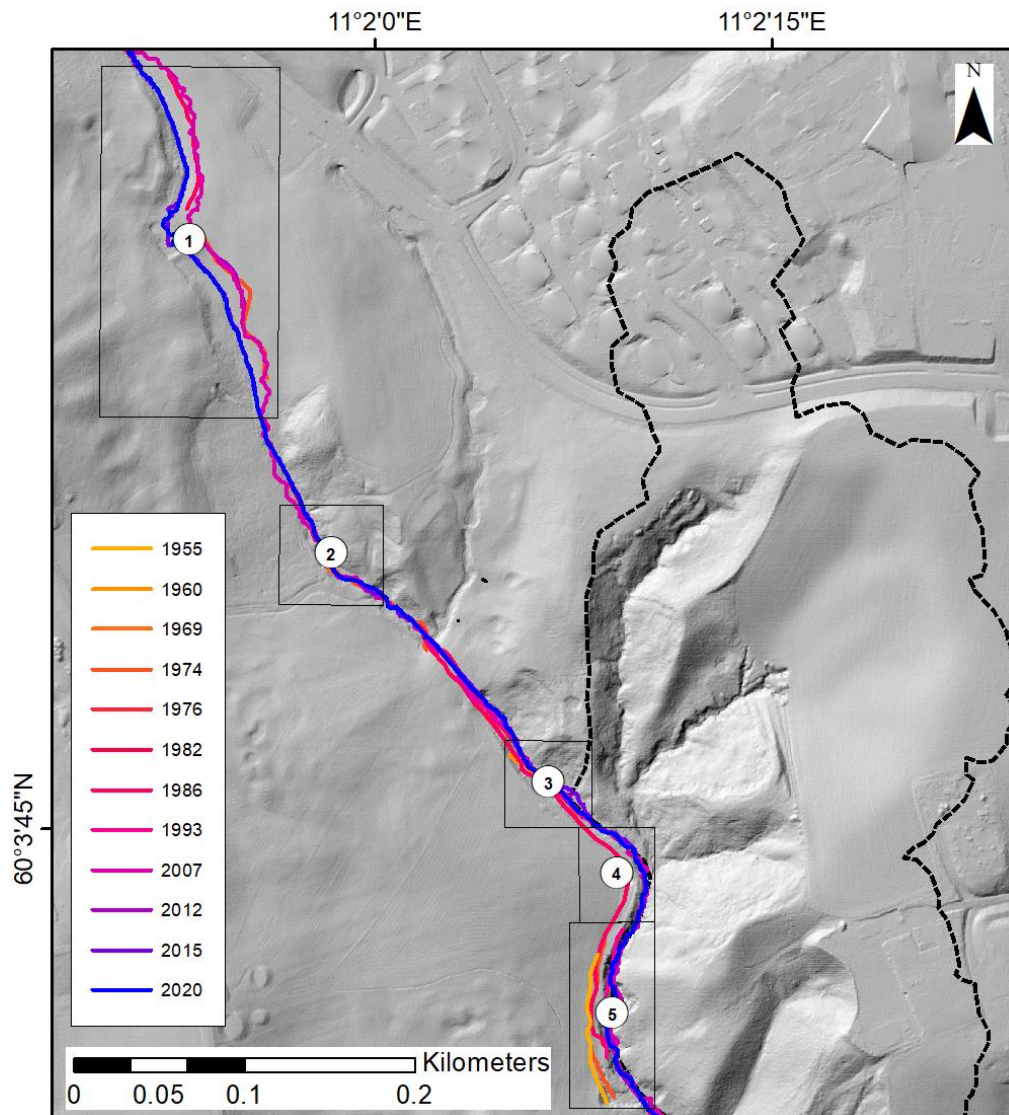
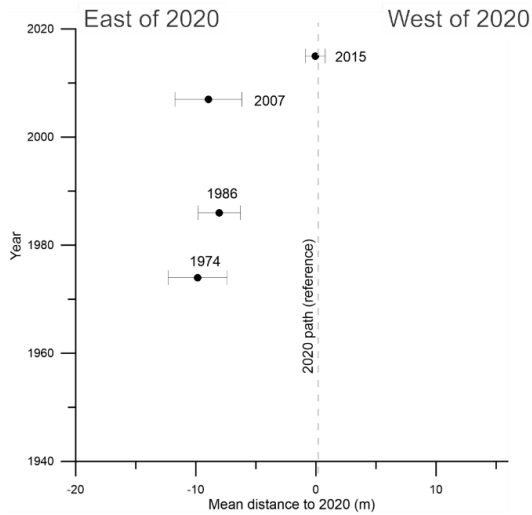
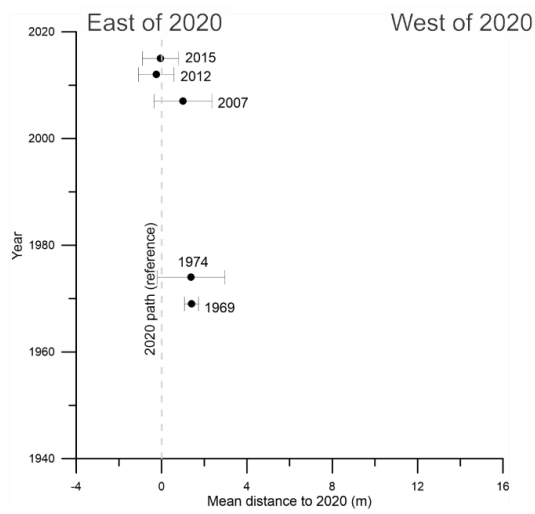


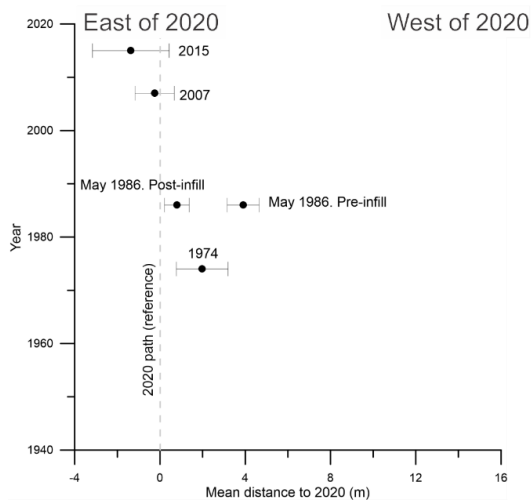
Figure 23. Hillshade map with the Brådalsbekken-Tistilbekken course at different times. Black polygons represent areas where more detailed analyses were done. Note: lines are discontinuous for the years where orthophotos were used. Vegetation coverage, or in some cases the quality of the photos, was not good enough to be used for the correct location of the creek.



AOI_1	Rate (m/y)
1974-1986	0.15
1986-2007	0.04
2007-2015	0.68
2015-2020	0



AOI_2	Rate (m/y)
1969-1974	0
1974-2007	0.01
2007-2012	0.25
2012-2015	0.07
2015-2020	0



AOI_3	Rate (m/y)
1974-May 1986	0.16
May 1986-Nov. 1986	6.3
Nov 1986-2007	0.05
2007-2015	0.13
2015-2020	0.27

Figure 24. Migration of Brådalsbekken-Tistilbekken for areas 1 to 3 (Figure 23). Graphs showing the mean distance of the paths compared to the 2020 creek at different times and migration rates.

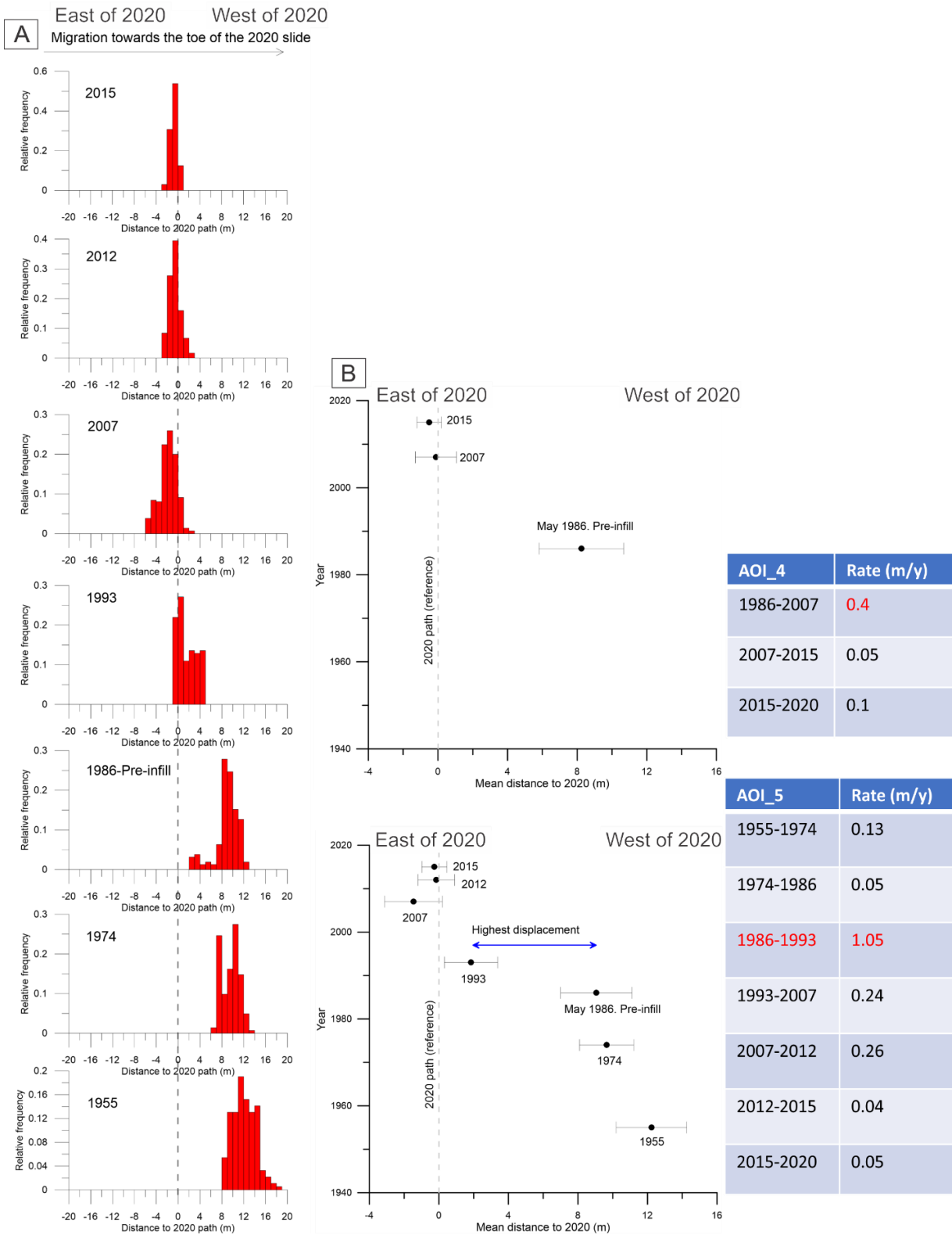


Figure 25. Migration of Brådalsbekken-Tistilbekken for the areas 4 and 5 (Figure 23). (A) Histogram showing the distribution of points representing the location of the creek for the at different times. (B) Graphs showing mean distance of the paths compared to the 2020 creek at different times and migration rates.

13. Changes in the long profile of the Brådalsbekken and Tistilbekken

The long profile of Brådalsbekken and Tistilbekken have changed with time, mainly driven by human activities such as land infill. In this section we show the changes corresponding to the period 2007 and 2020. Figure 26 shows which parts of Brådalsbekken and Tistilbekken were analysed.

13.1 Methodology

The creeks paths were delineated using the 2007 and 2020 DTMs. This required as a first step the computation of flow direction and flow accumulation with the *Hydrology* toolbox from ArcMap. Then, the lines representing the creek path were simplified using the *Simplify Line* tool in ArcMap (*Bend Simplify*, 5 m tolerance). The lines representing the creeks were then divided with sample points (locations at which the information will be collected) with 1 m spacing. The coordinates of each sample point were calculated using the *Interpolate Function* of Shapely (a Python library; Gillies 2020).

For the 2007 line, the coordinates of the sample points are then projected on the 2020 line using the *Project* function of Shapely (Gillies 2020). Thus, the distances used on the graphs correspond to the 2020 line, while the attributes of the sample points are defined using their original position.

The altitude of the sample points is interpolated from the DEM using *the interpolate.griddata function* of SciPy and a linear model (The SciPy community, 2021).

To compute the slope, knickpoints have been manually defined and a linear regression performed using all the sampling points between the knickpoints.

13.2 Results

The profile of Brådalsbekken-Tistilbekken has changed between 2007-2020 because of land changes that have taken place in the area. The most significant change is the increase in the slope of the Tistilbekken upstream from the culvert, which passed from 1.3° to $\sim 3^\circ$ in a section of ca. 200 meters (Figure 26; Figure 27).

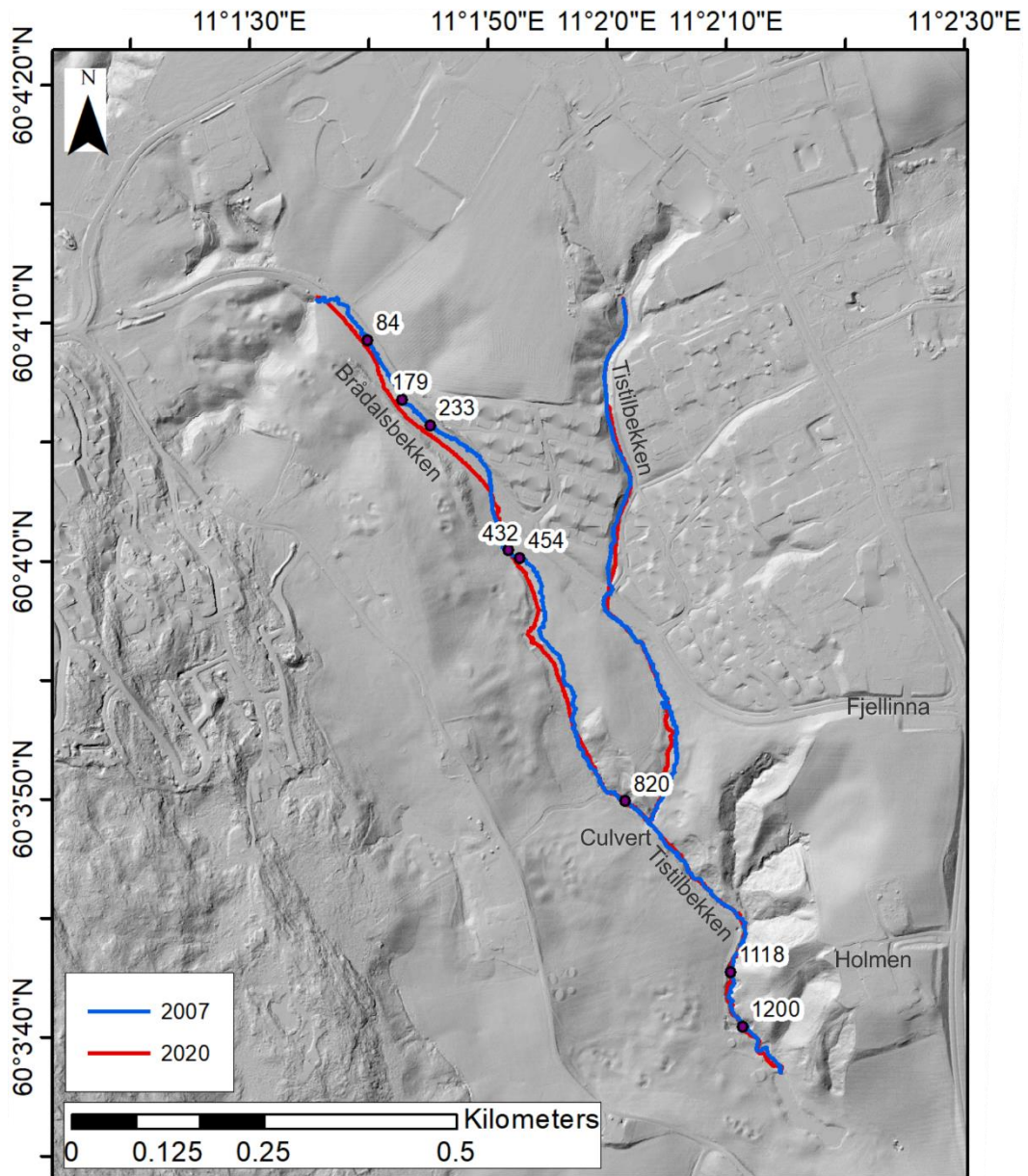


Figure 26. Map showing the sections of Brådalsbekken and Tistilbekken in which changes were analysed. The numbers correspond to slope breaks in which slope calculations of Figure 27 were done.

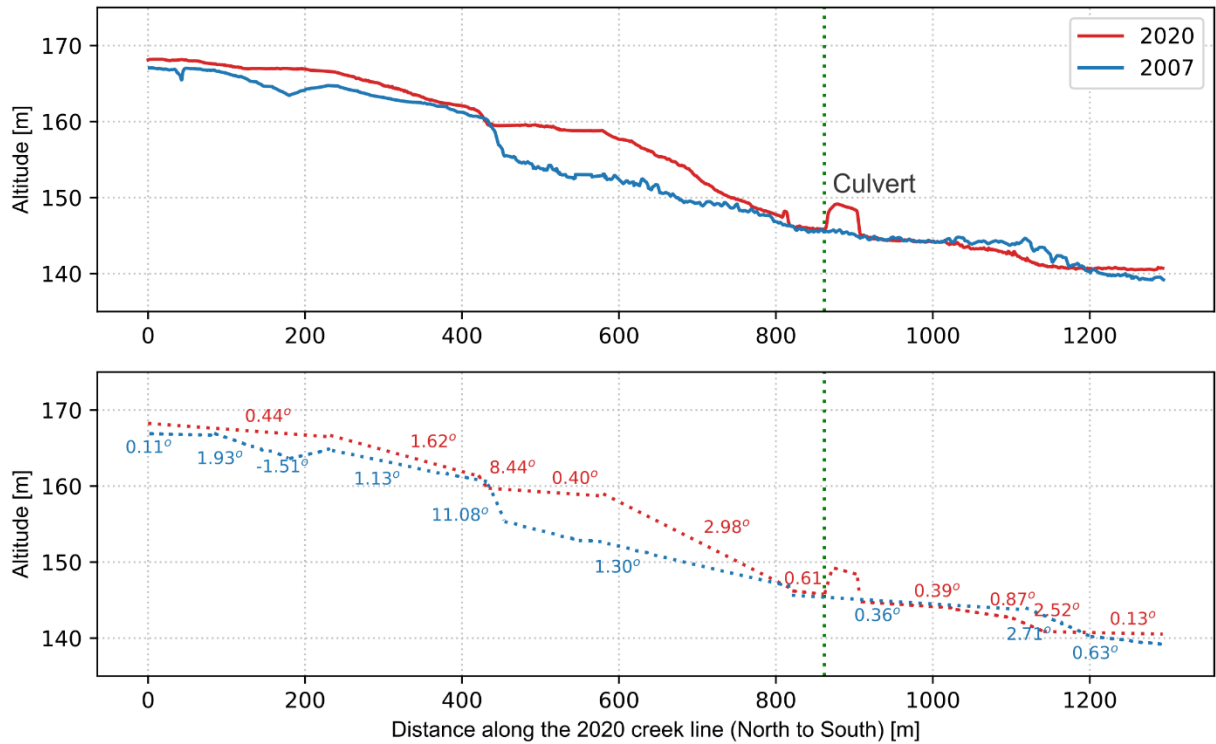


Figure 27. Brådalsbekken-Tistilbekken. Long profiles and slopes in time.

The sector of Tistilbekken from the catchment area to its confluence with Brådalsbekken has not changed significantly between 2007 and 2020 (Figure 28).

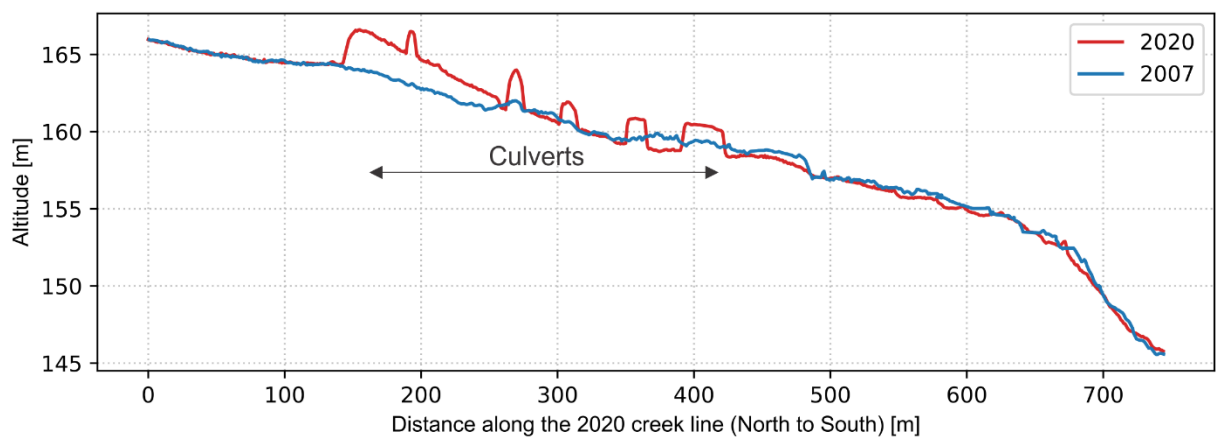


Figure 28. Long profile of Tistilbekken in time, upstream the confluence with Brådalsbekken.

14. Changes observed in cross sections of the streams

To explore vertical changes along Brådalsbekken and Tistilbekken, cross sections between 2007 and 2020 were produced.

14.1 Methodology

The elevation and distance along each profile was obtained by using the *Stack profile* tool from ArcMap. For each profile, the tool created tables containing the height and along-profile-distance for 2007, 2015 and 2020 DTMs. After that, the output tables were used in Grapher™ to generate the profiles shown in Figure 29.

Appendix 5 exposes the reasons why the 2013 LiDAR dataset is not used for these analyses.

14.2 Results

The main observations arising from the analysis of the cross-sections in the lower section of Tistilbekken is shown in Figure 30 and Figure 29. See Appendix 6 for the complete set of cross-sections.

The main observations are:

- Right downstream of the large golf course culvert in Tistilbekken (Figure 1), no significant surface changes are observed between 2007 and 2020.
- ca. 130 m downstream the culvert, incision is observed. Profile 5 shows the creek bed of 2007 2 meters above the one of 2015 and 2020 (Figure 30).
- The profiles 2 and 3 show the surface of 2007 located below the one from 2015 and 2020, meaning accumulation (Figure 30).

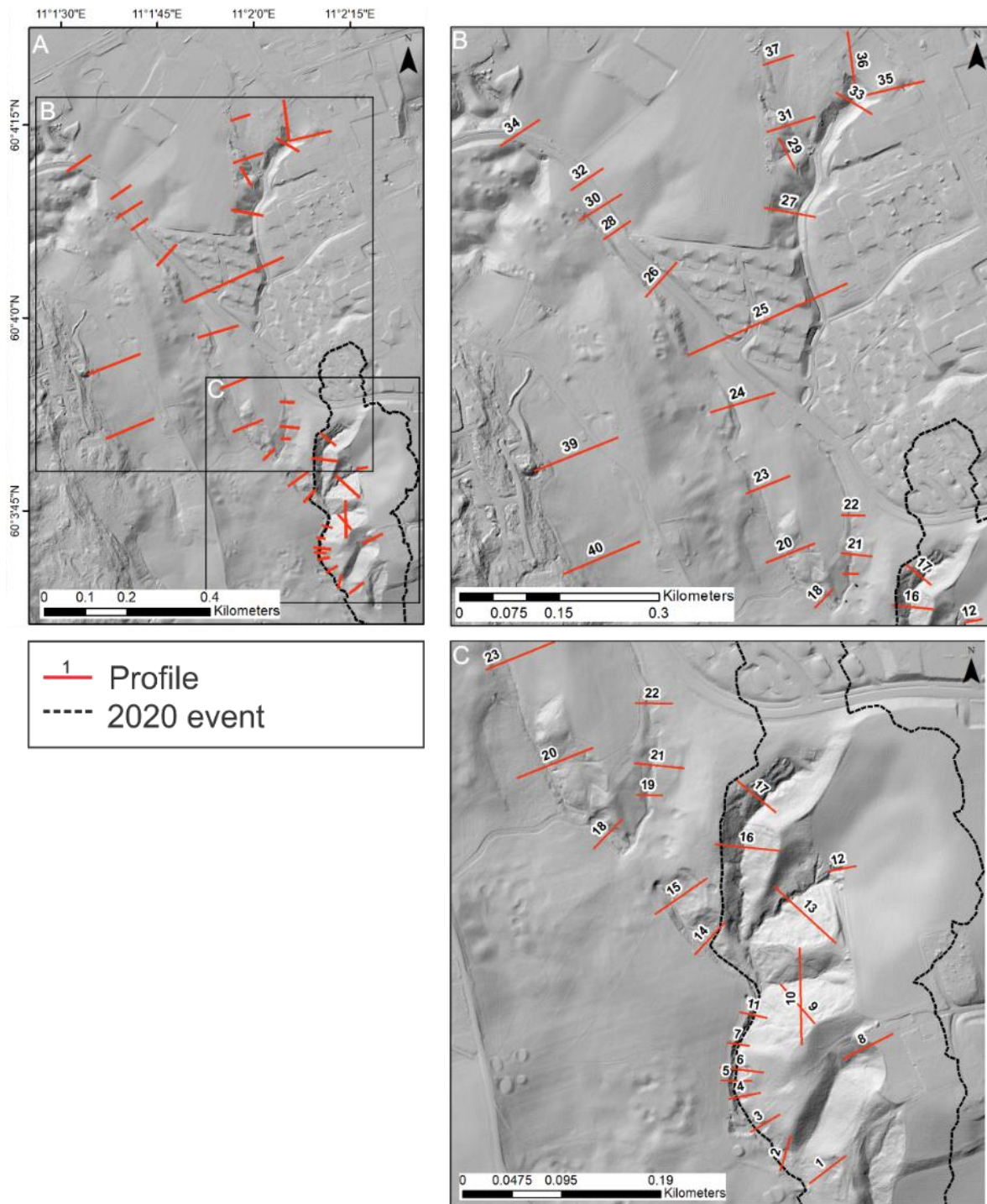


Figure 29. (A) Map with location of cross-sections, (B) Location of the cross-sections in the upper and central part of the study area, (C) Location of the cross-sections in the lower part of the study area. 2020 hillshade is used as a base map.

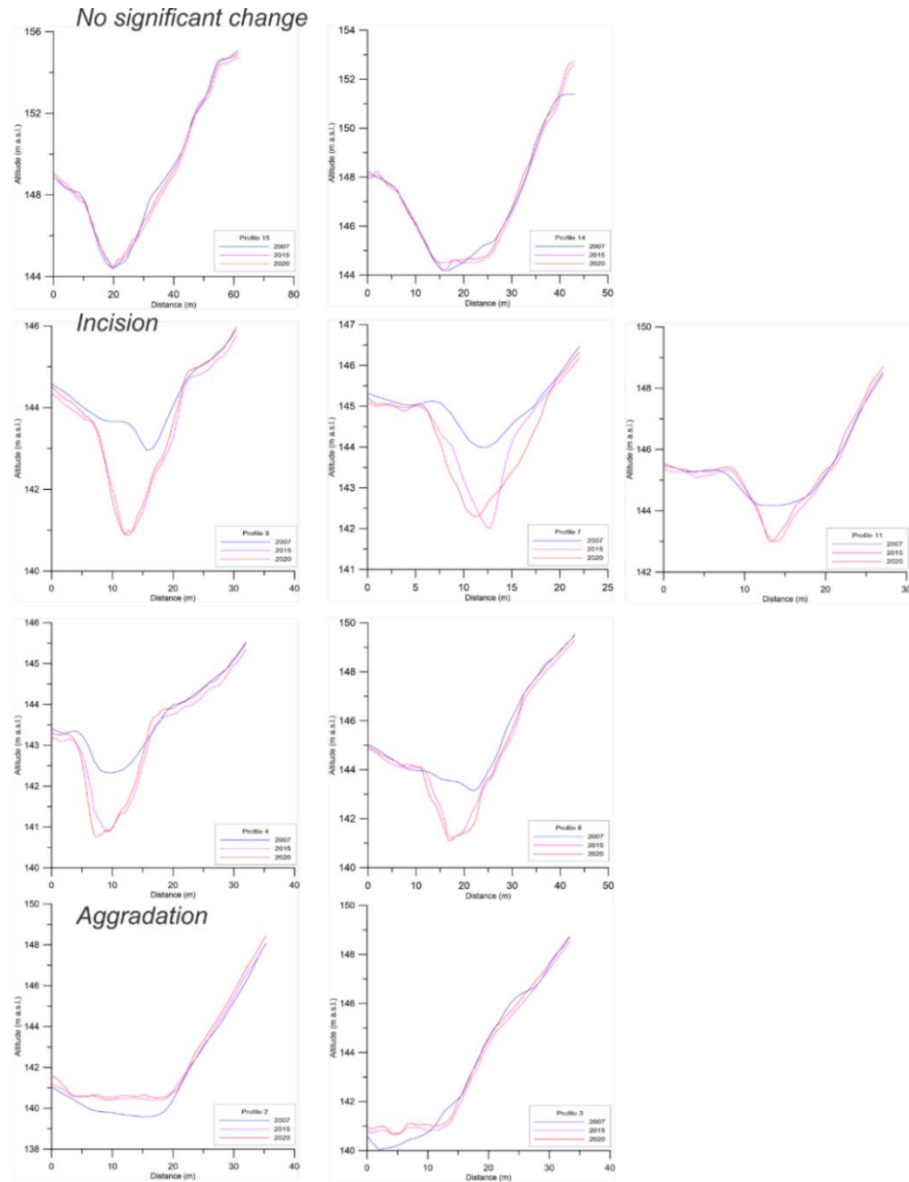
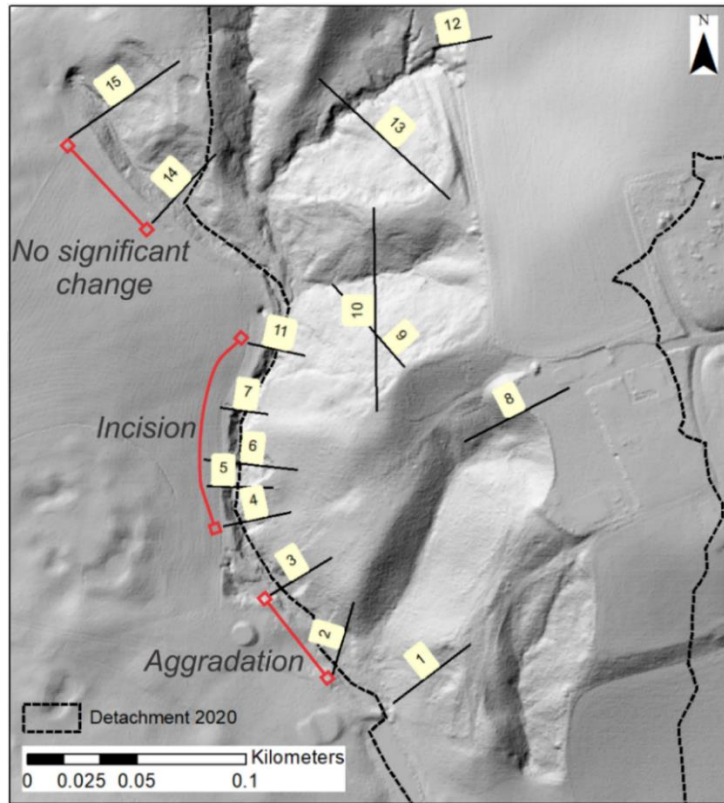


Figure 30. Map with location of cross sections with the 2020 hillshade as a base map, and cross sections in the lower section of Tistilbekken. All profiles are drawn from left to right.

15. Streambed changes in the lower section of Tistilbekken

Fluvial erosion can be detected by comparing the height of the bed at two different times. In this chapter we identify changes in Tistilbekken in the sector extending downstream the culvert to the pond.

15.1 Methodology

The Cloud Compare software was used to analyse the height differences between the 2007, 2015, and 2020 LiDAR point clouds in a buffer area of 10 meters around the main creek downstream the culvert. The buffer was mapped in ArcMap using the *Buffer* tool, and then converted to 3D features with the *Interpolate Shape* tool (Figure 31).

In Cloud Compare, a filter was applied to keep only the points representing the ground, which means that vegetation and unclassified points were removed. Then, with the *Segment* tool, we extracted the points of 2007, 2015 and 2020 falling inside the buffer area.

After this, a mesh was produced for the point clouds used as a reference, and the *Cloud to Mesh Distance* tool was used to compute the height differences for the periods 2007-2015 and 2015-2020. For the period 2007-2015, the dataset of 2007 was used as a reference, while for the period 2015-2020 the 2015 dataset constituted the reference. The methodology is summarised in Figure 31A.

The obtained results of distances were later classified in ArcMap into three categories: 1) Distances smaller than -0.3 m representing points where the surface was higher in the reference dataset than in the compared one, which means erosion occurred. 2) Differences between -0.3 m to 0.3 correspond to the threshold of detection based on the error of the DTMs. 3) Differences higher than 0.3 m represent points where the surface was lower in the reference dataset than in the compared one, which means accumulation.

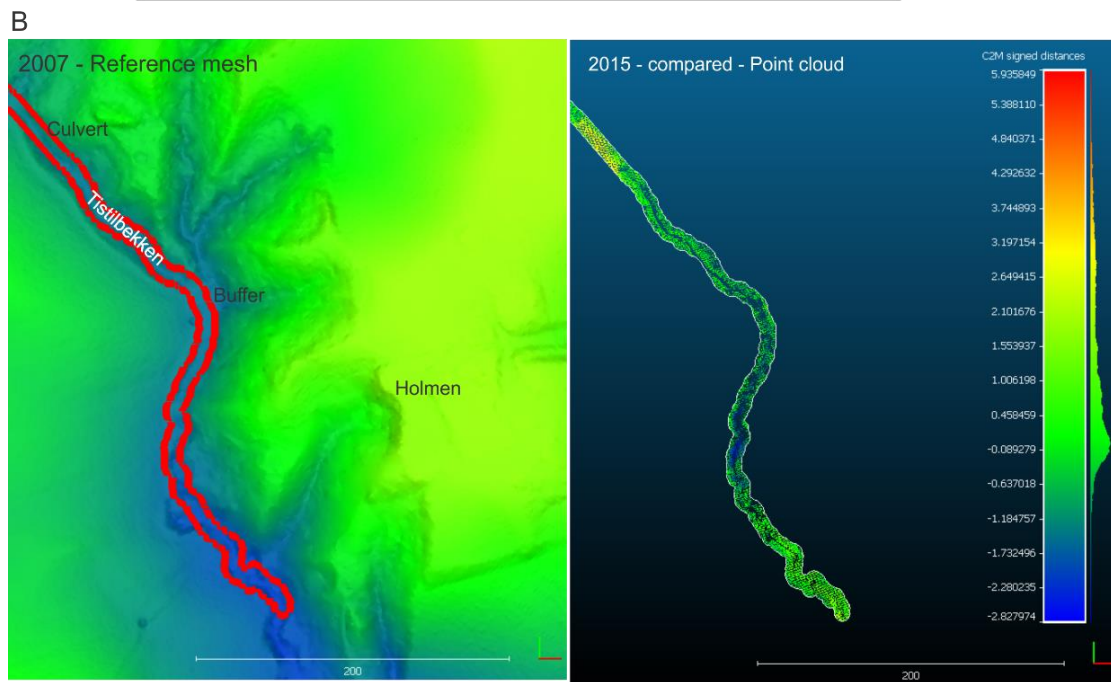
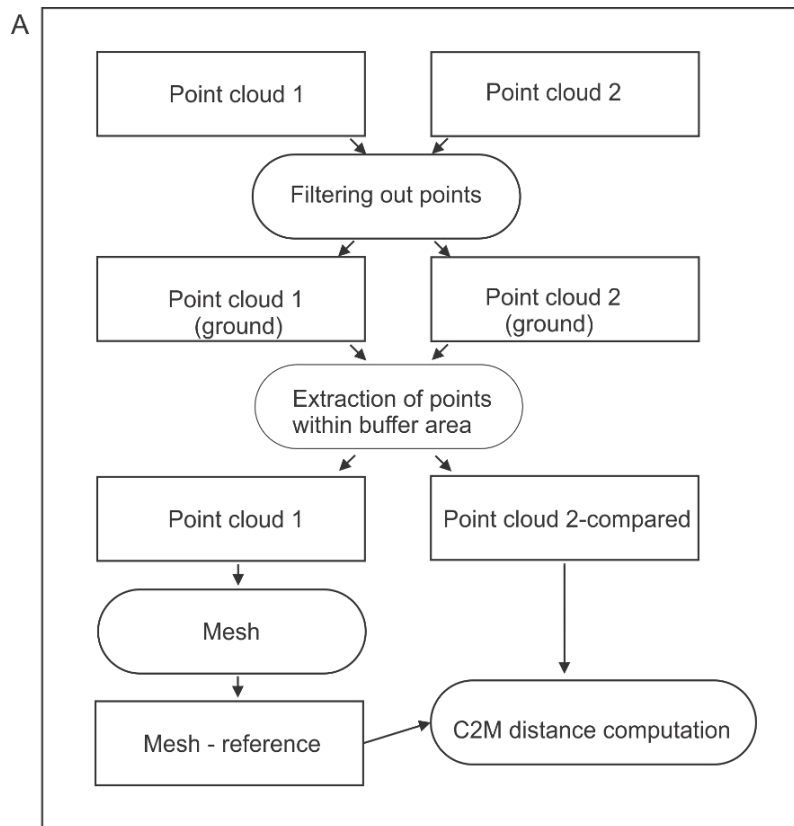


Figure 31. (A) Scheme showing the methodology applied for the computation of height differences. (B) View of the mesh and point clouds used as input data for the analysis of height differences downstream the culvert.

15.2 Results

The computation of height differences between datasets are presented in Figure 32, and the main observations are summarised below:

- The main changes occurred between 2007-2015; no significant changes are observed between 2015-2020.
- Between 2007-2015 a zone of erosion is observed in Tistilbekken, in the vicinity of Holmen. In the zone undergoing erosion, some old pipes were exposed and visible in orthophotos (Figure 32). Upstream of this zone, no significant changes were detected, except for the construction of the culvert (built around 2010).
- Downstream the zone of erosion, the 2007 surface is above the one of 2015, meaning accumulation.

These results, that show a change in the stream bed conditions, match well with the morphological features observed in the area (Figure 33). Along the section where most of the erosion was detected, several scars of small slides are observed in the DTMs of different years. These scars are very well preserved and present sharp edges. In the section showing accumulation, a flat surface is observed at the sides of the channel. This is also seen at the toe of a scar of a past slide, which is well preserved, but shows smoother edges than the previously mentioned scars.

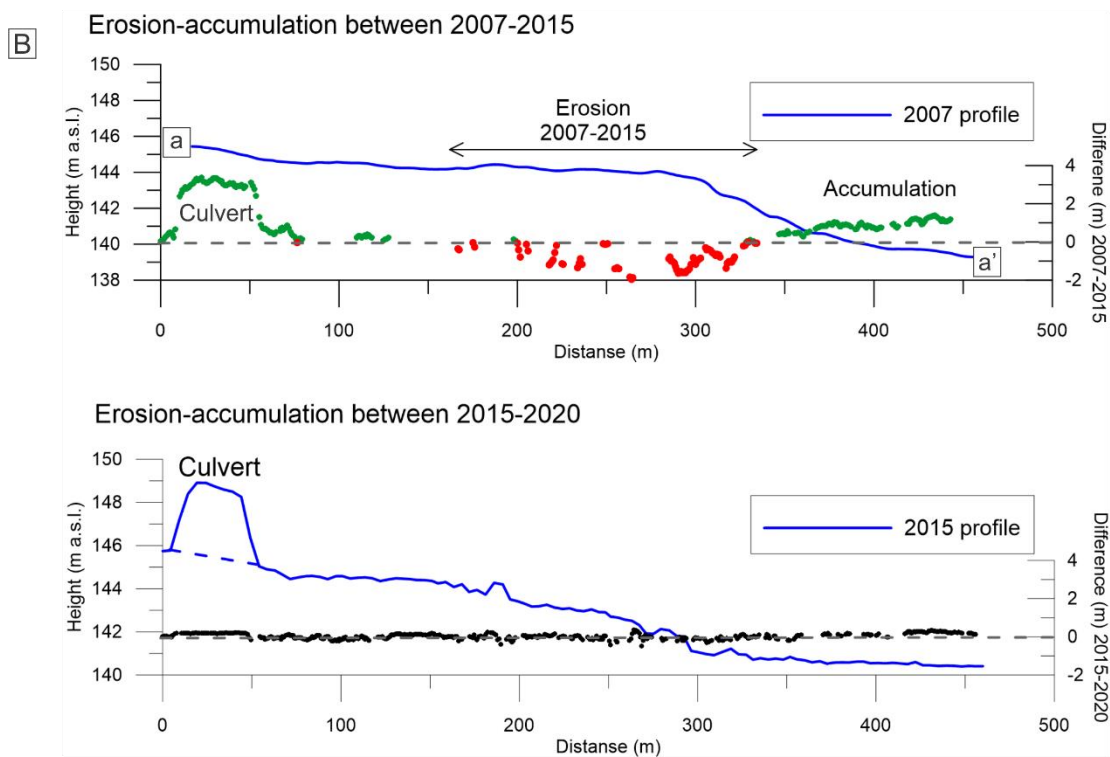
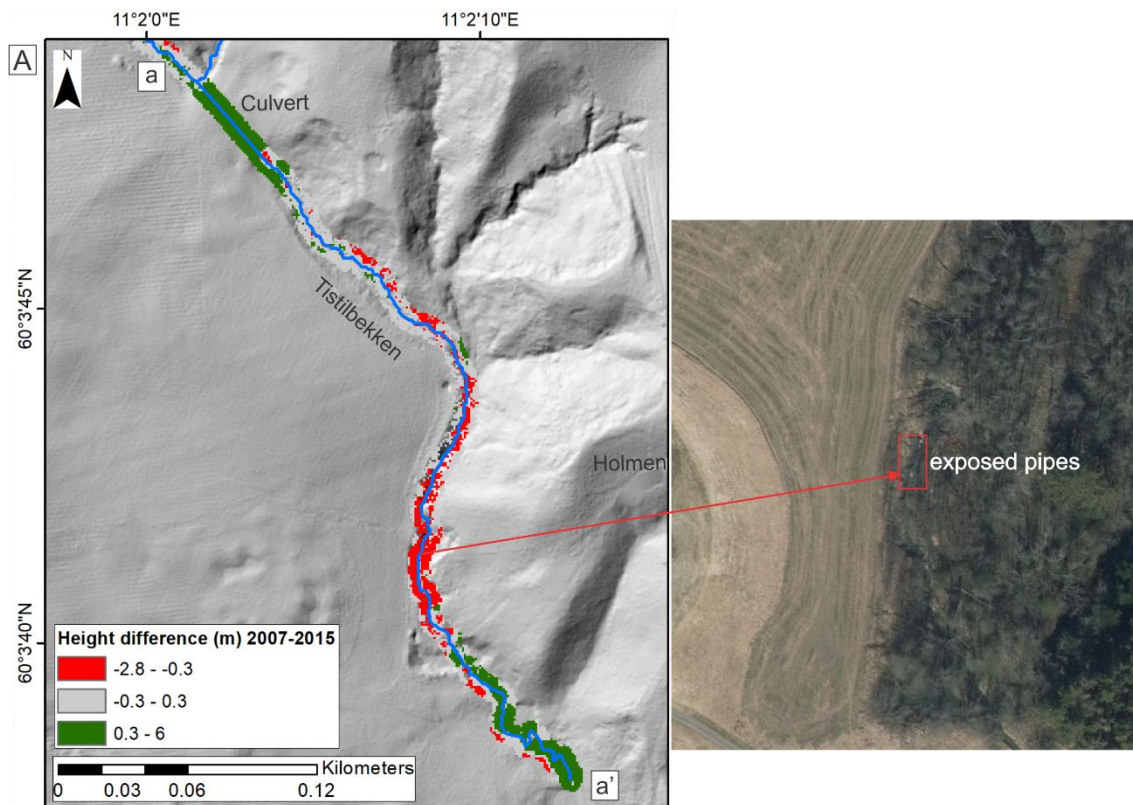


Figure 32. (A) Map showing changes in the creek bed in Tistilbekken between 2007 and 2015. (B) Erosion and accumulation in 2007-2015 and 2015-2020.

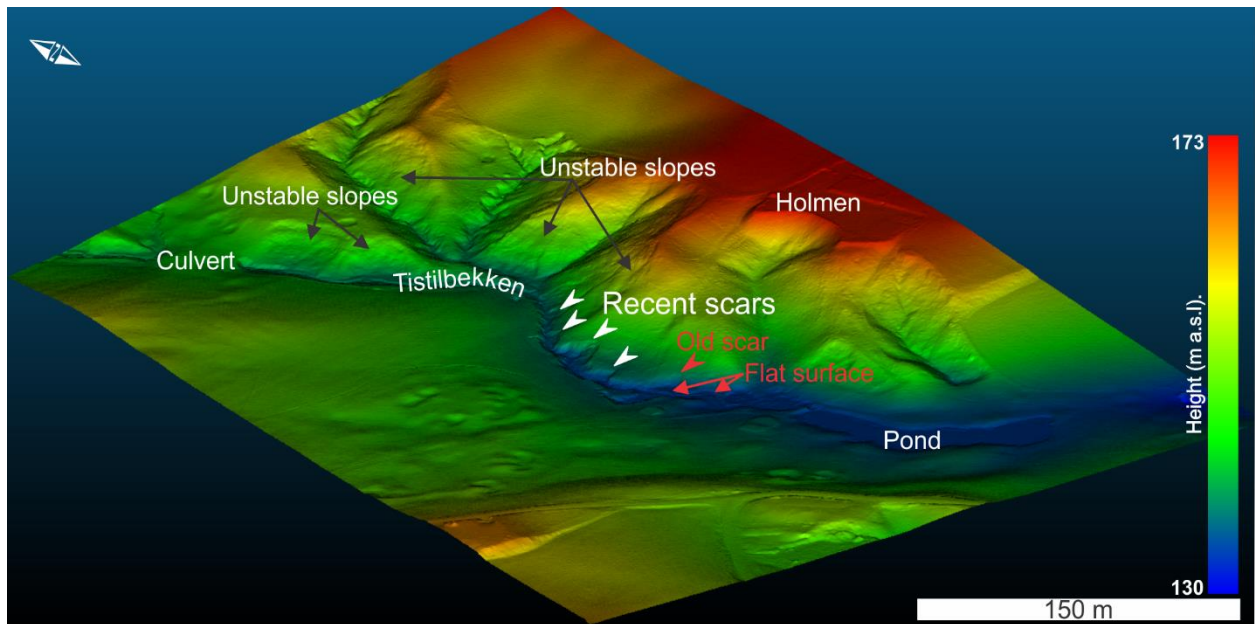


Figure 33. 3D view of the lower section of Tistilbekken and main morphological features observed.

16. Slope changes at the bottom of Tistilbekken creek

In this chapter, we analyse the changes in the lateral slopes of Tistilbekken creek in a buffer of 10 m in the section downstream the culvert down to the pond (Figure 1). The average steepness of the slopes surrounding the creek is calculated.

16.1 Methodology

Definition of the creek path: The creek path was delineated using the 2007 and 2020 DTMs. This required as a first step the computation of flow direction and flow accumulation with the *Hydrology* toolbox from ArcMap. Then, the lines representing the creek path were simplified using the *Simplify Line* tool in ArcMap (Bend Simplify, 5 m tolerance). The line representing the creek was then divided in 200 sample points (locations at which the information was collected) equally spaced. The coordinates of each sample point were calculated using the *interpolate function* of Shapely (a Python library; Gillies 2020). Finally, the slope angles were analysed inside a 10 m buffer along the lines.

For the 2007 line, the coordinates of the sample points are then projected on the 2020 line using the *project function* of Shapely (Gillies 2020). Thus, the distances used on the graphs correspond to the 2020 line, while the attributes of the sample points are defined using their original position.

Altitude: The altitude is interpolated at the position of each sample point using the *interpolate.griddata function* of SciPy and a cubic model (The SciPy community 2021).

Slope: For the 2007 and 2020 DTMs, a slope map was made using the *Slope* tool from ArcMap. This tool determines the gradient for each cell of a raster. For each cell of the slope raster, a script checks if the distance to the closest point of the line is shorter than 10 m using the *distance function* of Shapely (Gillies 2020). If this condition is met, the script finds the closest sample point and registers the cell's value to this sample point. Once all the cells have been

projected, the slope is averaged for each sample point using a weighted mean to account for the slope. Indeed, the real terrain surface in a cell that is not flat is greater by a factor $1/\cos(\text{slope})$. This process is done for both sides of the creek together and individually, thus producing three graphs (both banks, eastern bank and western bank). The 2007 sample points do not necessarily project at the same distance as the 2020 sample points. Therefore, to find the difference between the two years, the 2007 curve must be interpolated. This allows calculating the difference between the two curves. These differences are then registered to the 2020 sample points and exported as a shapefile.

16.2 Results

We have analysed the changes in the slopes of Tistilbekken in a section of ca. 400 meters. The profile of the creek shows changes in altitude which reflect incision and accumulation, as documented in chapter 15.

Figure 34 shows that the altitude in the section between 120 and 260 meters is lower in 2015 and 2020 than in 2007, while between 260 and 400 meters the altitude in 2015 and 2020 is higher than in 2007. The changes in altitude (showing erosion and accumulation) came together with changes in the slopes of the banks. Figure 34 and Figure 35 show that during 2007-2015 the slope of the banks increased in the sector 120-260 m, especially in the western bank. This section coincides with the one identified in chapter 15 as undergoing incision, but also with the sector where Jjunju & Rapp (2021) identified increased speed of the flow during a hydrologic modelling. From 290 meters and down to the pond, the slopes of the banks became gentler (Figure 34 and Figure 35), and this coincides with the sector undergoing accumulation, as described in chapter 15. Between 2015-2020 no significant changes were observed.

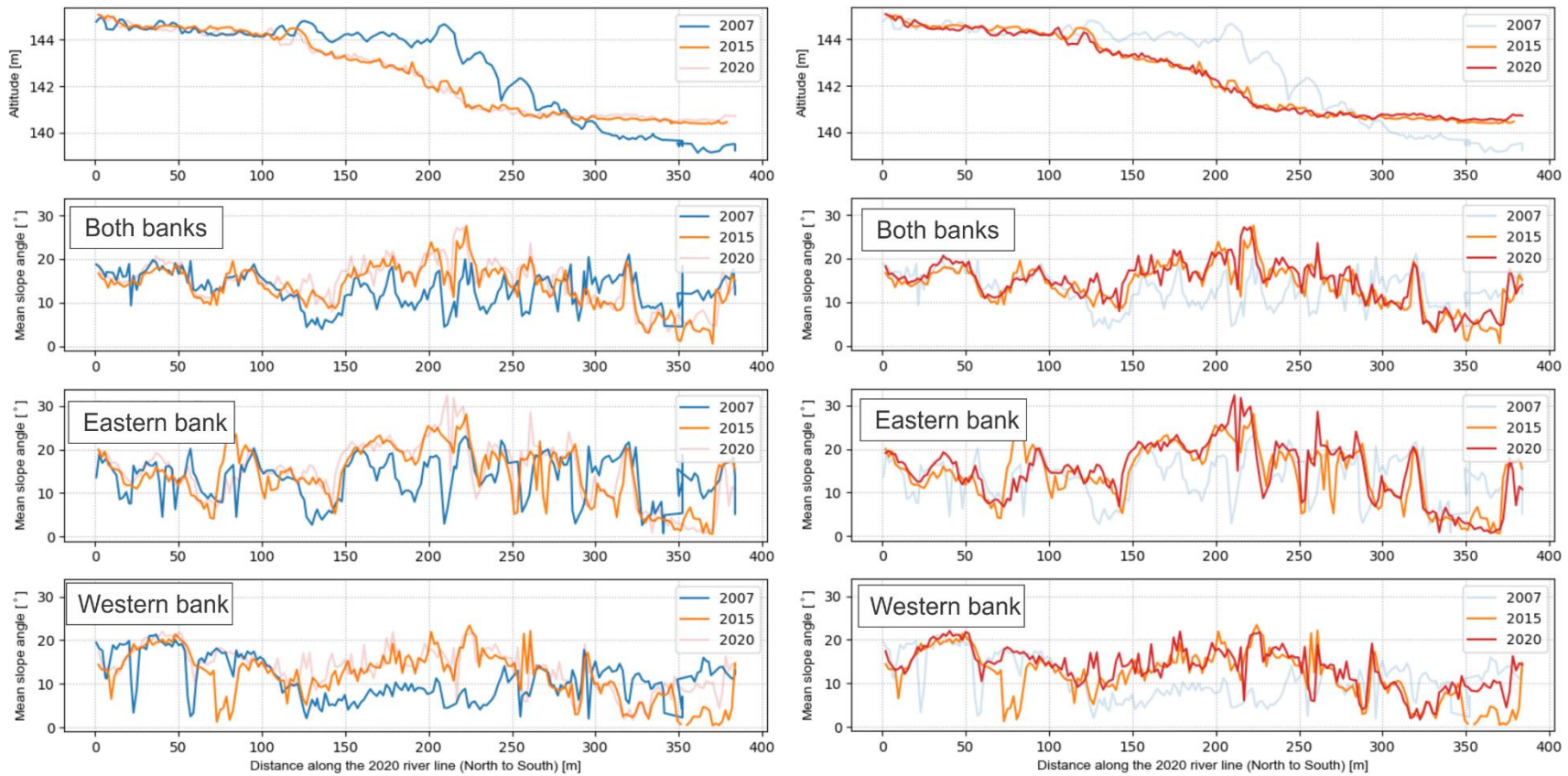


Figure 34. Altitude and mean slope angles in the banks of the creek along the 2007, 2015 and 2020 creek lines on a buffer of 10 m. See map in the following figures.

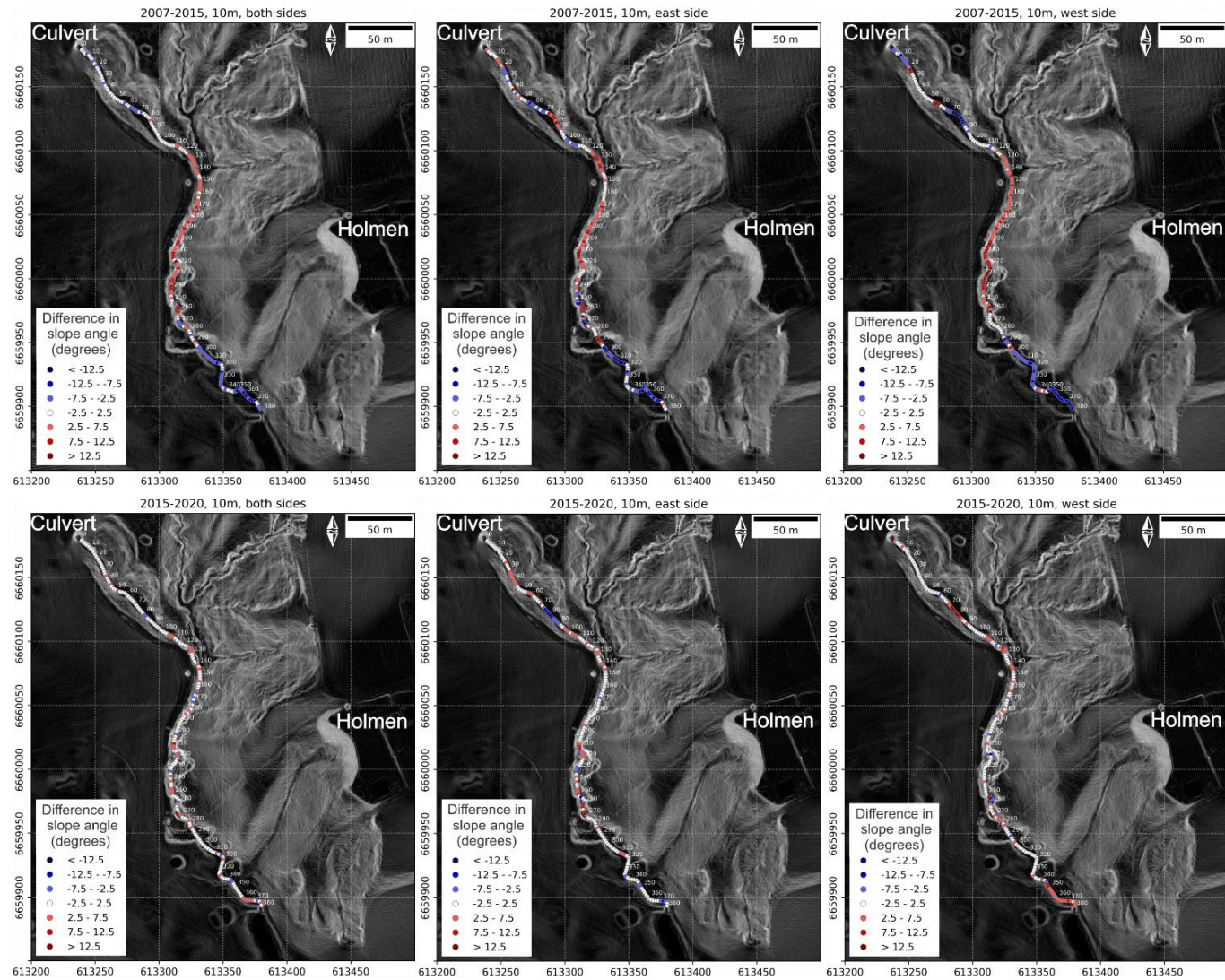


Figure 35. Difference of mean slope angle inside a 10 m buffer along the creek lines between 2007-2015 and 2015-2020. Positive values mean the slope got steeper and negative values than the slope got gentler during the period considered. The 2015 slope raster is shown in the background for the period 2007-2015 and the one from 2020 for the period 2015-2020.

17. Stream Power Index

The Stream Power Index (SPI) is a measure of the erosive power of flowing water at any point in a catchment (Moore et al. 1991). It is a geomorphologic index based on the contributing area of a stream and its local slope. Slopes changes in a watershed result into changes on the SPI. In this chapter, we present the spatial and temporal evolution of the SPI for Brådalsbekken and Tistilbekken.

17.1 Methodology

The SPI is defined as $SPI = \alpha \cdot \tan(\beta)$, where α is the cumulative upslope area draining through a point per unit contour length and $\tan(\beta)$ is the local slope angle. There will be a constant increase in the SPI in a fluvial course with constant slope because of an increase in the contributing areas. For this report, the SPI was computed by NVE using the GRASS GIS software (2017).

The computation for the years 1969, 1974, 1982, and 1991 was done using photogrammetric models, while for 2007, 2015 and 2020, LiDAR DTMs were used. The results of the GRASS computation were used to produce graphs with Grapher™. The input data to build the creek and the SPI profiles was obtained with the *Stack Profile* tool from ArcMap along the path of the creek at the time considered.

17.2 Results

The SPI profiles of Brådalsbekken and Tistilbekken show changes with time. In Figure 36 the central part of the profile of the creek is steeper in 2020 than in 1969. Increases in the slope along the profile are seen as increases in the SPI values (Figure 36). In 2020, the sector showing highest values was in the vicinity of Holmen (Figure 32). Towards the lower part of the profile, the decrease in the SPI values is controlled by a decrease in the local slope.

For the upper part of Tistilbekken (upstream the culvert), we present the SPI for the period 1991-2020. This is when the most significant terrain changes have taken place. We can observe that the lower part of the profile, the slope increased with time. In 2020, higher values were observed in the lower part of the profile, and this is because the contributing area is bigger than the sectors located upstream, but also because of the higher local slope (Figure 37).

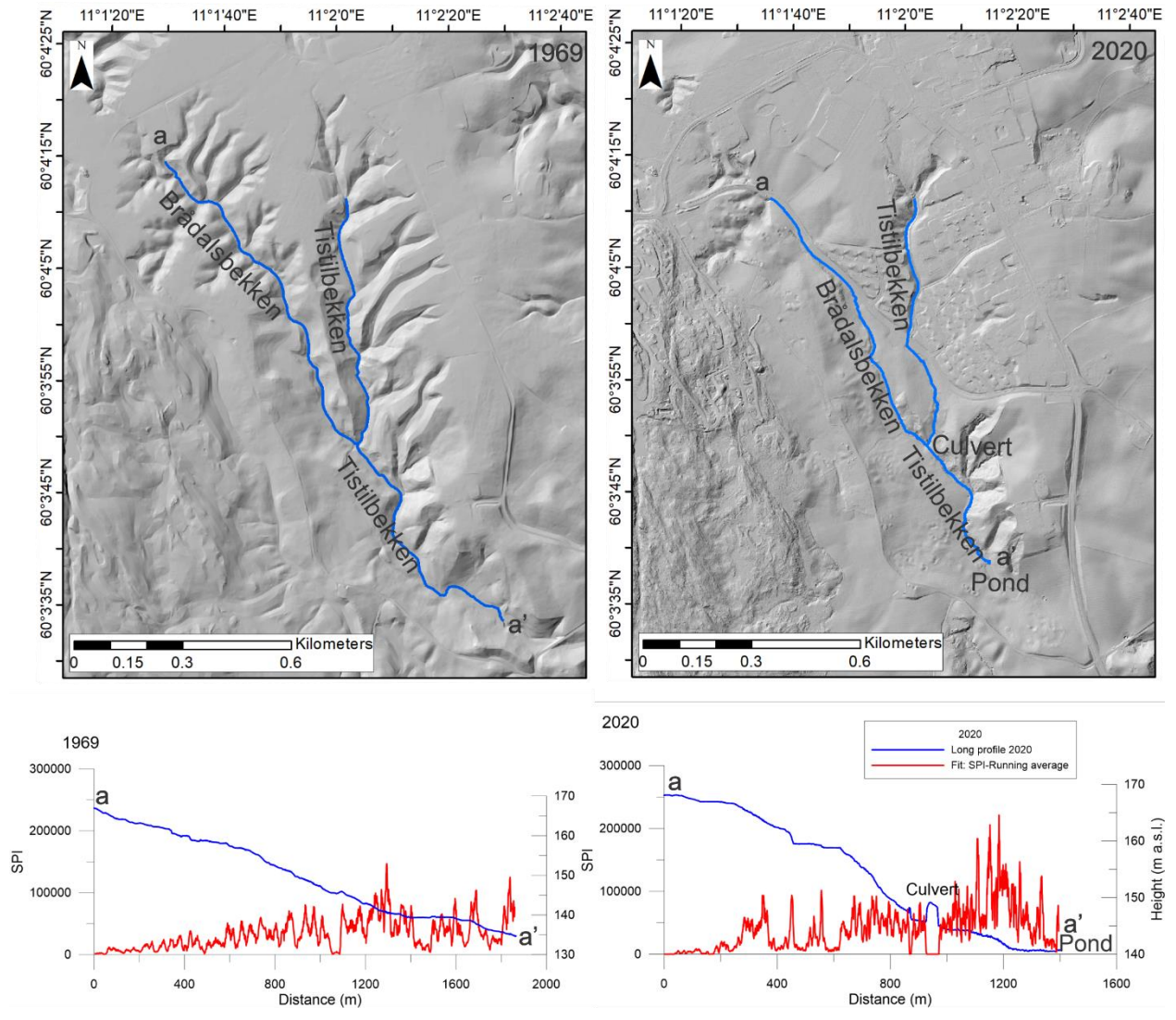


Figure 36. SPI results for Brådalsbekken-Tistilbekken for 1969 and 2020. Note: 1) The running average was computed for a moving window of 15 rows. 2) the resolution of the dataset differs, therefore only the trend is comparable.

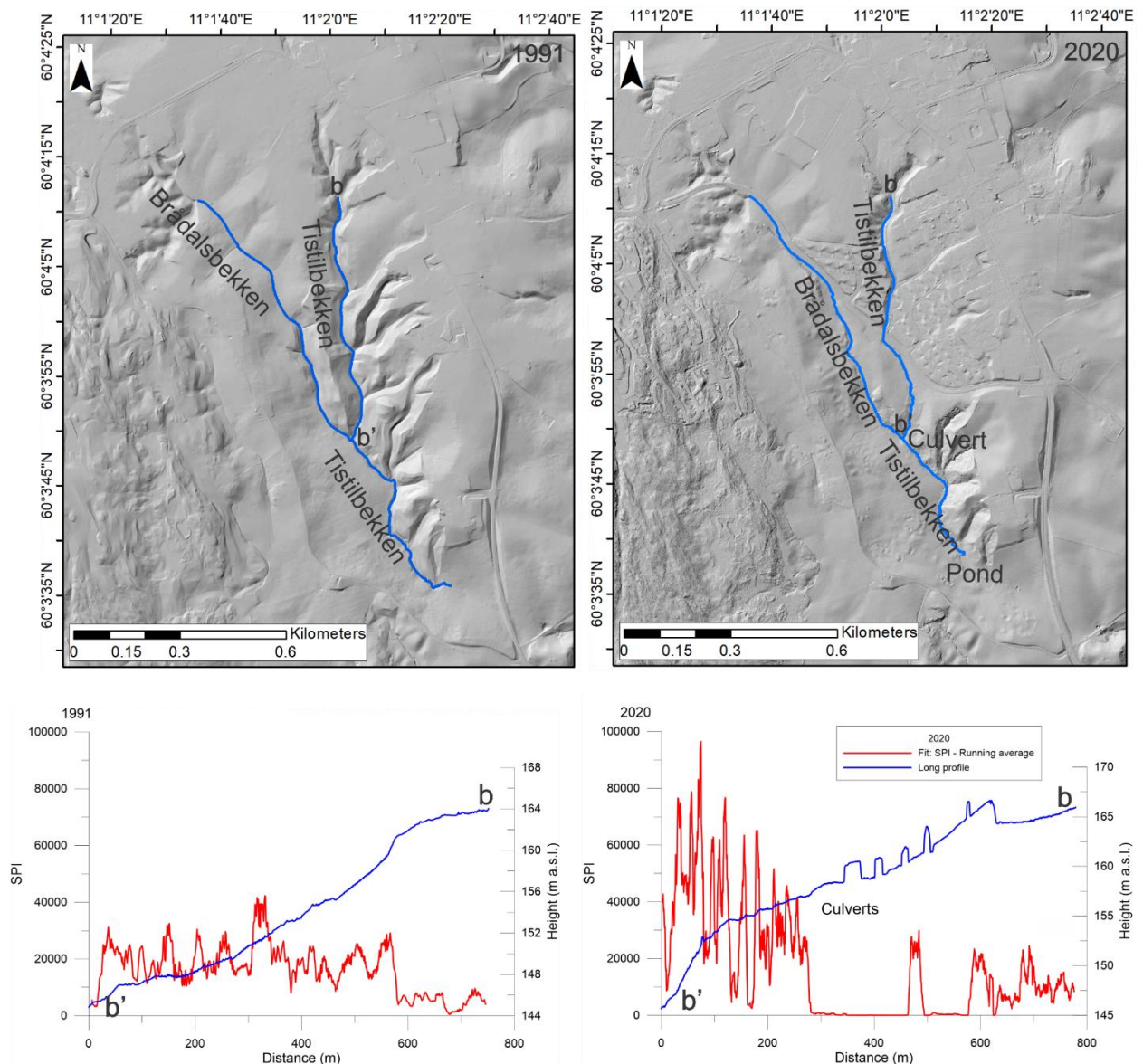


Figure 37. SPI results for the upper part of Tistilbekken for 1991 and 2020. Note: 1) The running average was computed for a moving window of 15 rows. 2) The resolution of the dataset differs, therefore only the trend is comparable.

18. Bedrock topography and sediment thicknesses

Reconstruction of the bedrock topography can provide valuable information about the landscape development of a region. The thicknesses of loose material (sediments) below the surface may be key information in landslide risk assessment and planning and development of infrastructure. In this chapter, we present the reconstruction of the bedrock topography for Ask and adjacent areas.

18.1 Methodology

The bedrock depth was determined based on the compilation of underground and surface data (Table 10; Figure 38; Figure 39). Some of the geotechnical borehole information used is available in NADAG (NGU 2021b). In addition, data from groundwater wells were used (NGU 2021c). For surface and near surface information, aerial pictures and DTMs were used to detect sites where bedrock is cropping out. In these sites, the bedrock height was extracted from the 2020 DTM. See Figure 2 for the extension of the 3D model.

A 3D Leapfrog model of a smaller area, around the landslide locality, for bedrock and sediment layers was made by Multiconsult (2021). The point cloud from this model was compared and partly used for the NGU 3D model.

Bedrock depth from 5 seismic lines was carried out by Argeo (2021) and from the geotechnical drilling profiles was provided by Multiconsult as a point cloud. For each of the seismic lines three horizons corresponded to different wave velocities (2500, 3000, and 3500 m/s V_p) and represented potential locations of the bedrock. The medium velocity was used in our analysis.

Table 10. Datasets used as input data for the reconstruction of the bedrock topography.

Type of dataset		Amount
Boreholes with:	Assumed/confirmed bedrock	140
	Not confirmed bedrock depth (Minimum depth of bedrock)	52
Aerial Pictures:	Observed bedrock at surface	69
Seismic lines:	Refraction and MASW	5

Since the input data is represented by points, we used the *Kriging method* (3D Analyst from ArcMap) to produce a 2 m resolution surface. We aimed to have the best possible resolution in the area with high point density, which corresponded to the area where the landslide occurred (Figure 39).

The reconstructed bedrock topography below the sediments was then merged with the topography of bedrock above the surface from the 2020 DTM. Finally, the thicknesses of the sediments were computed with the *Raster Calculator* tool as the difference between the bedrock topography and the 2020 DTM.

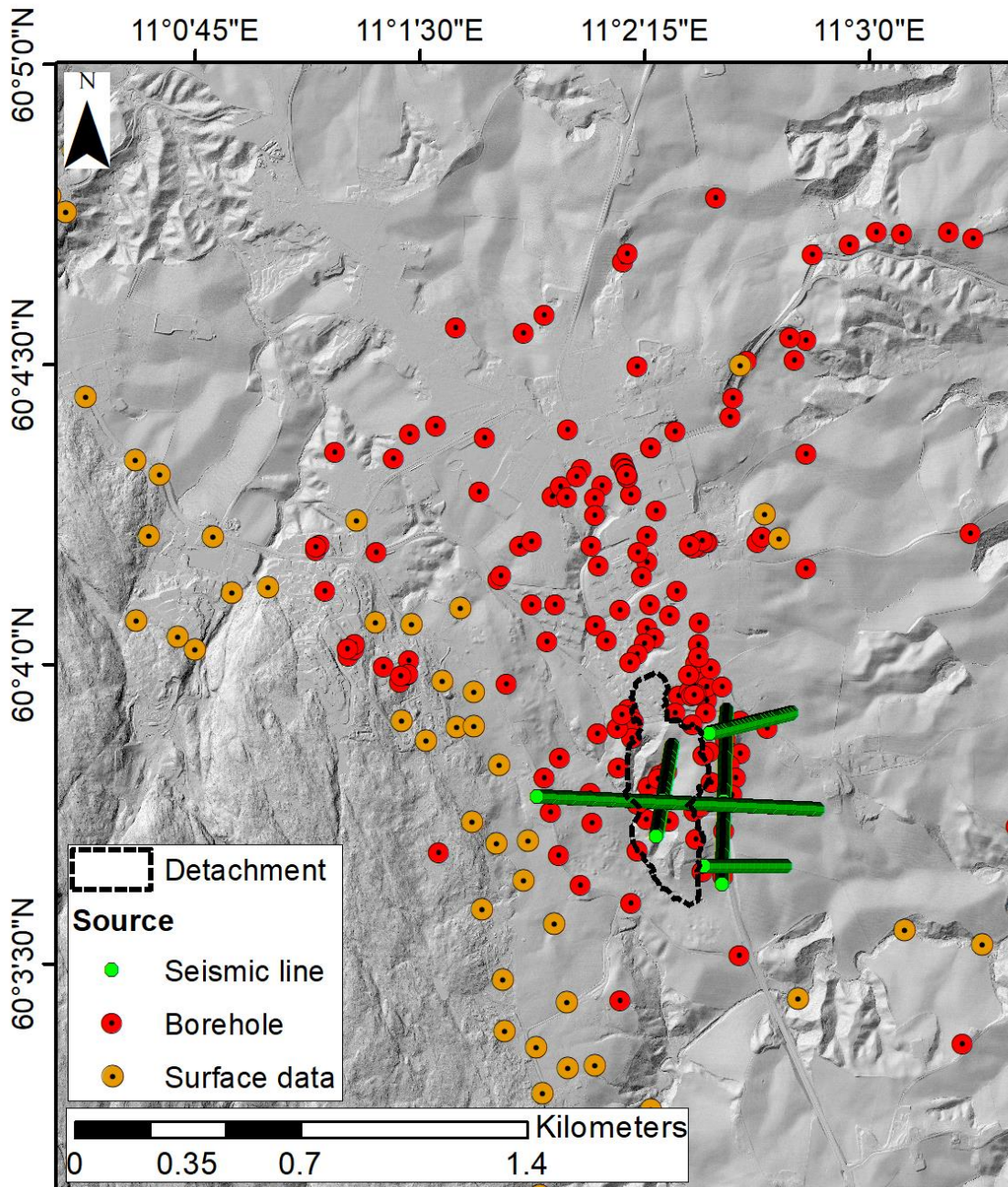


Figure 38. Distribution of data points used to reconstruct the bedrock surface.

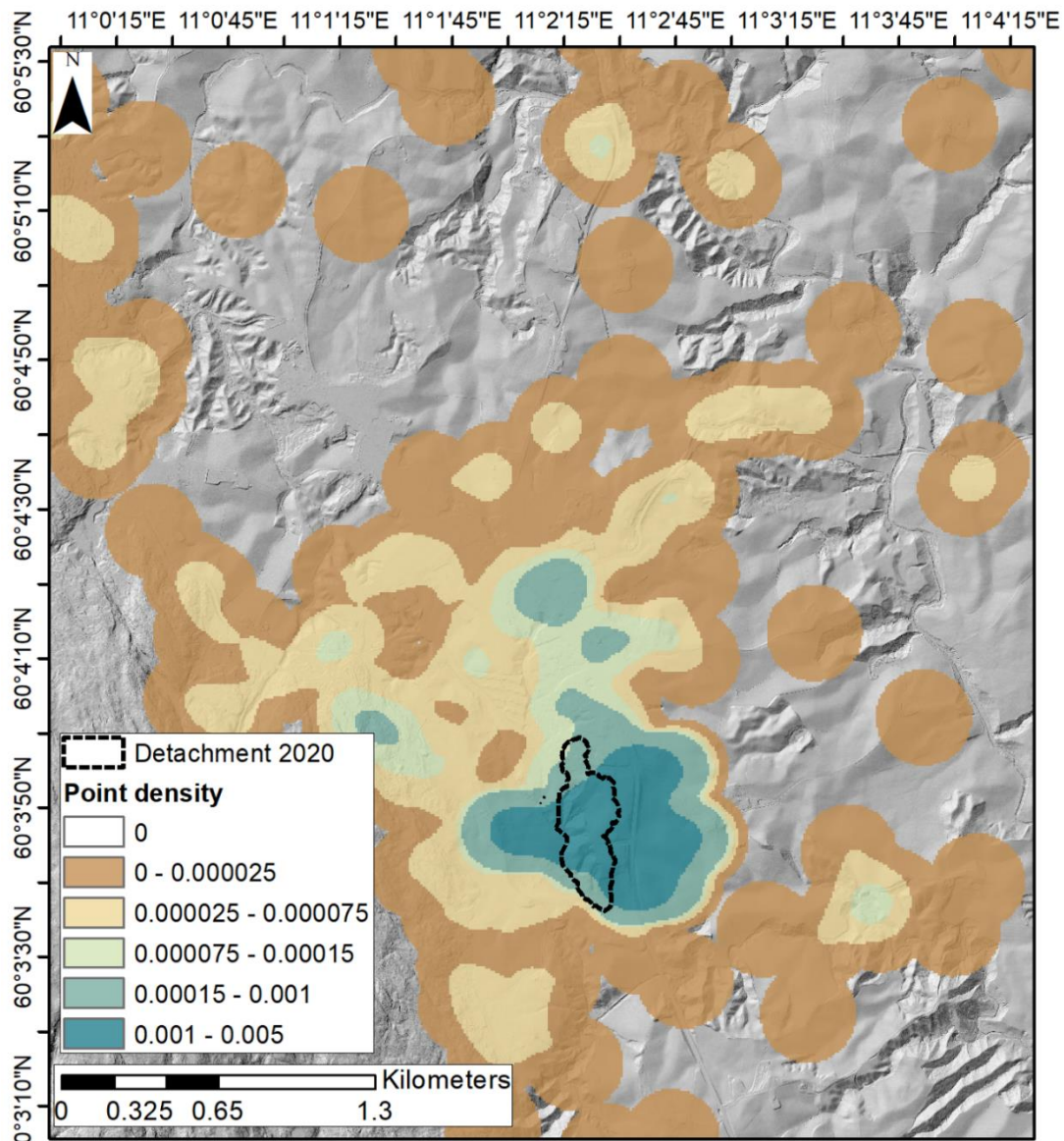


Figure 39. Point density map. The map represents the number of boreholes per square meter in a circular window of 200 meters radius, determined using a Kernel density function.

18.2 Results

We have reconstructed the depth to bedrock in an area of $\sim 14 \text{ km}^2$. The reconstructed bedrock topography shows elongated depressions that probably correspond to “valleys” eroded by the glacier in the bedrock (gneisses (Olerud 2002)). These “valleys” are in accordance with the pattern of regional discontinuities. The Brådalsbekken and Tistilbekken follow the orientation of the elongated depressions observed in the bedrock topography. Below Ask centre there is a north-south-lying ridge, which is narrow in the southern part with a somewhat wider plateau in north (Figure 40, Figure 41 and Figure 42).

In the headscarp of the 2020 quick clay landslide, bedrock depths range between 20-10 m, while at the toe of the mobilised landslide mass, bedrock is found between 30-50 m below the 2020 surface.

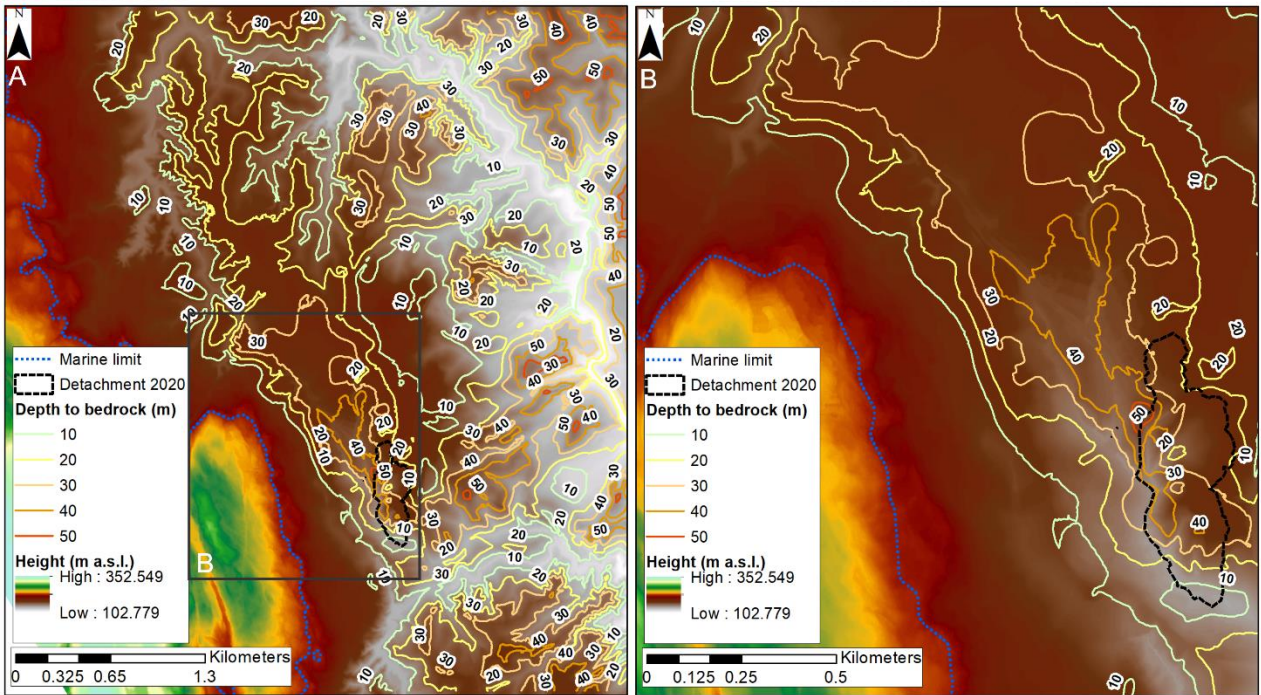


Figure 40. (A) Isopach map showing the contour lines of depth to bedrock (sediment thicknesses). (B) Isopach map with the contour lines corresponding to depth to bedrock in the area of the 2020 landslide.

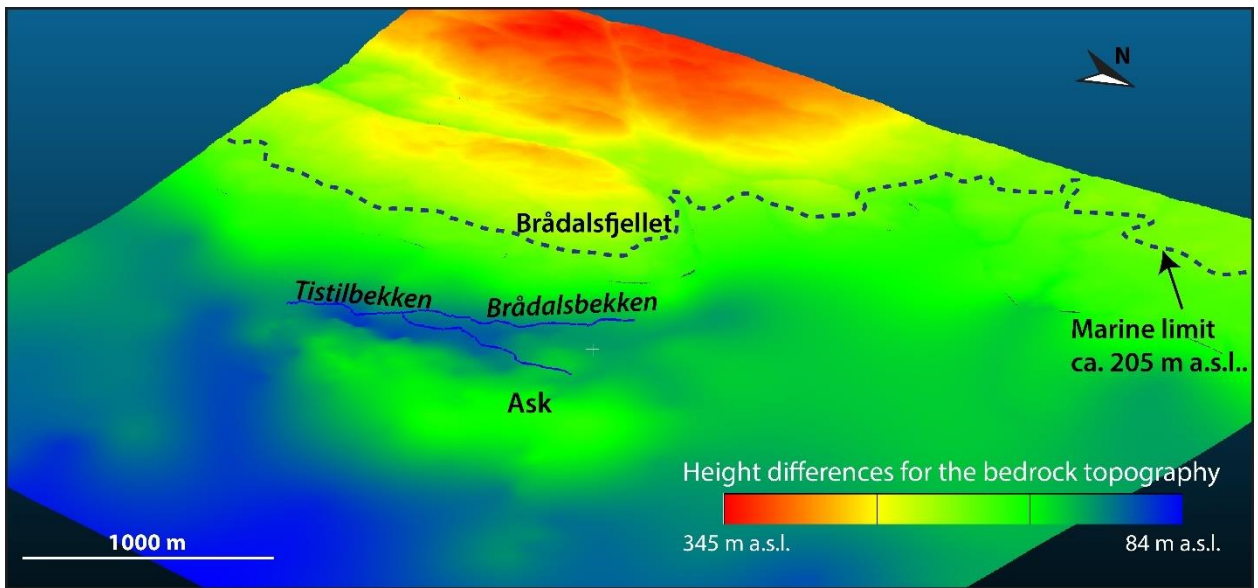


Figure 41. The Cloud Compare model of the bedrock topography. Areas below the Marine limit are covered by marine sediments.

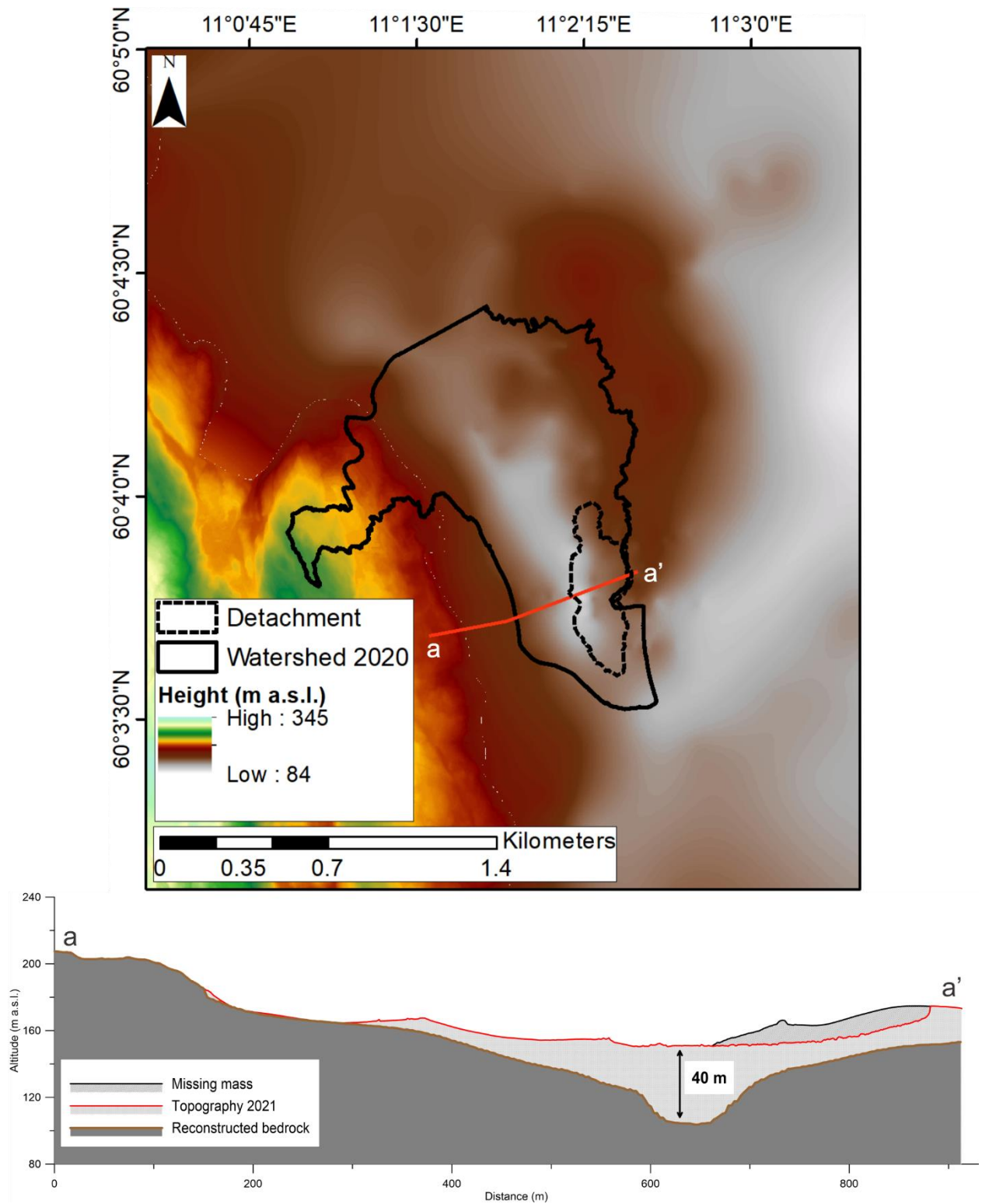


Figure 42. Map of reconstructed bedrock and a topographic profile. The red line represents the topography after the 30 December quick-clay landslide.

19. Closing remarks

This report has documented the methods used to analyse landscape changes in Ask area before the occurrence of the 30 December 2020 quick-clay landslide. The main results of this work are summarised below, but not discussed with regards to the underlying causes and/or triggering of the landslide. However, most of the results are used and discussed in the report of the Gjerdrum Committee, published 29 September 2021.

Some of the main results are:

- Since the 1970s the area has undergone a process of urbanisation, in which the construction of houses, buildings and roads increased. Along with urbanisation, a process of deforestation is observed.
- Soil infill and soil removal took place in several sectors of the study area, but mainly in the upper and central part of Brådalsbekken-Tistilbekken.
- The position of Brådalsbekken and Tistilbekken, as well as their long profiles have changed with time. In the sector where the landslide occurred, we observed as a general trend a migration of the creek towards the east. In this same sector we detected downcutting, an increase of the average slope of the banks and mapped several small detachments at the toe of the slope.
- The landslide mobilised about 1.35 million m³ of marine sediments. In the detachment area, signs of slope instabilities are observed in the LiDAR DEM of 2007. Ca. 30 % of the mobilised material remains over the sliding surface and the rest deposited mainly along the Tistilbekken and Tangeelva valleys.
- The toe of the detachment area located in a sector where the coverage of marine sediments was thicker than the surroundings.
- The reconstructed bedrock topography is in accordance with the pattern of regional discontinuities. Below Ask centre there is a north-south-lying ridge.

20. References

Argeo 2021: Refraksjonsseismikk, Gjerdrum. Innsamling og Tolkning av refraksjon og overflatebølgeseismikk over leirskredet i Gjerdrum. Argeo report ARG-21014-01, p. 33.

Bargel, T.H. 2005: Spor etter istiden i Oslo og Akershus. Gråsteinen 10, NGU.

Brasington, J., Langham, J. & Rumsby, B. 2003: Methodological sensitivity of morphometric estimates of coarse fluvial sediment transport. *Geomorphology*, v. 53(3-4), p. 299-316.

COWI 2018: Ortofoto rapport-Historiske Ortofoto-NLF-0883 Nittedal-Sedsmo-Fet-Sørum 1986. COWI 08-Rapport.

Gillies, S. 2020: The Shapely User Manual. Available at:
<https://shapely.readthedocs.io/en/stable/manual.html> (last visit 09/09/2021)

GRASS Development Team 2017: Geographic Resources Analysis Support System (GRASS) Software, Version 7.2. Open-Source Geospatial Foundation. Electronic document: <http://grass.osgeo.org>.

Gregersen, O. & Moholdt, R. 2006: Resultat av sjaktgravinger. Nystulia Gjerdrum, Boligfelt B9 Ask sentrum. NGI Teknisk Notat 20031570, date 2006-05-18, 10 p.

Jaboyedoff, M., Carrea, D., Derron, M.H., Oppikofer, T., Penna, I.M., & Rudaz, B. 2020: A review of methods used to estimate initial landslide failure surface depths and volumes. *Engineering Geology*, v. 267, 105478.

Jjunju, E., & Rapp, Ø. 2021: Vurdering av vannføringen og erosjonspotensialet i Tistilbekken Gjerdrum. Project: Erosjon Tistilbekken Gjerdrum. SWECO Report No 10223798-001.

Kartverket 2021a: "Høydedata" from Norwegian Mapping Authority,
<https://hoydedata.no/LaserInnsyn/>

Kartverket 2021b: Orthophoto from Norwegian Mapping Authority,
<https://www.norgebilder.no/>

Moore, I.D., Grayson, R.B. & Ladson, A.R. 1991: Digital terrain modelling: a review of hydrological, geomorphological, and biological applications. *Hydrological Processes*, vol. 5(1): 3-30.

Multiconsult 2021: Kvikkleireskred Ask Gjerdrum 3D-modell. Multiconsult note 10223695-07-RIG-NOT-001, date 01.07.2021.

NGU 2021a: Surficial deposits map, http://geo.ngu.no/kart/losmasse_mobil/

NGU 2021b: NADAG (geotechnical data), <http://geo.ngu.no/kart/nadag/>

NGU 2021c: GRANADA (groundwater wells), http://geo.ngu.no/kart/granada_mobil/

O’Driscoll, M., Clinton, S., Jefferson, A., Manda, A. & McMillan, S. 2010: Urbanization Effects on Watershed Hydrology and In-Stream Processes in the Southern United States. *Water*, vol. 2, 605-648; doi:10.3390/w2030605.

Olerud, S. 2002: Berggrunnskart Nannestad, 1915III, M 1:50 000. NGU.

Regjeringen 2021: Gjerdrum-utvalget. <https://nettsteder.regjeringen.no/gjerdrumutvalget/>

The SciPy community 2021: Interpolation (scipy.interpolate). Available at: <https://docs.scipy.org/doc/scipy/reference/interpolate.html> (last visit 09/09/2021)

Wheaton, J.M., Brasington, J., Darby, S.E. & Sear, D.A. 2010: Accounting for uncertainty in DEMs from repeat topographic surveys: improved sediment budget. *Earth Surface Processes and Landforms*, vol. 35, p. 136-156.

Østmo, S.R. & Olsen, K.S. 1978: Nannestad 1915 III, kvartærgeologisk kart M 1:50 000. NGU.

21. Acknowledgement

The authors gratefully thank all people that contributed with datasets, analyses and good discussions during the development of this study:

NGU: Francois Noel, Pierrick Nicolet and Anne Liinamaa-Dehls.

NVE: Rengifo Zenon Ortega Mora, Hallvard Berg, Amund Frogner Borge, Ellen Davis Haugen, Kjetil Indrevær.

Multiconsult: Ruth Hetland, Marit Isachsen.

Parts of the Gjerdrum external expert committee: Steinar Nordal (NTNU), Hanne B. Ottesen (Statens vegvesen), Tone M. Muthanna (NTNU).

List of appendices

Appendix 1. The LiDAR method	65
Appendix 2. Aerial photogrammetry	66
Appendix 3. Forest cover	67
Appendix 4. Creek migration – Tistilbekken	69
Appendix 5. The 2013 dataset	70
Appendix 6. Cross section profiles for change detection in the streams	72
Appendix 7. Stream power index	80

Appendix 1. The LiDAR method

LiDAR (Light Detection and Ranging) is an optical remote analytic technology, and it is called airborne LiDAR when the laser system is mounted on an aircraft (Figure 43A). The LiDAR acquisition consists on the emission of an infrared pulse whose reflection (returned pulse) is captured and recorded by a sensor. The distance between the sensor and the target (terrain and objects) is computed from the round-trip time travel of the pulse.

The points composing a point cloud are classified depending on type of object that has reflected the laser pulse (ground, vegetation, infrastructure, water, etc). Filtering these points by using their classification value allows obtaining a point cloud composed of only the points corresponding to the ground, and therefore the construction of digital terrain models (Figure 43B and C). The resolution of the digital terrain models depends on the amounts of points per unit area. In our study, the DEMs used range from 25 cm to 1 m of resolution. The application of a shading function to a DEM (hillshade) helps to the visualisation of the different features in the surface (e.g. landforms such as landslides, ravines, bedrock exposures, etc) by applying a light source with a user-defined orientation.

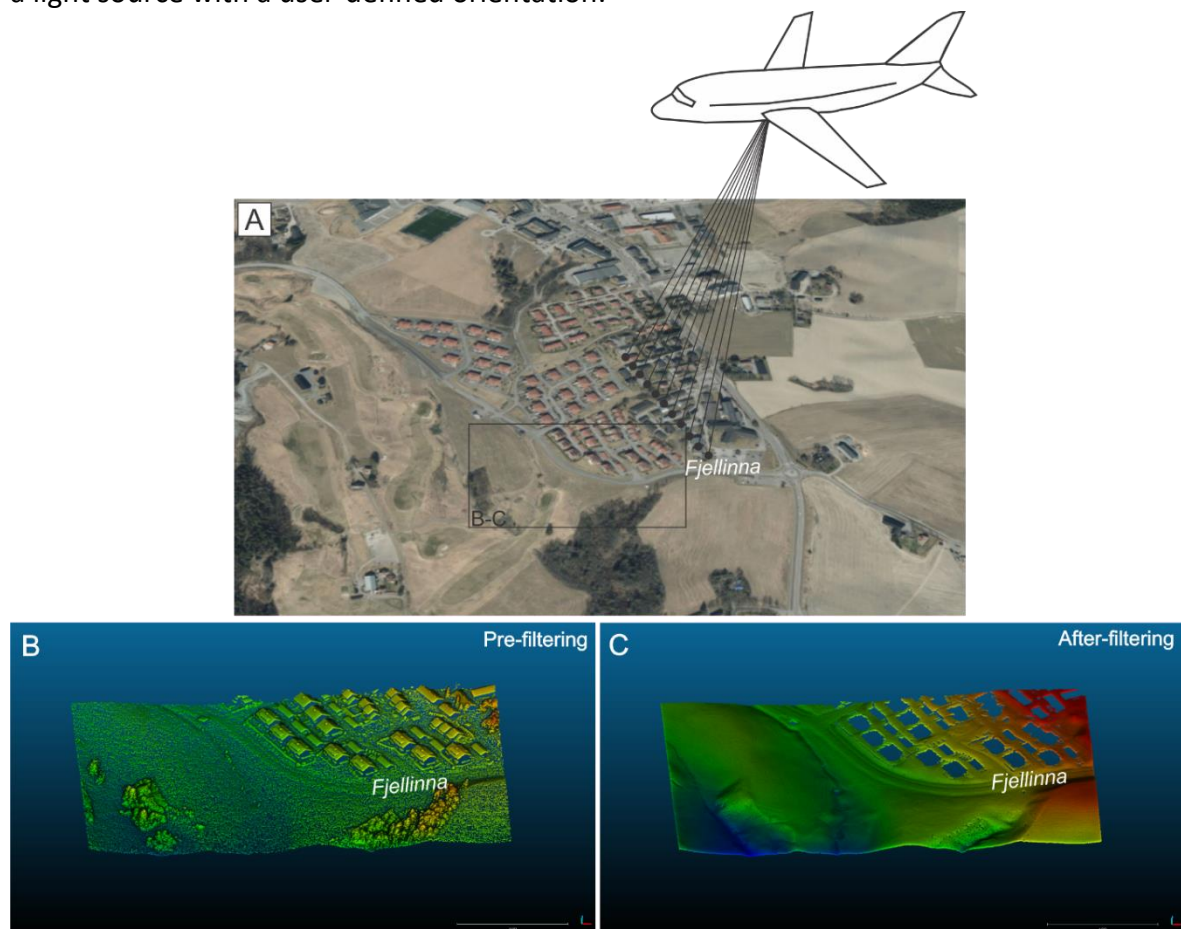


Figure 43. (A) Scheme showing the methodology for the acquisition of point clouds with airborne LiDAR. (B) Point cloud before filtering points corresponding to the ground. (C) Point cloud after filtering all points not corresponding to ground.

Appendix 2. Aerial photogrammetry

Aerial pictures from the projects Ask juli 1969, Ask juni 1974, Ask 15 mai 1982, and Ask 17 mai 1991 were used to build digital terrain models by using photogrammetry. Photogrammetry is a methodology that allows building 3D models from overlapping two dimensional photographs, e.g. aerial photos. The photogrammetric models used in this study were done by COWI AS for NVE. COWI AS used the program DTMaster from Inpho to generate DTM grids (regular grid points) as a terrain model.

Table 11 shows the accuracy test carried out for the photogrammetry models, using as ground control points GPS measurements carried out by NGI in 2006 (Gregersen and Moholdt, 2006).

Table 11. Control of accuracy for the photogrammetric models using as GCP GPS measurements from 2006 in Nystulia area.

ID	X	Y	Z 2006	H1969	H1974	H1982	H1991	Dz (1969-2006)	Dz (1974-2006)	Dz (1982-2006)	Dz (1991-2006)
6/06	613319.5	6660404.3	163.137	163.54	163.47	162.896	163.02	-0.403	-0.333	0.241	0.117
5/06	613330.4	6660388.9	162.879	162.578	163.35	163.254	163.099	0.301	-0.471	-0.375	-0.22
7/06	613312.7	6660424.8	164.757	165.277	165.244	165.16	164.847	-0.520	-0.487	-0.403	-0.09
8/06	613328.4	6660444.9	167.913	168.456	168.525	168.634	168.143	-0.543	-0.612	-0.721	-0.23
9/06	613335.5	6660430.4	166.042	166.758	166.751	166.697	166.404	-0.716	-0.709	-0.655	-0.362
10/06	613361.4	6660420.4	165.69	166.039	166.587	166.452	166.33	-0.349	-0.897	-0.762	-0.64

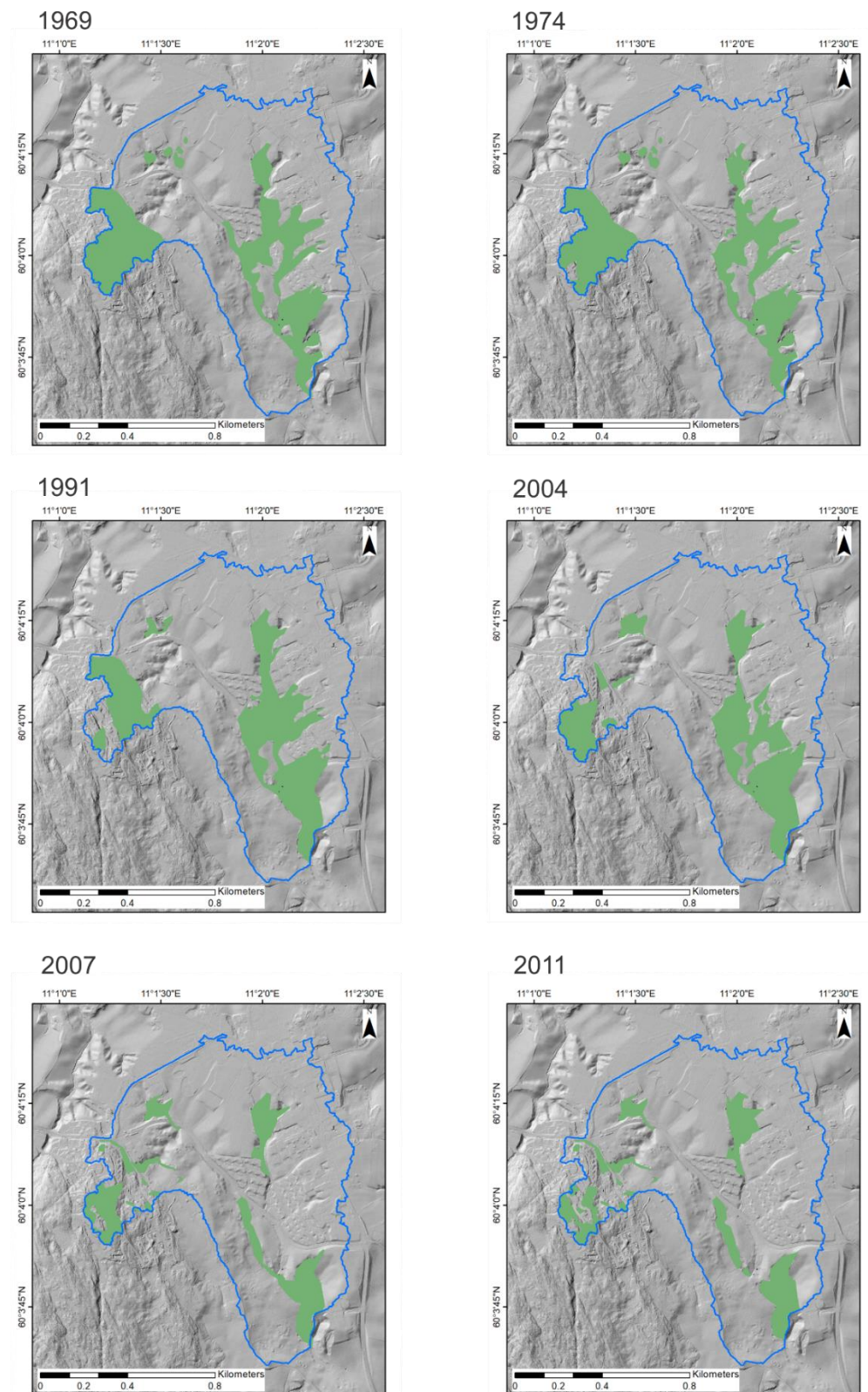
Accur-acy	1991
Min (m)	-0.64
Max (m)	0.117
MAE	0.2765
RMSE	0.492

Accur-acy	1982
Min (m)	-0.762
Max (m)	0.241
MAE	0.526
RMSE	0.561

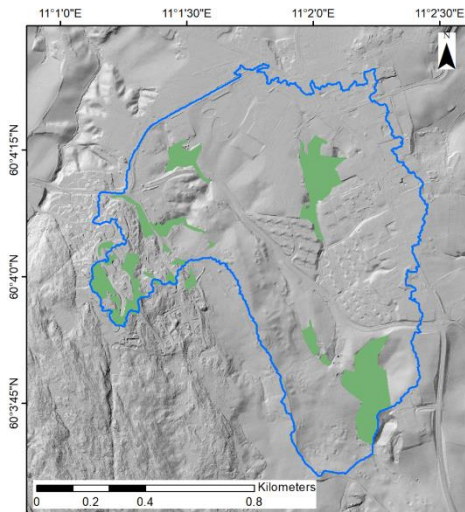
Accur-acy	1974
Min (m)	-0.897
Max (m)	-0.333
MAE	0.585
RMSE	0.613

Accur-acy	1969
Min (m)	-0.716
Max (m)	0.301
MAE	0.472
RMSE	0.333

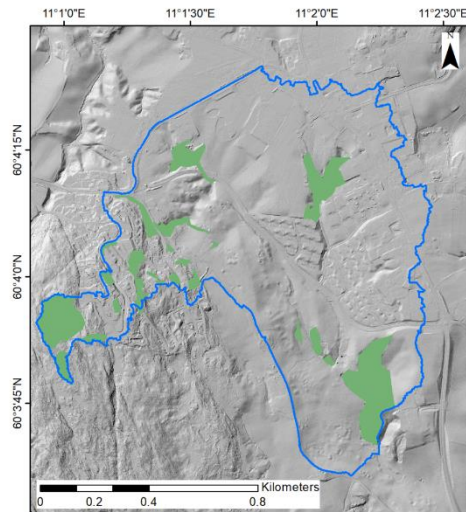
Appendix 3. Forest cover



2013



2016



2020

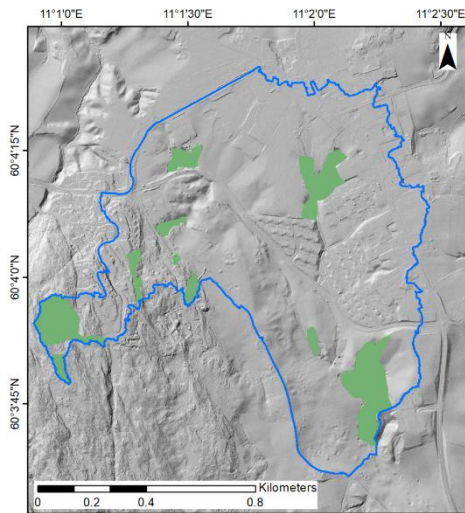
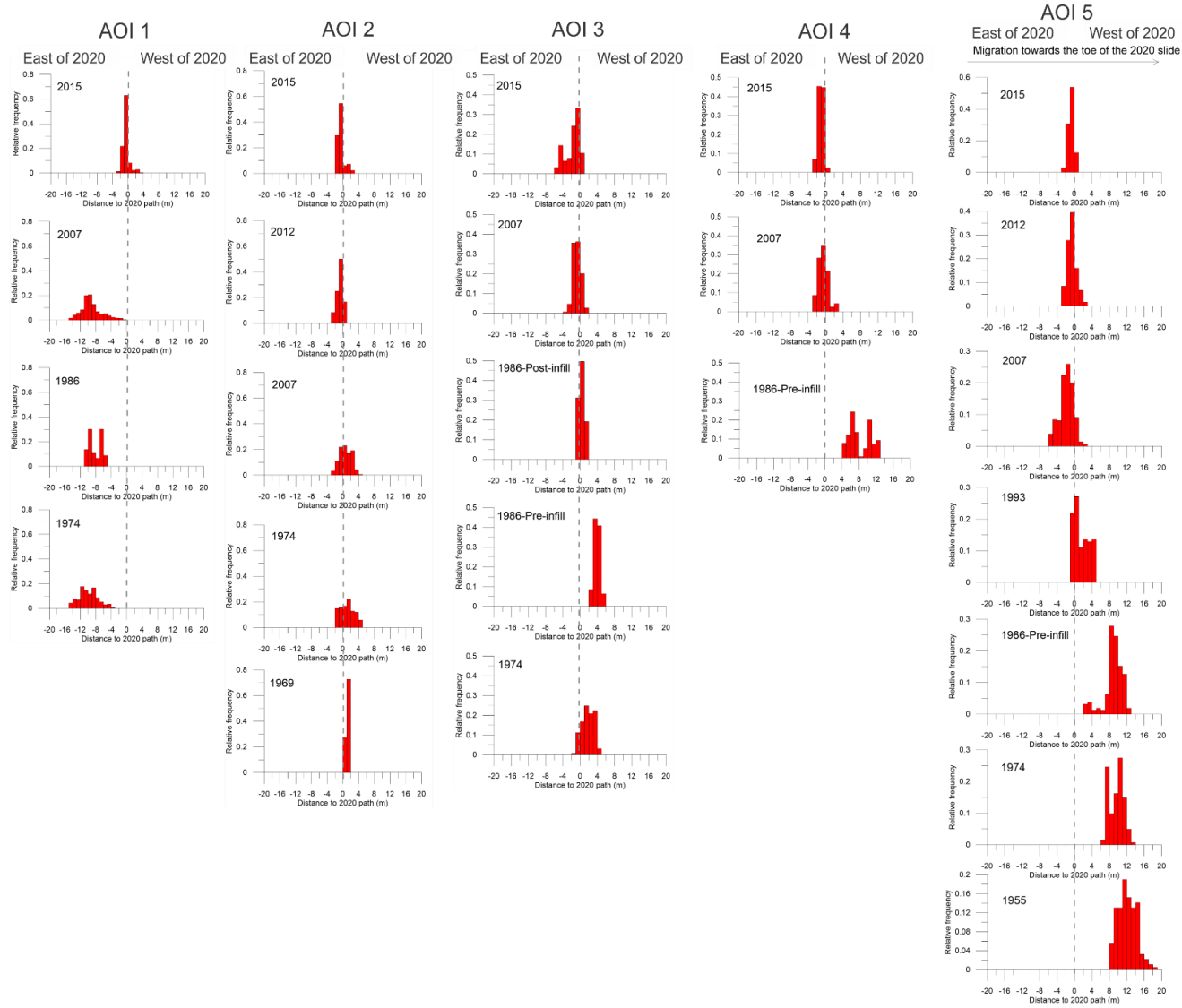


Figure 44. Maps showing the vegetation coverage at different times.

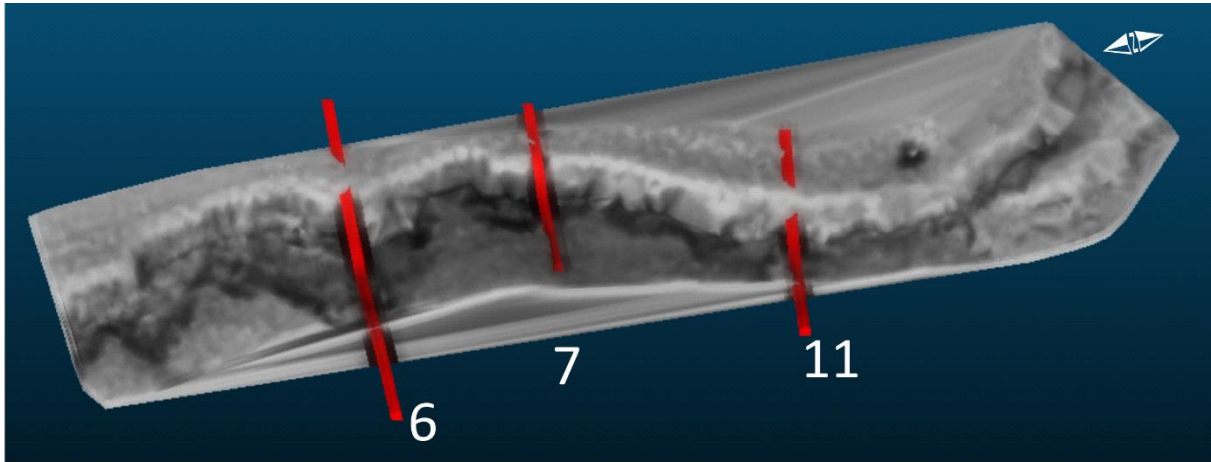
Appendix 4. Creek migration – Tistilbekken



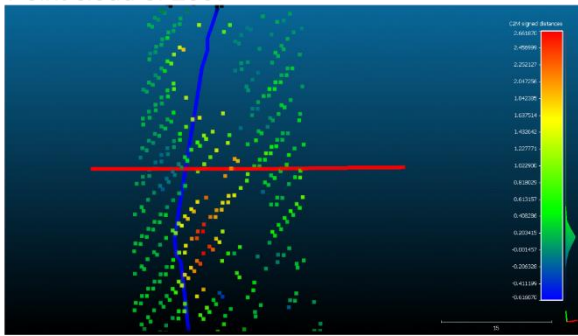
Appendix 5. The 2013 dataset

For the analysis of the cross sections, specially in the area where the landslide occurred, we did not used the dataset of 2013. In slopes without changes, the cross sections for 2007, 2015 and 2020 showed a good match, while this was not the case for 2013.

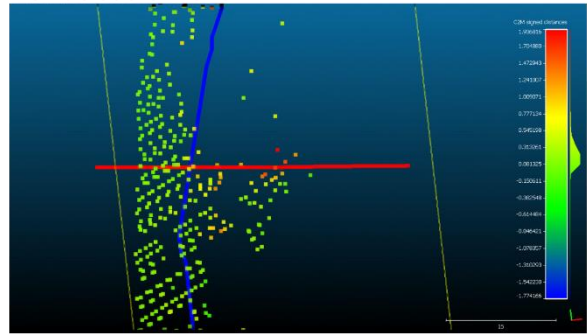
The datasets of 2007 and 2013 have the same point density but the dataset of 2007 (acquired in may), specially in forested areas, has a higher amount of points classified as «ground» than the dataset of 2013 which was acquired in July (Figure 45). The dataset of 2013 was acquired at a time where the vegetation coverage was denser, therefore less points representing the ground were acquired and then the interpolation is coarser.



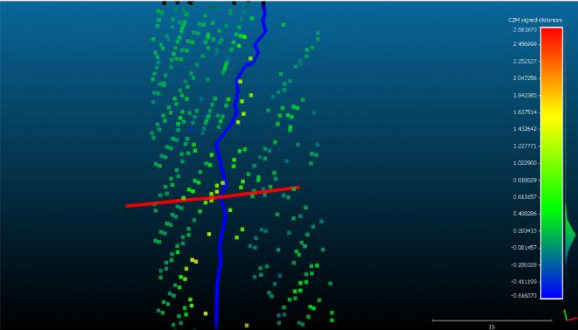
Profile 6
Point cloud of 2007



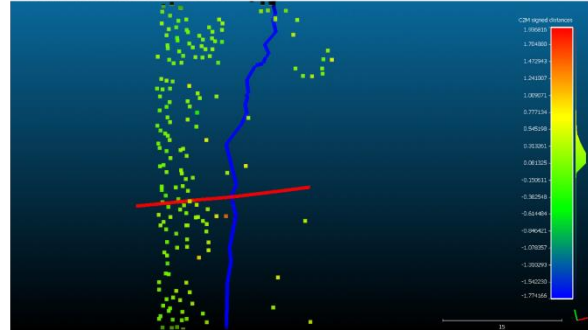
Profile 6
Point cloud of 2013



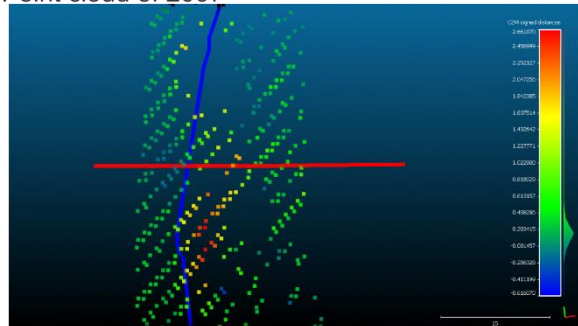
Profile 7
Point cloud of 2007



Profile 7
Point cloud of 2013



Profile 11
Point cloud of 2007



Profile 11
Point cloud of 2013

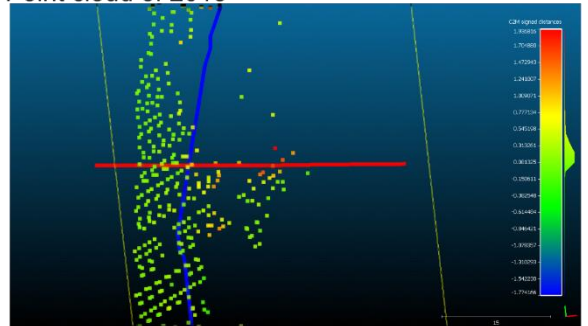


Figure 45. Profiles in the lower part of Tistilbekken and views of the point clouds at 2007 and 2013 in the vicinity of each profile. Note: the blue line represents the location of the creek in 2020.

Appendix 6. Cross section profiles for change detection in the streams

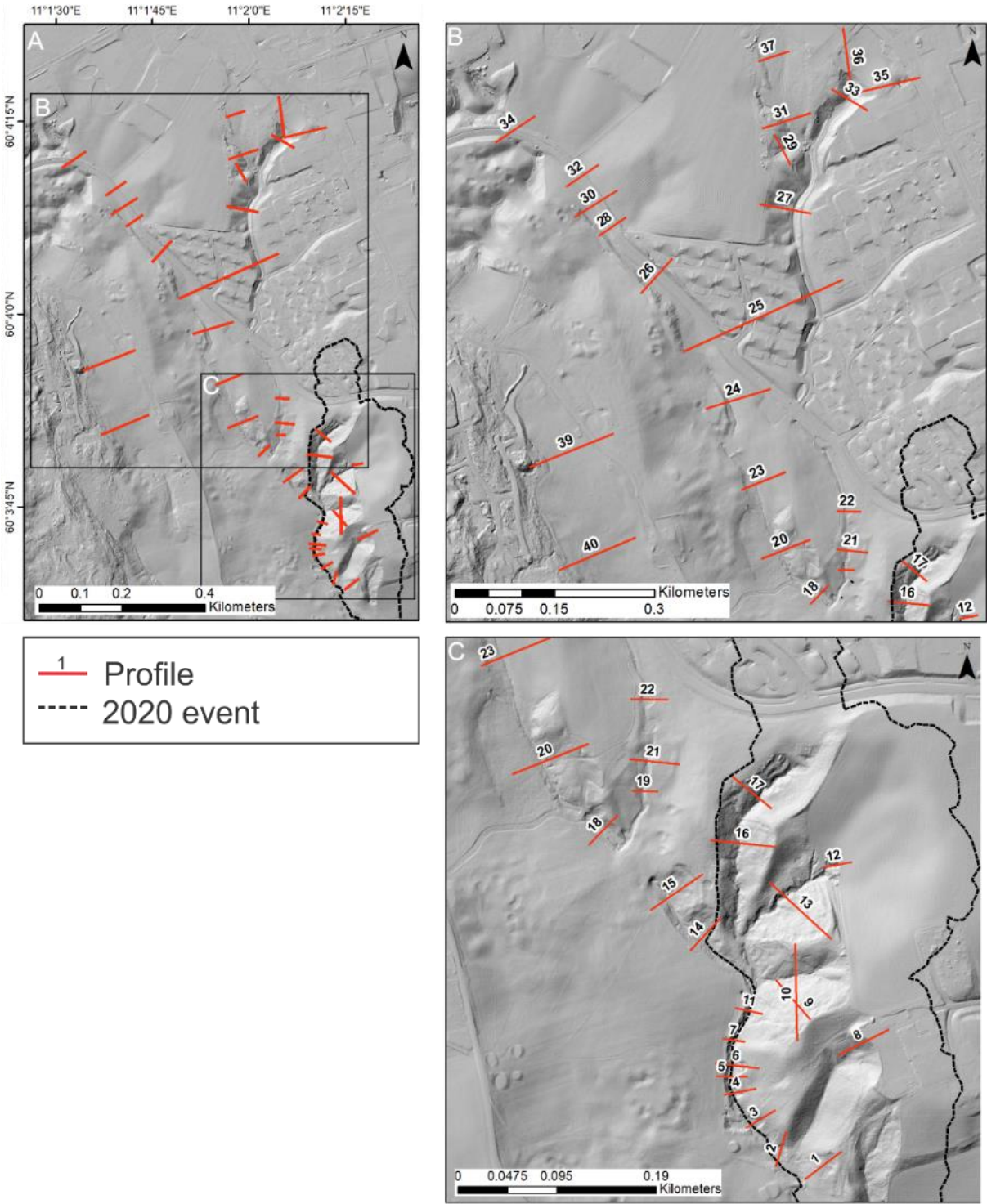
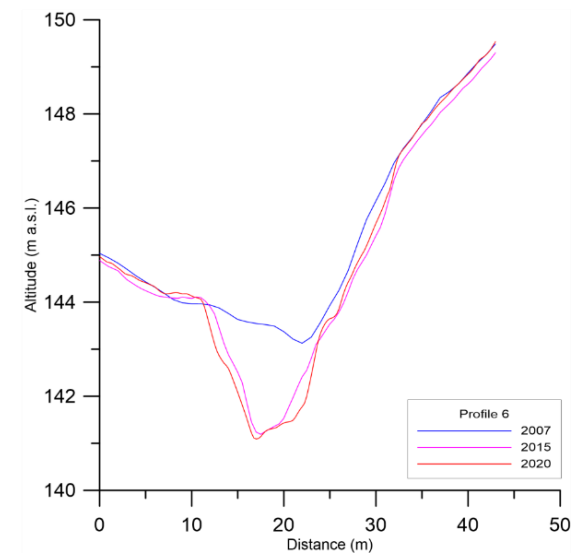
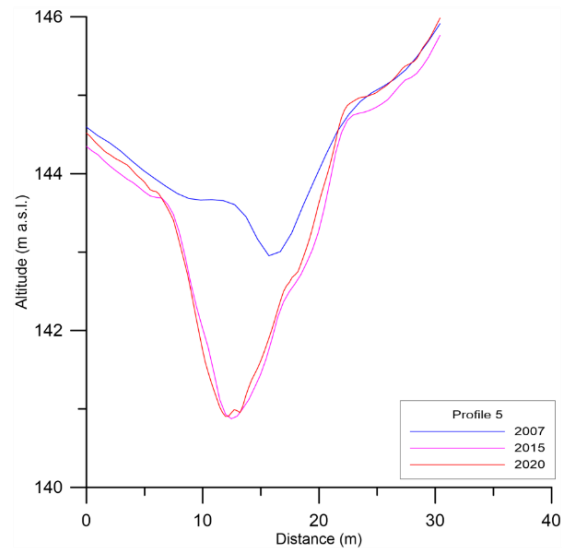
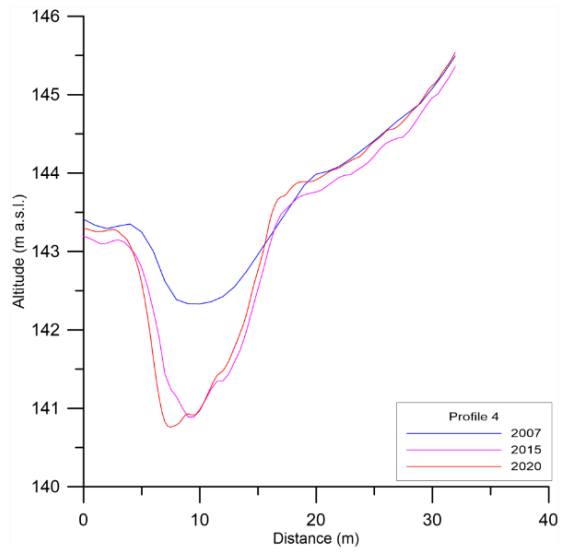
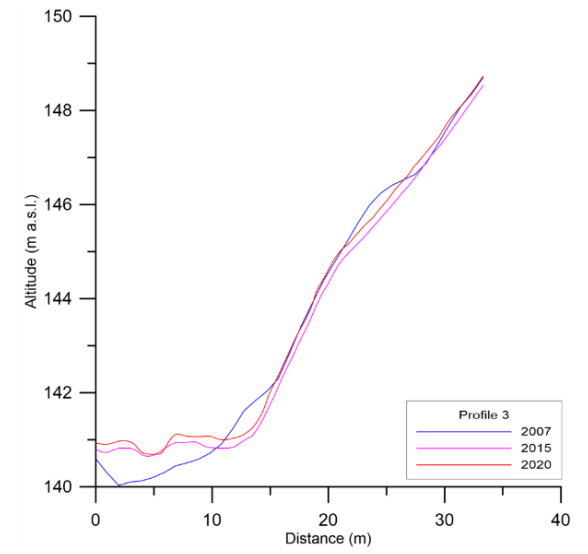
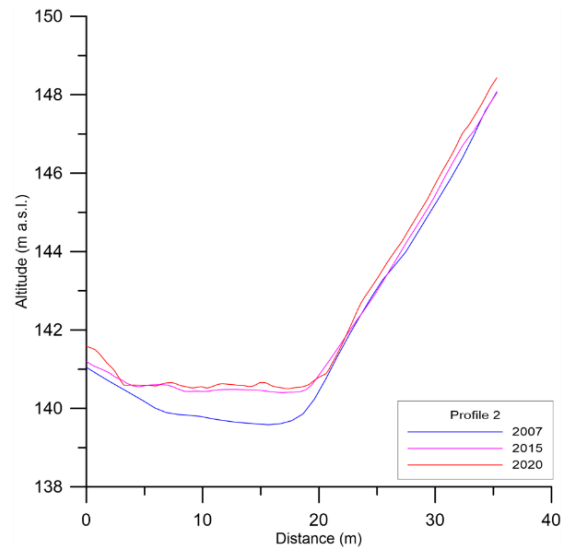
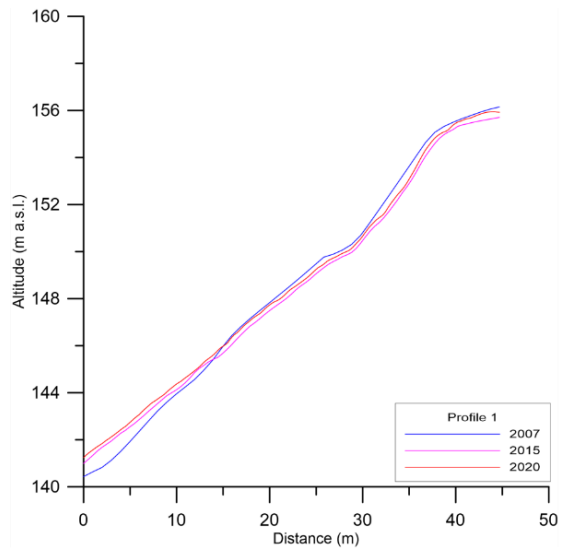
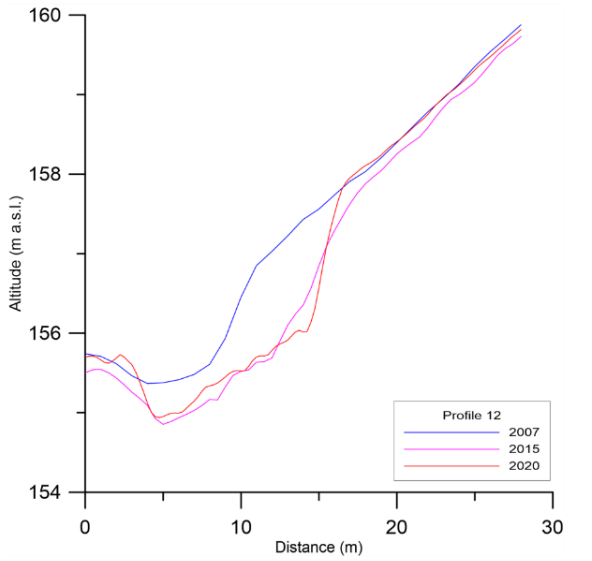
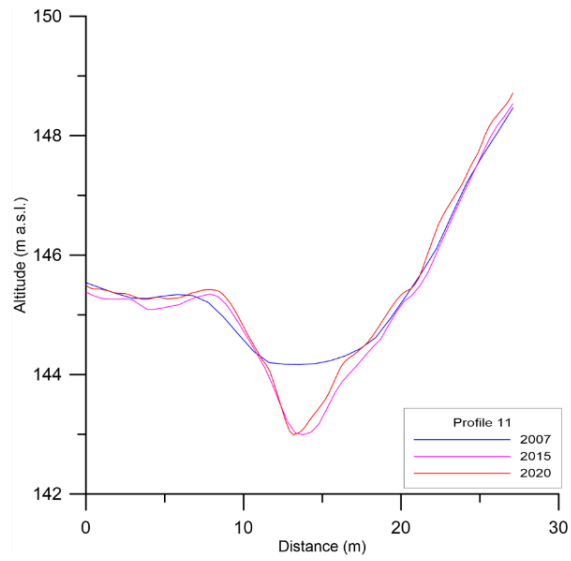
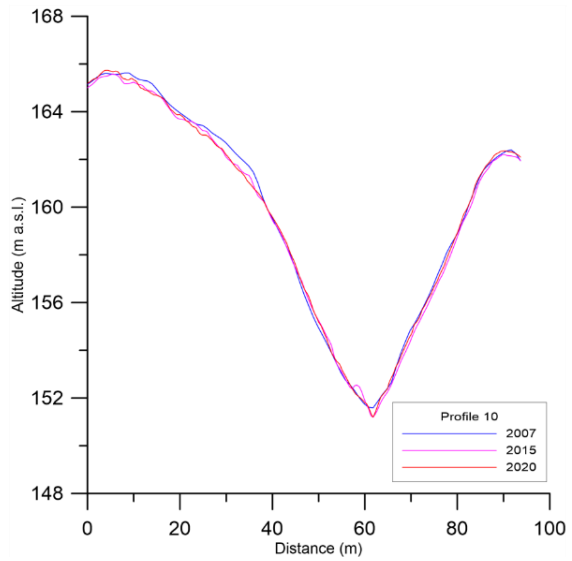
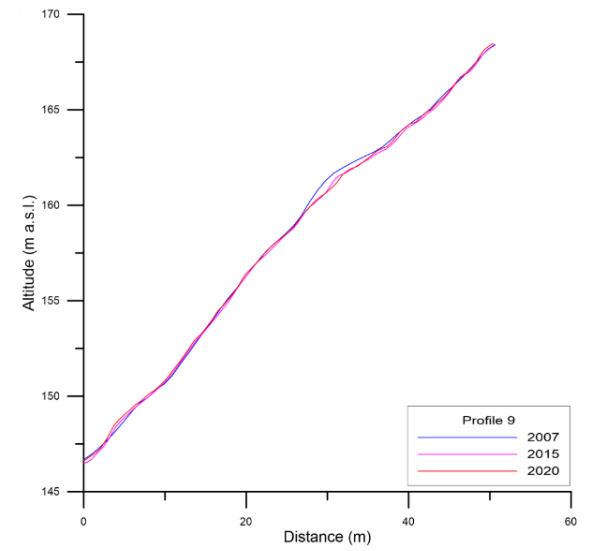
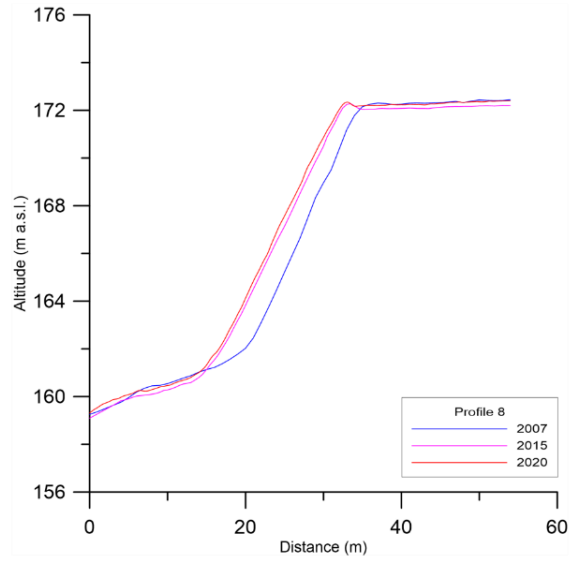
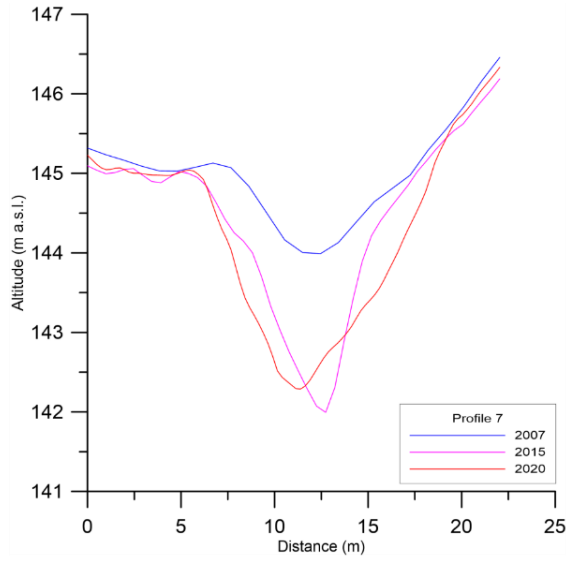
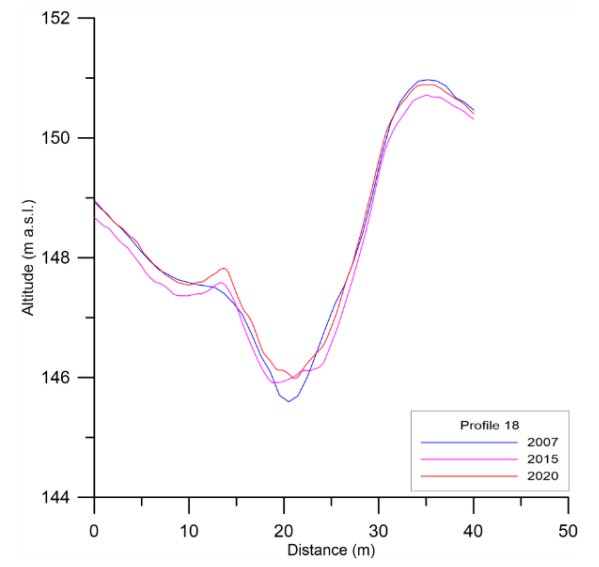
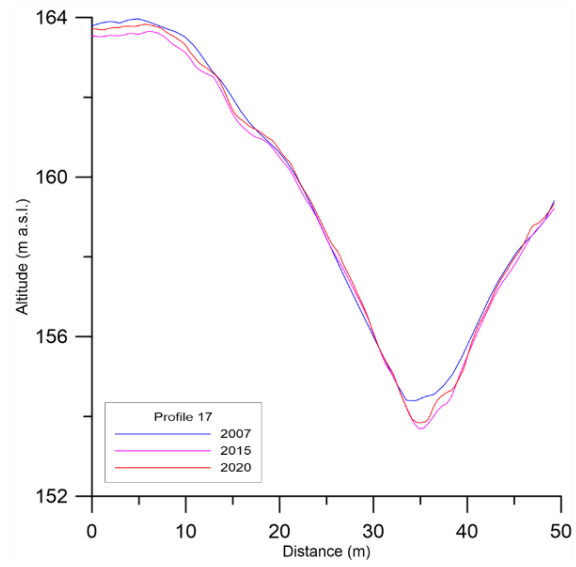
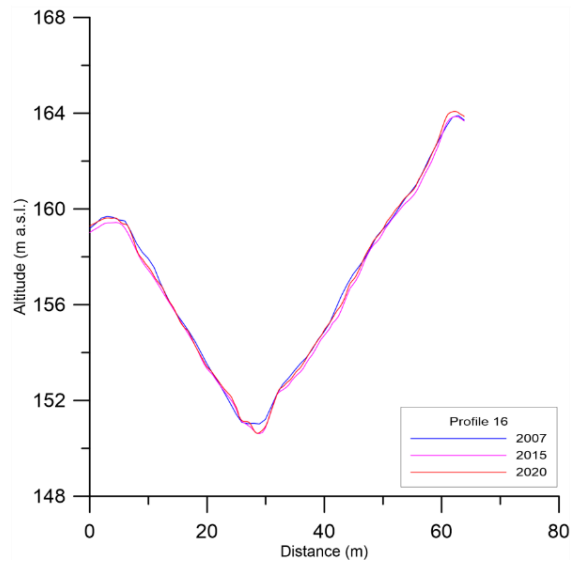
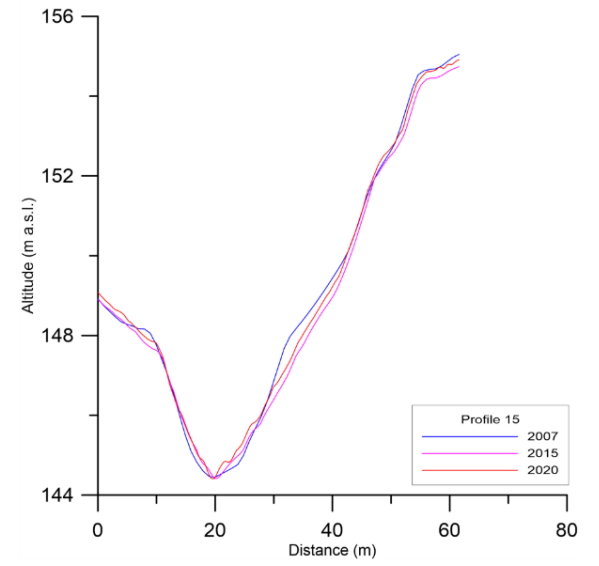
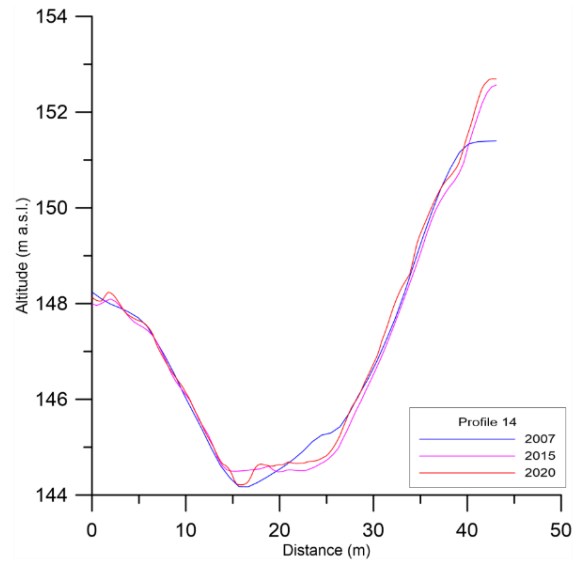
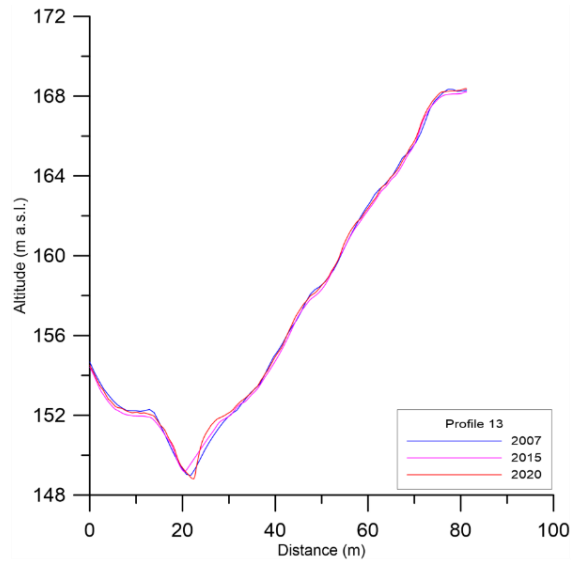
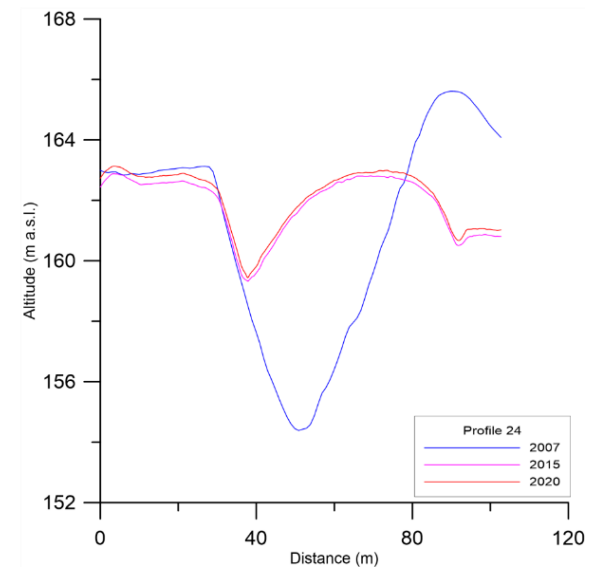
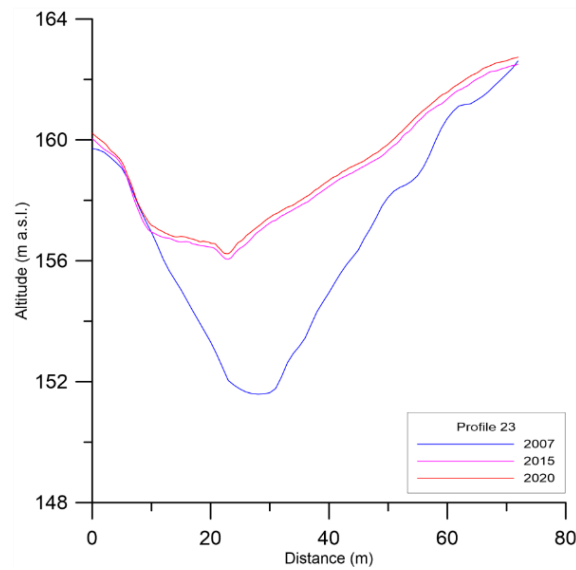
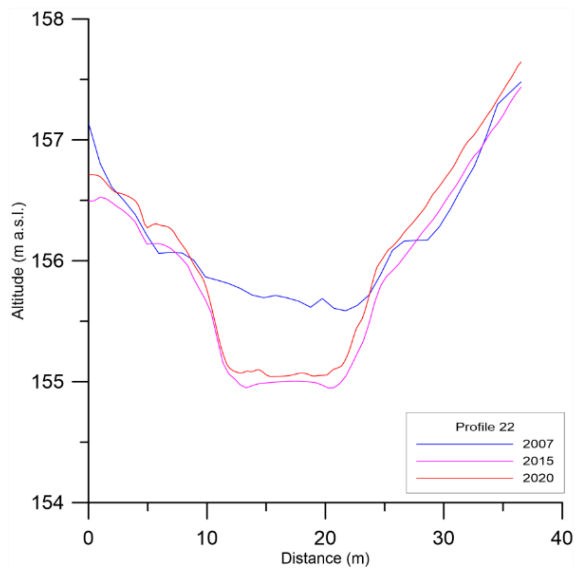
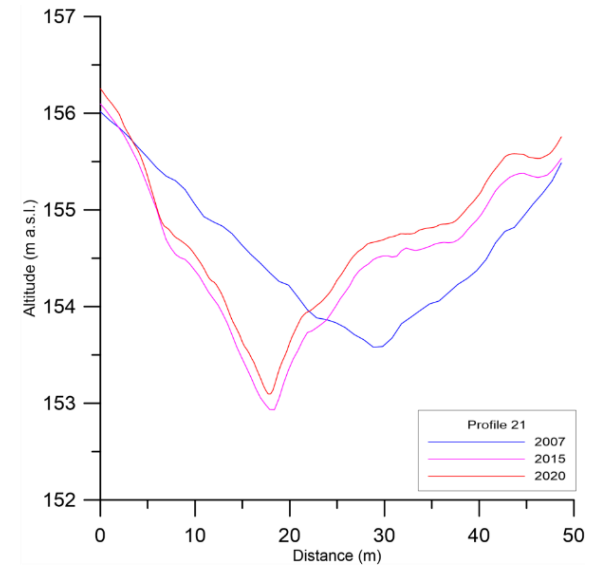
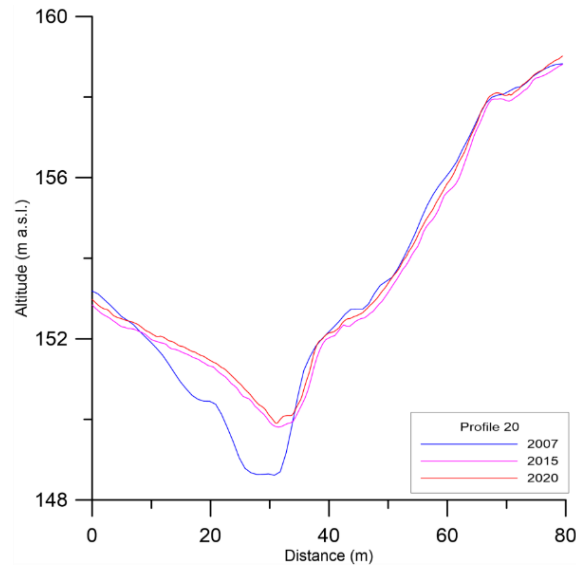
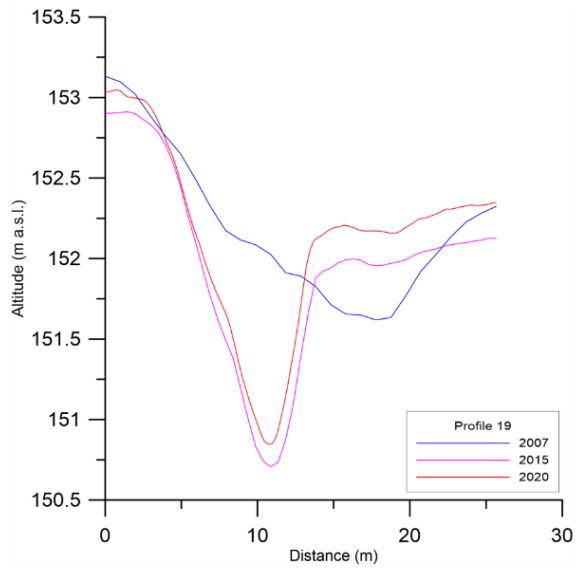


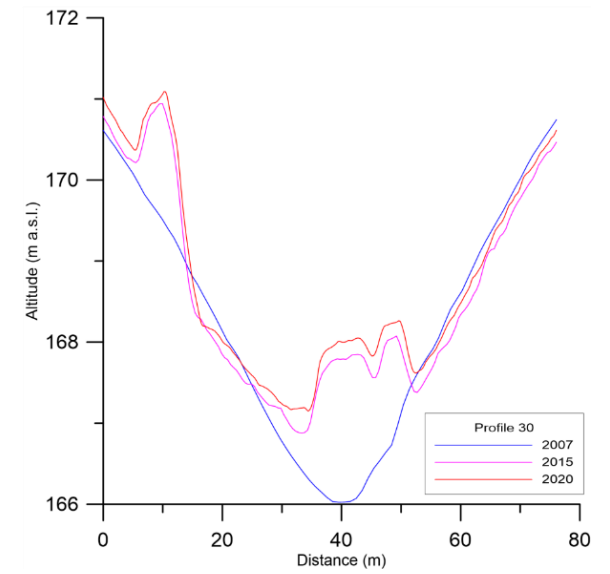
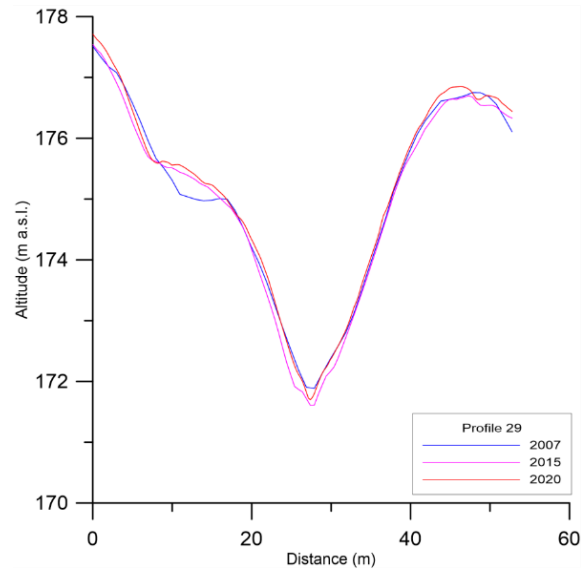
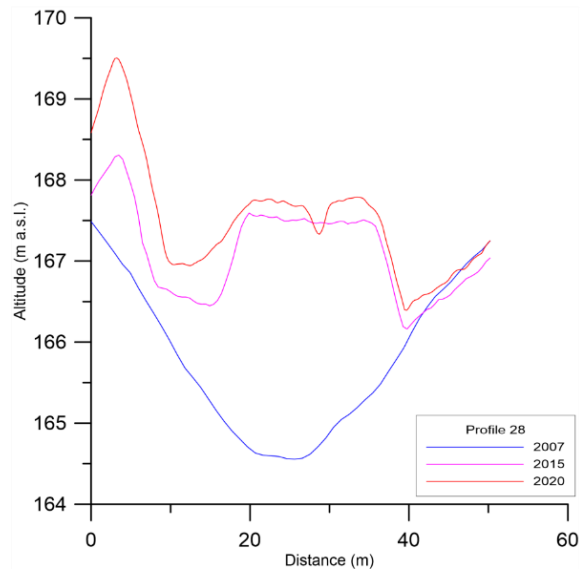
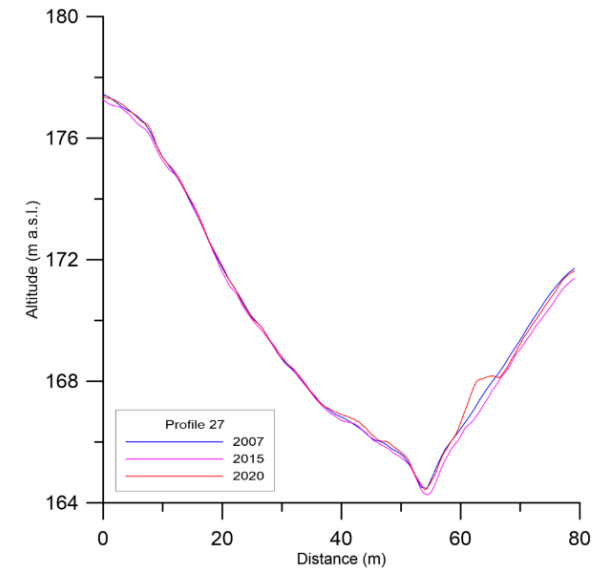
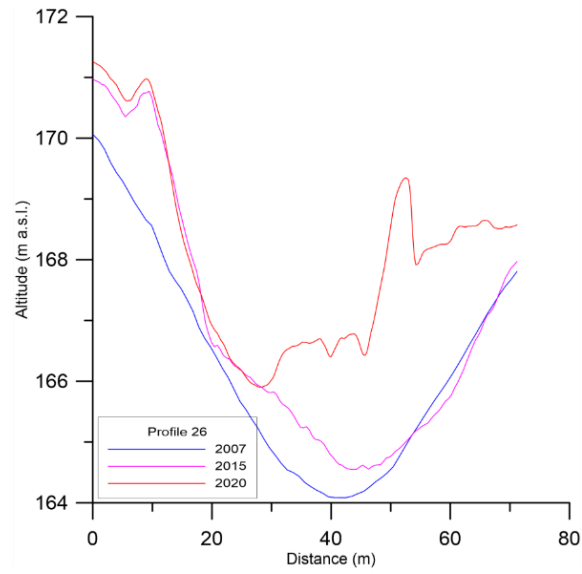
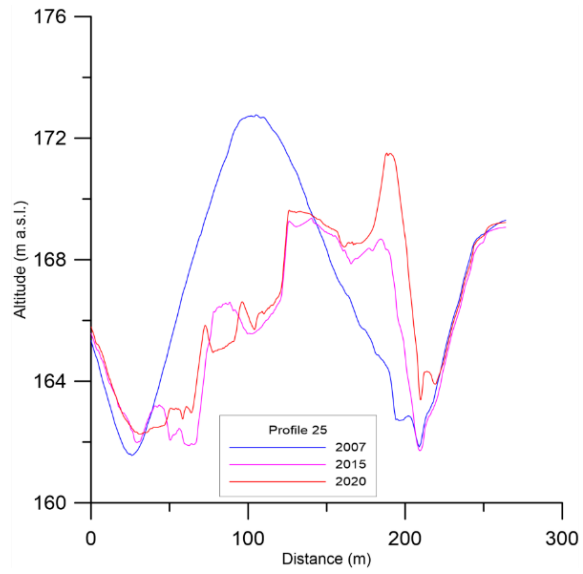
Figure 46. Maps of all the cross profiles are shown above. Most of the profiles are drawn from W to E, the profiles 10 and 36 are drawn from S to N, and profiles 9, 13, 29 and 33 are drawn from N to S.

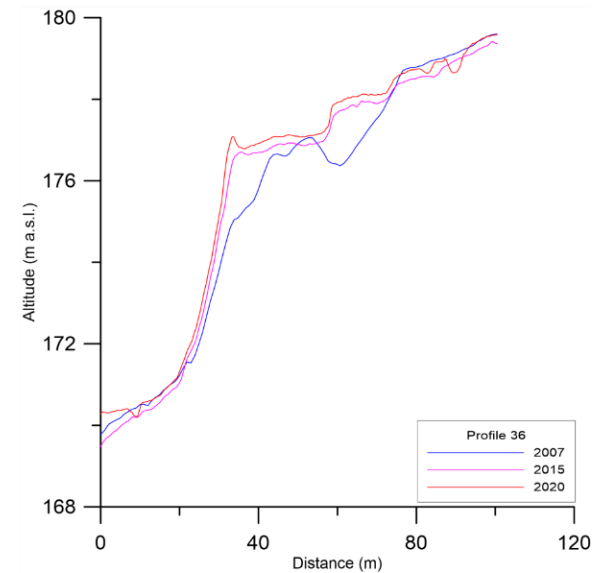
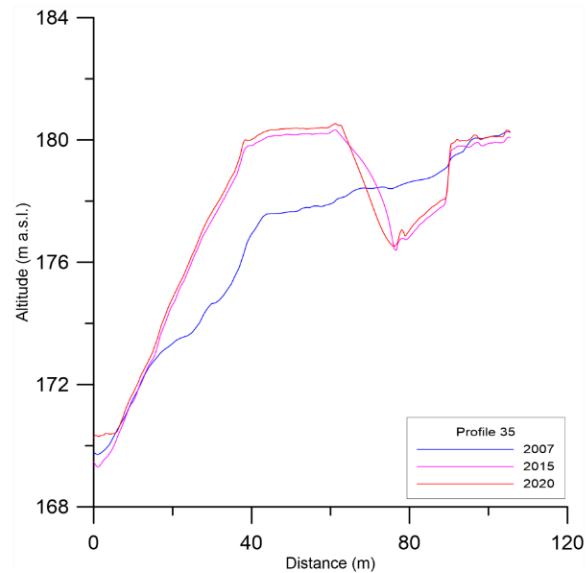
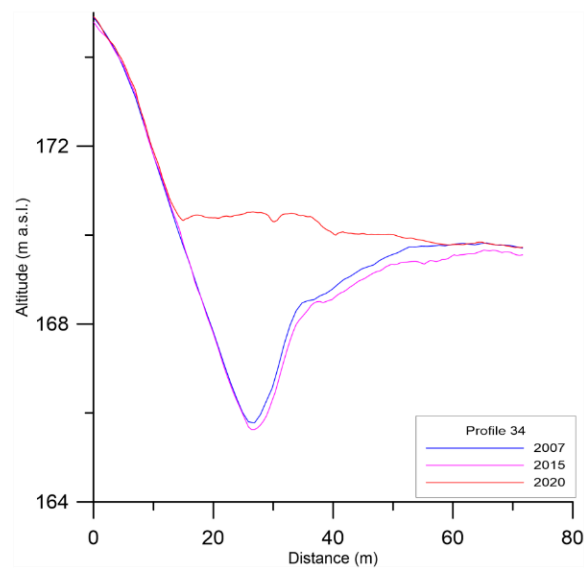
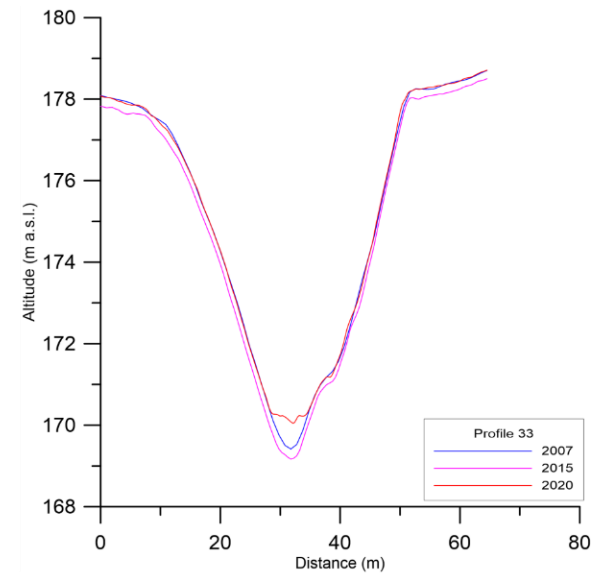
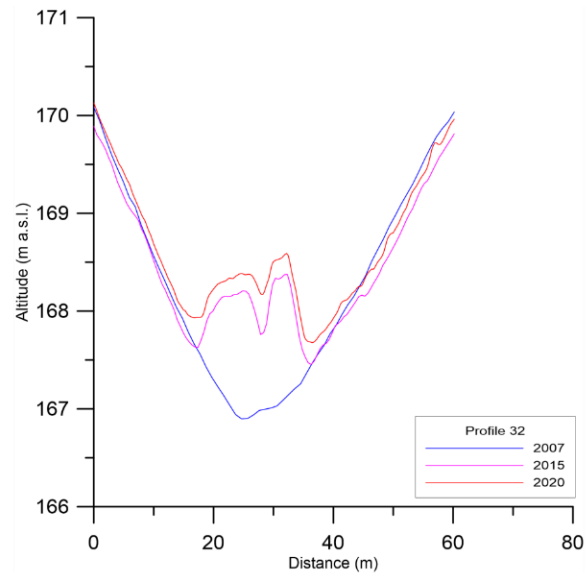
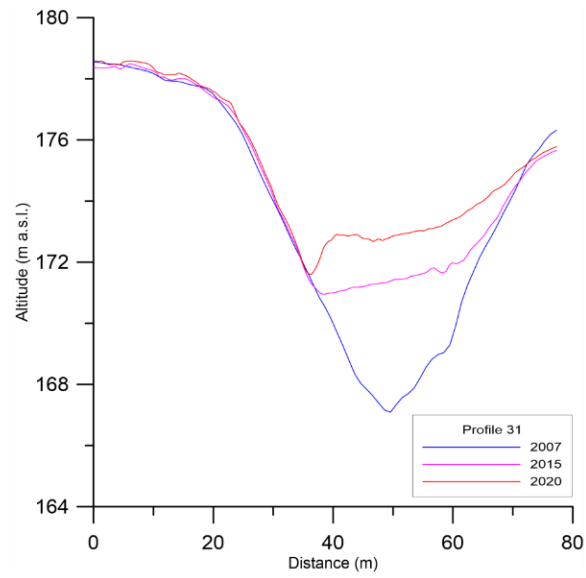


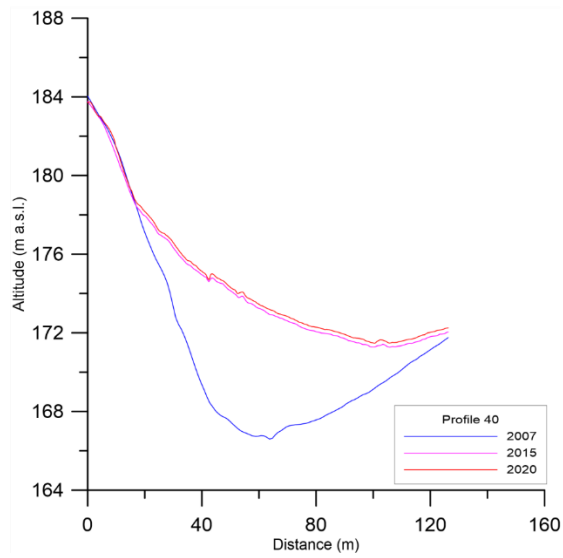
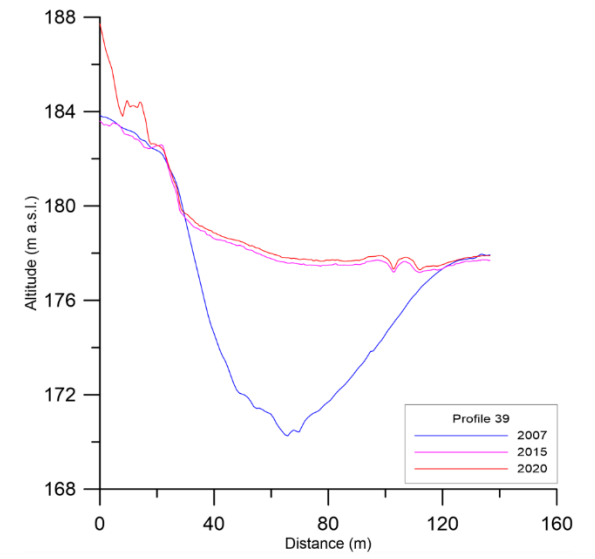
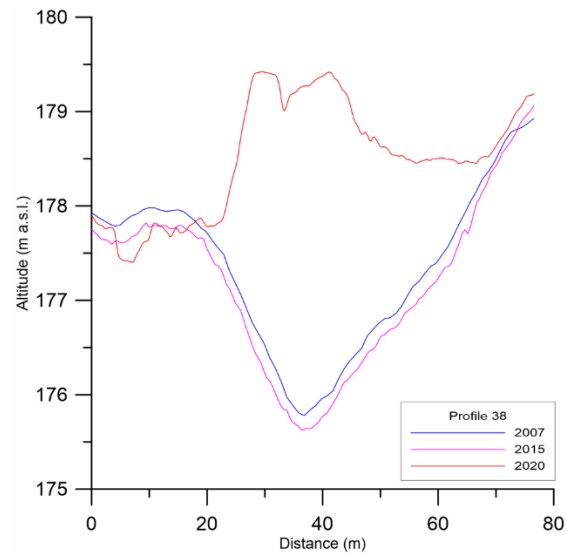
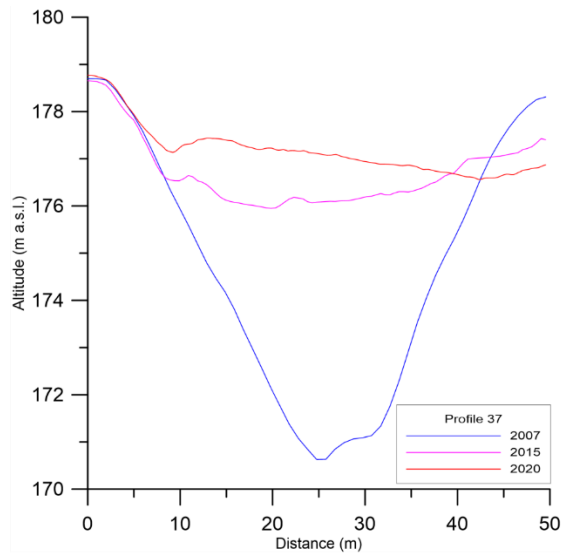












Appendix 7. Stream power index

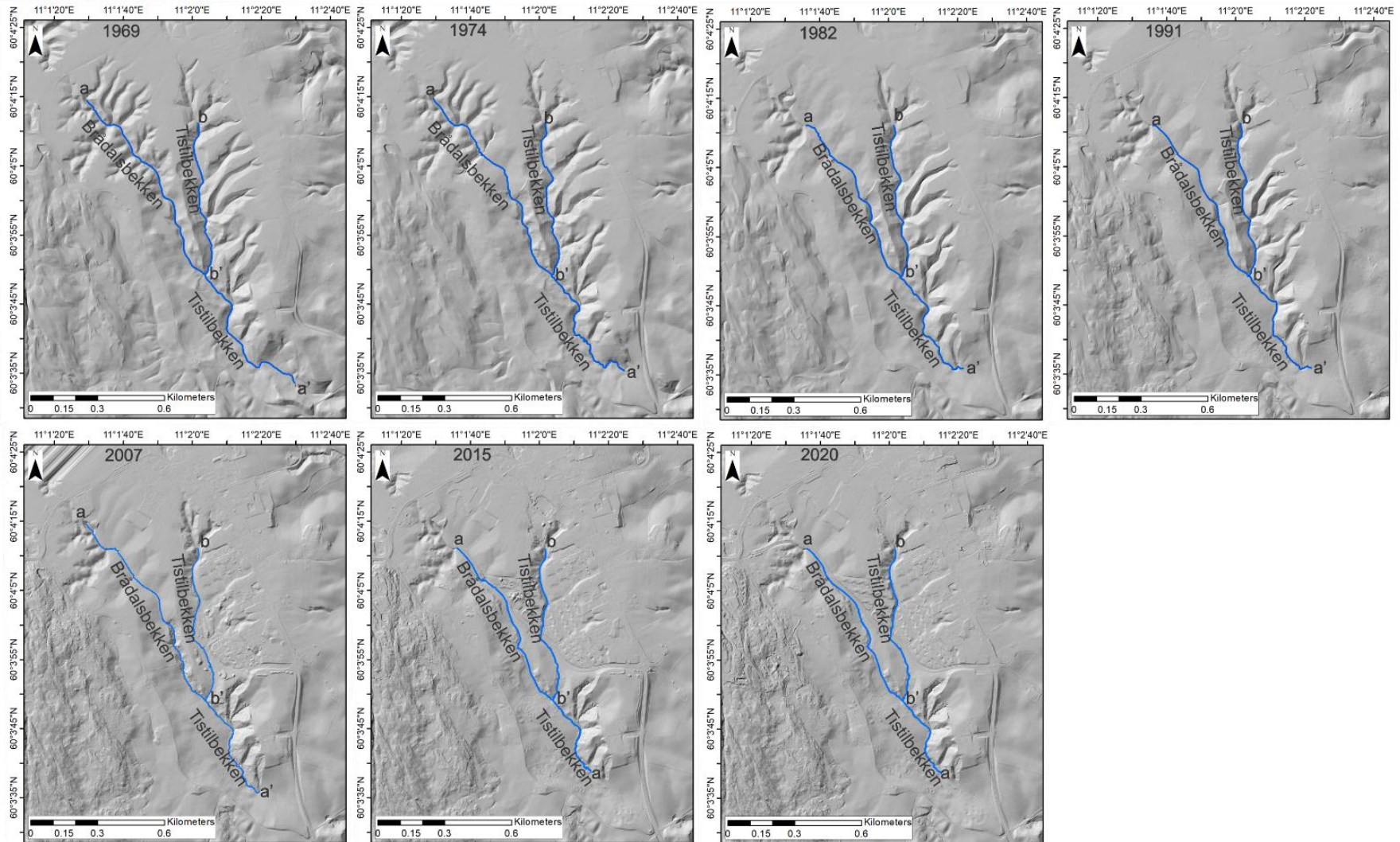


Figure 47. Hillshade maps showing the path of Brådalsbekken and Tistilbekken over various years.

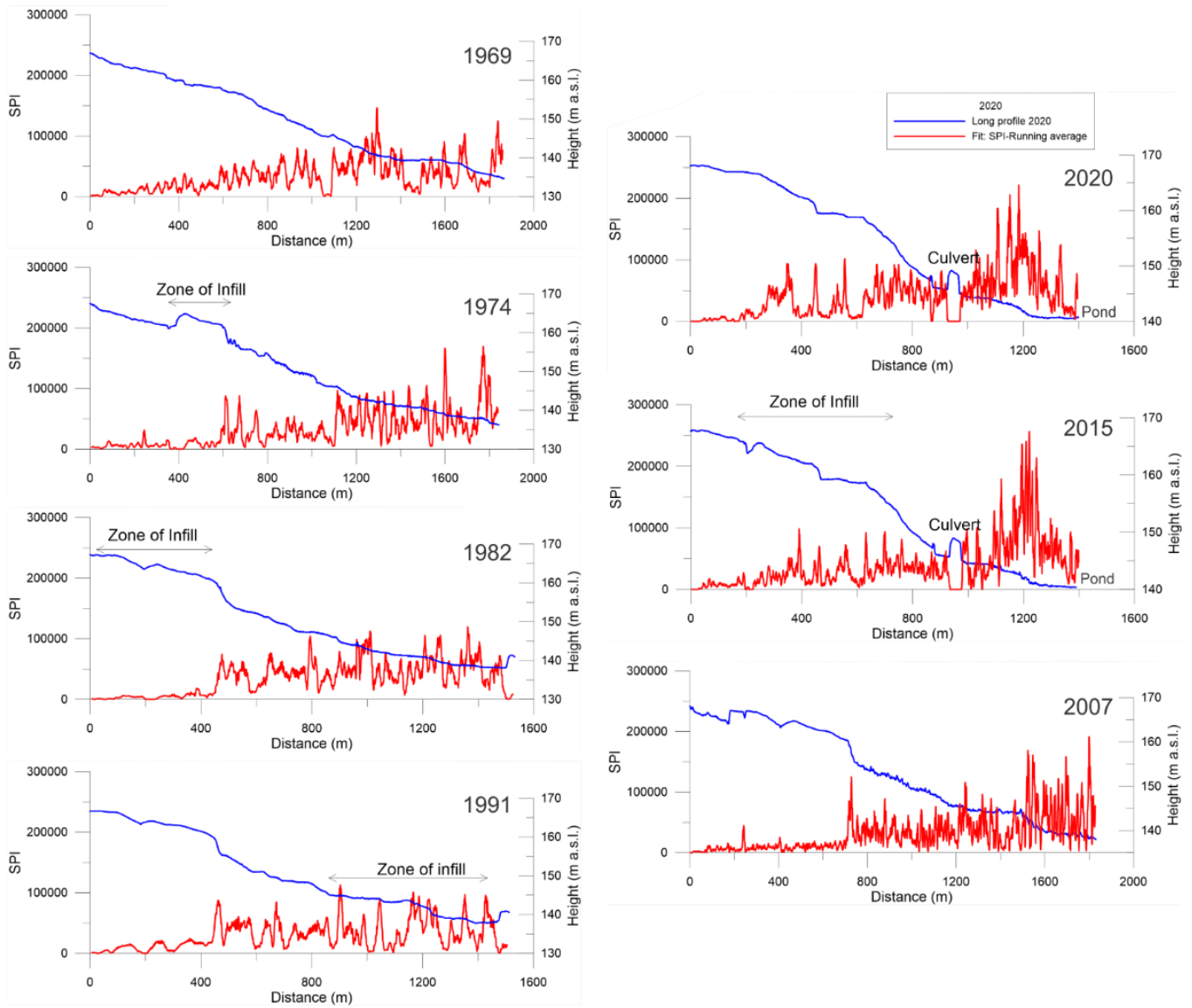


Figure 48. Variation in SPI along the profile of Brådalsbekken-Tistilbekken for the different periods analysed.

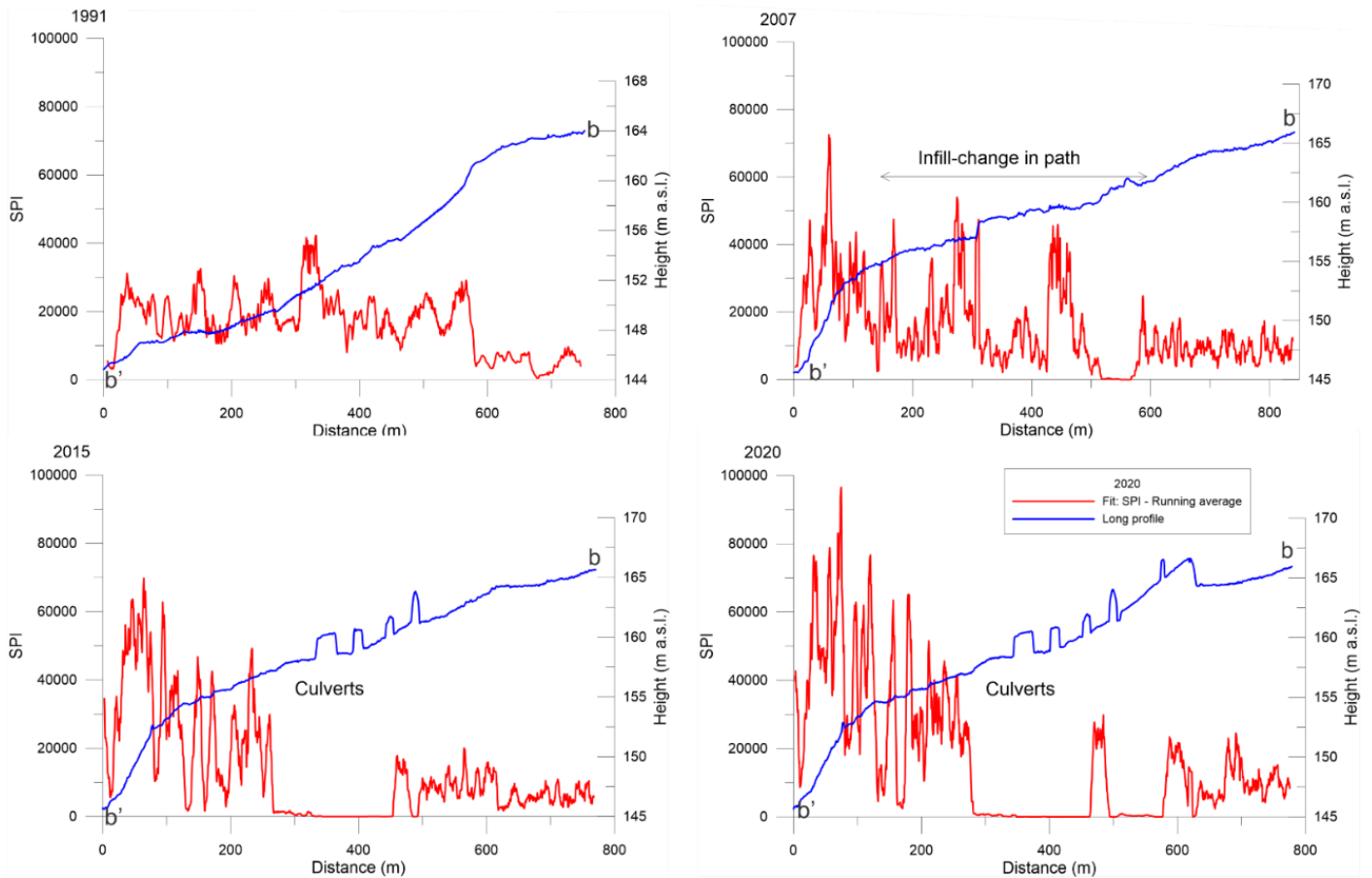


Figure 49. Variation in SPI along the profile of the upper section of Tistilbekken for the different periods analysed.



GEOLOGICAL
SURVEY OF
NORWAY

· NGU ·

Geological Survey of Norway
PO Box 6315, Sluppen
N-7491 Trondheim, Norway

Visitor address
Leiv Eirikssons vei 39
7040 Trondheim

Tel (+ 47) 73 90 40 00
E-mail ngu@ngu.no
Web www.ngu.no/en-gb/